Structure-based discovery of potent and selective small-molecule inhibitors targeting signal transducer and activator of transcription 3 (STAT3)

Qiuyao Huang [a, 1], Yan Zhong [b, 1], Bingbing Li [a, 1], Shumin Ouyang [b], Lin Deng [a], Jianshan Mo [b], Shuo Shi [b], Nan Lv [b], Ruibo Wu [b], Peiqing Liu [b], Wenhao Hu [a], Xiaolei Zhang [b, **], Yuanxiang Wang [a, *]

[a] Guangdong Key Laboratory of Chiral Molecule and Drug Discovery, School of Pharmaceutical Sciences, Sun Yat-Sen University, Guangzhou, 510006, China
[b] Guangdong Key Laboratory of New Drug Design and Evaluation, School of Pharmaceutical Sciences, Sun Yat-Sen University, Guangzhou, 510006, China

ARTICLE INFO

ABSTRACT

STAT3 has been validated as an attractive anticancer target due to its important roles in cancer initiation and progression. However, discovery of potent and selective STAT3 small-molecule inhibitors with druglike properties is still challenging. In this study, two series of substituted 2-phenylquinolines and 2-arylimidazo[1,2-a]pyridines were designed through structure-based drug discovery approach by condensing the privileged structures of **STX-119** and **SH4-54**. Our study has resulted in the discovery of a number of highly potent and selective STAT3 inhibitors, exemplified by compound **39** with the privileged structure of 2-phenylimidazo[1,2-a]pyridine, which selectively inhibits phosphorylation of STAT3 and suppresses subsequent signaling pathway. Moreover, **39** inhibits cell growth, migration and invasion of human triple negative breast cancer (TNBC) cells lines. Consistently, it achieves significant and dose-dependent tumor growth inhibition in both cell line-derived and patient-derived xenograft tumor models in mice. These results clearly indicate that **39** is a highly potent and selective STAT3 inhibitor.

1. Introduction

As a transcription factor, STAT3 transduces extracellular signals to the nucleus and then activates transcription of target genes. Under physiological conditions, it mediates cell proliferation, differentiation, apoptosis, survival, and other important cellular processes in response to stimulation of a large number of cytokines and growth factors [1,2]. However, constitutive STAT3 activation has been detected in almost 70% of human solid and hematological tumors, and is generally associated with poor clinical prognosis [3,4]. In view of its critical roles in cancer initiation and progression, STAT3 has attracted considerable interest as a potential target in cancer therapy [5–10]. On the other hand, aberrant STAT3 activation has been reported to mediate acquired resistance to a broad spectrum of chemotherapies, radiotherapies and targeted therapies, by up-regulating the expression of antiapoptotic proteins and surviving protein (such as Bcl-2, survivin, c-Myc, cyclin-D1, and Mcl-1) and down-regulating tumor suppressor gene (such as p53) [11–15]. Therefore, inhibition of STAT3 represents a new advance to reverse STAT3-addicted cancer cell resistance. Furthermore, constitutively activated STAT3 is also reported to play critical roles in modulation of tumor microenvironment and immune response through up-regulation of immunosuppressive factors and down-regulation of immune activation factors [16–18]. It has been validated that the combination of immune checkpoint inhibitors and STAT3 specific inhibitors can enhance the efficacy of cancer immunotherapy and demonstrates a synergistic antitumor effect [19–22]. Accordingly, the development of potent and selective

STAT3 inhibitors has multifaceted applications in cancer therapy and is highly desirable.

In the canonical STAT3 signaling pathway, STAT3 is activated by phosphorylation of tyrosine residue 705 (Tyr705) within its Src homology 2 (SH2) domain, followed by forming a homodimer via reciprocal interaction between the phosphorylated Tyr705 (pY705) within one monomer and the SH2 domain of the other. Activated STAT3 homodimers then translocate from the cytoplasm to the nucleus, where they bind to STAT3-specific DNA-response elements and regulate the expression of target genes. As the SH2 domain plays a pivotal role in STAT3 signaling cascade, significant efforts have been made to discover STAT3 inhibitors targeting the SH2 domain. These STAT3 SH2 domain inhibitors consist of small peptidomimetics, natural products and synthetic nonpeptidic small-molecules [1–4]. However, most of these inhibitors suffer from unfavorable cell permeability and druglike properties, or weak to modest binding affinity, highlighting the challenge in developing potent and selective small-molecule STAT3 SH2 domain inhibitors.[1,2] For instance, the previously discovered peptidomimetic STAT3 SH2 domain inhibitors usually demonstrate high binding affinities to STAT3 in biochemical assays, but display undesired cell permeability and druglike properties [1]. On the other hand, synthetic nonpeptidic STAT3 SH2 inhibitors as exemplified by the compounds 1-5 [23–27] in Fig. 1, which possess good cell permeability compared to peptidomimetic inhibitors, usually exhibit weak to moderate binding affinities to STAT3.

Recently, Wang and coworkers discovered a potent STAT3 degrader SD-36 (6) based upon the proteolysis targeting chimera (PROTAC) concept, by employing a ligand for cereblon/cullin 4A E3 ligase and a peptidomimetic STAT3 SH2 domain inhibitor [28,29]. The degrader SD-36 is capable of effectively and selectively degrading STAT3 protein and exhibits highly potent anticancer activities. However, developing selective and potent nonpeptidic STAT3 SH2 inhibitors which serve as the starting point for discovering STAT3 degraders, may provide more promising clinical candidates with desirable druglike properties.

In this context, we performed structure-based drug design approach to facilitate the discovery of highly potent and selective STAT3 small-molecule inhibitors. Two series of novel STAT3 small-molecule inhibitors were designed and synthesized with the privileged structures of 2-phenylquinoline and 2-arylimidazo[1,2-a] pyridine, respectively. Further optimization led to the identification of compound 39 as the most promising STAT3 small-molecule inhibitor. Our data demonstrated that compound 39 selectively bound to STAT3 SH2 domain, inhibited STAT3 activation and subsequent signaling pathway, and ultimately suppressed cell growth, migration and invasion of human cancer cell lines. Moreover,

compound 39 demonstrated significant and dose-dependent tumor growth inhibition in both cell line-derived and patient derived xenograft tumor models in mice.

2. Results and discussion

2-Phenylquinoline-based STAT3 inhibitor. Our drug discovery campaign initiated with two previously reported STAT3 inhibitors, **STX-119** [23] and **SH4-54** [25], both of which are selective STAT3 inhibitors and have similar binding mode with the SH2 domain revealed by molecular modeling. Analysis of the X-ray structure of STAT3 SH2 domain (PDB ID: 1BG1) [30] suggested that there are three important sub-pockets within the SH2 domain, including pY705 binding site, Leu706 binding site and a side pocket (Fig. 2A). The molecule docking of **STX-119** with STAT3 SH2 domain revealed that 2-phenylquinoline bound to the pY705 binding site alongside the side pocket, and 5-(furan-2-yl)-1,3,4-oxadiazol targeted to the Leu706 sub-pocket (Fig. 2B). Molecule modeling studies on **SH4-54** showed that the salicylic acid group and tosylamide moiety accessed to the pY705 sub-pocket and side pocket, respectively, and cyclohexylphenyl occupied to the Leu706 sub-pocket (Fig. 2C). While these two compounds display modest inhibitory activity against human cancer cell lines [23,25], the privileged structures embedded in them attracted our attentions, such as 2-phenylquinoline in **STX-119** and cyclohexylbenzene in **SH4-54**. 2-Phenylquinoline is a well-known privileged structure and has been found to be the core structure of many bioactive substances [31–35]. Cyclohexylbenzene is also claimed to be a privileged structure due to its common presence in various bioactive compounds [36–40]. Since cyclohexylphenyl of **SH4-54** was shown to occupy an essentially similar binding pocket as compared to 5-(furan-2-yl)-1,3,4-oxadiazol of **STX-119**, we surmised that fusing cyclohexylphenyl of **SH4-54** with 2-phenylquinoline of **STX-119** would result in identification of novel STAT3 inhibitors with privileged structures and improved potencies. It is important to note that C2-phenyl of **STX-119** bound to the side pocket (Fig. 2B), a specific site for STAT3 over other STAT members which provides structure basis for the high selectivity of **STX-119**. Novel inhibitors derive from 2-phenylquinoline may also display high selectivity for STAT3. Therefore, the initial series of compounds were designed by condensing 4-cyclohexylaniline or (4-cyclohexylphenyl)methanamine with 2-phenylquinoline-4-carboxylic acid and several hydrophilic groups were also incorporated into the C7-positon of quinoline core to modulate their physicochemical characteristics.

As an initial screening, the 10 hybrid compounds were evaluated for their cell growth inhibitory activities in the cell viability assays against cancer cell lines which express constitutively active STAT3,
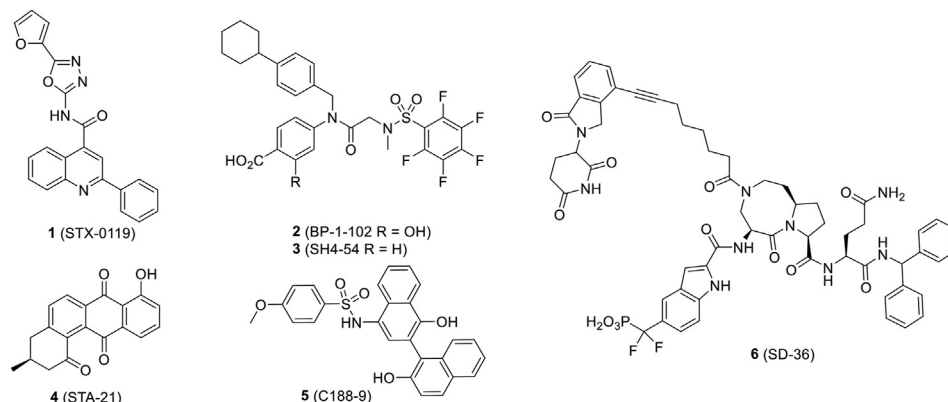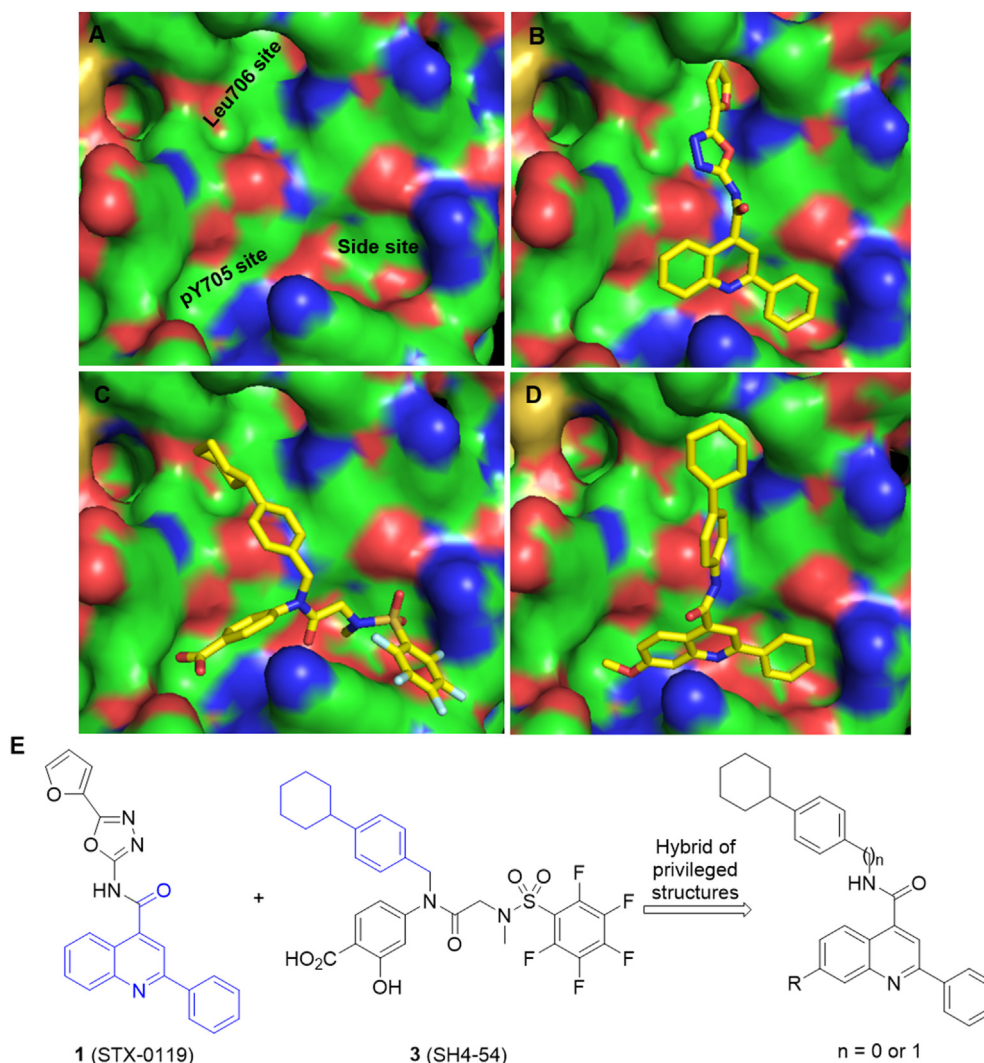

Fig. 1. Chemical structures of previously reported STAT3 inhibitors (1-5) and degrader (6).

Fig. 2. (A) Three pockets within STAT3 SH2 domain (PDB ID: 1BG1). (B) Binding mode of compound **1**. (C) Binding mode of compound **3**. (D) Binding mode of compound **8**. (E) Our design of new STAT3 inhibitors.

including MDA-MB-231 (breast cancer cell line), MGC-803 (gastric cancer cell line) and A549 (non-small cell lung cancer cell line). **SH4-54** and **STX-0119** were included as positive controls and the data are summarized in Table 1, which were comparable to the reported values. Compound **7** was obtained by fusing 4-cyclohexylaniline and 2-phenylquinoline-4-carboxylic acid together, and showed slightly decreased inhibitory activities with IC$_{50}$ values of 10 μM, 5.9 μM and 5.8 μM for MDA-MB-231, MGC-803 and A549, respectively. With the aim of improving the physicochemical characteristics of compound **7**, methoxy group was incorporated at the C7-postion of the quinoline ring and afforded compound **8**, which displayed enhanced potency with IC$_{50}$ values of 5.9 μM, 4.9 μM and 4.8 μM against the three tested cancer cells, respectively. However, incorporation of other hydrophilic groups, including hydroxy (**9**), 2-ethoxy-2-oxoethoxy (**10**) and carboxymethoxy (**11**), at the quinoline C7-postion of compound **7** was not well tolerated and led to completely abolished cell growth inhibitory activity. On the other hand, it seems that the design concept of condensation of (4-cyclohexylphenyl)methanamine with 2-phenylquinoline scaffold was unsuccessful, and the hybrid compounds **12**, **13**, **15** and **16** were found to be completely inactive with IC$_{50}$ values greater than 100 μM, even though hydroxy substituted quinoline derivative **14** displayed weak cancer cell growth

inhibition. It is interesting to note that the structural differences between **13** and **8** are the groups that were designed to access to the Leu706 pocket, 4-cyclohexylbenzylamine for **13** and 4-cyclohexylaniline for **8**. The huge difference in the cellular activity of **13** and **8** revealed that 4-cyclohexylphenylamines is preferred than 4-cyclohexylbenzylamine when 2-phenylquinoline is used as the core structure.

Upon the basis of its potent cell growth inhibitory activity and privileged chemical structure, compound **8** was selected as a starting point for further optimization. Before the next round of optimization, compound **8** was first docked to the three hot spots within the SH2 domain to determine whether it has the binding modes as we predicted. The docking result confirmed our proposal and demonstrated that cyclohexylphenyl fragment of compound **8** occupied to the Leu706 sub-pocket (Fig. 2D). Therefore, in an effort to explore the structure-activity relationship (SAR) on this position and to identify more potent STAT3 inhibitors, cyclohexyl of compound **8** was replaced by a diverse of groups, including halogen (**17-19**), alkyl (**20, 22, 23**), alkoxy (**21**), aryl (**24-28**) and heteroaryl (**29-33**).

As shown in Table 2, replacement of cyclohexyl group of compound **8** with halogen atoms led to compounds **17-19** with significantly decreased potency against the three test cancer lines.

Table 1
Antiproliferative activity of quinoline derivatives **7-16** against human cancer cell lines.[a]
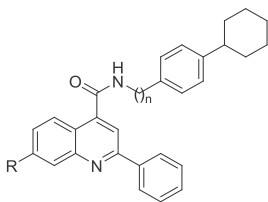
Compd	R	n	IC$_{50}$ (μM)		
			MDA-MB-231	MGC-803	A549
7	H	0	10.0 ± 2.03	5.9 ± 0.58	5.8 ± 0.72
8	OMe	0	5.9 ± 0.68	4.9 ± 0.69	4.9 ± 1.12
9	OH	0	>100	>100	>100
10	OCH$_2$CO$_2$Et	0	>100	>100	>100
11	OCH$_2$CO$_2$H	0	>100	>100	>100
12	H	1	>100	20.1 ± 3.21	>100
13	OMe	1	>100	>100	>100
14	OH	1	50 ± 5.16	14.6 ± 2.28	16.6 ± 1.15
15	OCH$_2$CO$_2$Et	1	>100	>100	>100
16	OCH$_2$CO$_2$H	1	>100	>100	>100
SH4-54			2.0 ± 0.24	5.6 ± 0.14	5.0 ± 0.15
STX-119			18.25 ± 3.09	7.43 ± 1.74	11.59 ± 3.09

[a] Data are calculated based on three independent experiments.

Compound **17** displayed very weak inhibitory activity with the IC$_{50}$ values ranging from 15.5 μM to 25.5 μM and compounds **18**, **19** were found to be completely inactive with IC$_{50}$ values greater than 50 μM. The similar tendency was also observed in the series of simple alkyl and alkoxy derivatives **20-23**, indicating that the size of the substitution has a significant effect on inhibitory potency. In the series of aryl substituted compounds **24-28**, significant discrepancy in the cellular inhibitory potency was observed. Interestingly, replacement of the cyclohexyl group of **8** with phenyl led to the compound **24**, which exhibited enhanced inhibitory effects with IC$_{50}$ values of 5.3 μM, 2.6 μM and 3.0 μM against the three tested cancer cells, respectively. In contrast, *para*-isopropylphenyl derivative **25** did not show any antiproliferative effects in the three type cancer cells. *Para*-fluorophenyl derivative **26** and *para*-methylthiophenyl derivative **28** displayed slight inhibitory activity against the proliferation of the three tested cancer cells. *Para*-methoxyphenyl derivative **27** exhibited moderate inhibitory activity against MGC-803 and A549 cells with the IC$_{50}$ values of 5.8 and 4.9 μM, respectively, but displayed much weaker activity against MDA-MB-231 cells with the IC$_{50}$ value greater than 20 μM. In addition to aryl group, compounds with various heteroaryl groups (**29-33**) were also examined. While thiophenyl (**29**), pyridinyl (**30**), and indolyl (**33**), decreased the inhibitory potency, furanyl derivative **31** showed more potent antiproliferative effects against MGC-803 cells with an IC$_{50}$ value of 2.1 μM when compared to **8**.

Compound **31** also retained the antiproliferative potency against A549 cells, but exhibited decreased inhibitory activity against the growth of MDA-MB-231 cells, with IC$_{50}$ values of 5.5 μM and 10.3 μM, respectively. Benzofuranyl derivative **32** showed antiproliferative activity comparable to compound **8** against the three tested cancer cell lines with the IC$_{50}$ values of around 5.0 μM. These results indicate that cyclohexyl group of compound **8** can also be replaced by phenyl, furanyl, or benzofuranyl.

Imidazo[1, 2-*a*]pyridine-based STAT3 inhibitor. In an effort to identify more potent STAT3 inhibitors with privileged structure, we turned our attention to optimize the 2-phenylquinoline moiety.

Table 2
Antiproliferative activity of quinoline derivatives **17-33** against human cancer cell lines.[a]
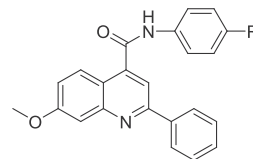
Compd	R	IC$_{50}$ (μM)		
		MDA-MB-231	MGC-803	A549
17	Br	25.5 ± 2.48	15.5 ± 2.15	21.4 ± 2.10
18	F	>100	>100	>100
19	Cl	>100	50.4 ± 4.71	>100
20	Me	>100	>100	>100
21	OMe	>100	>100	>100
22	*n*-Butyl	>100	39.6 ± 4.25	40.9 ± 6.68
23	*iso*-Propyl	>100	>100	>100
24	phenyl	5.3 ± 0.28	2.6 ± 0.90	3.0 ± 0.32
25	4-isopropylphenyl	>100	>100	>100
26	4-fluorophenyl	11.2 ± 2.66	40.4 ± 3.18	29.9 ± 4.16
27	4-methoxyphenyl	21.0 ± 4.32	5.8 ± 0.54	4.9 ± 0.43
28	4-methylthiophenyl	20.2 ± 2.24	15.6 ± 3.42	15.6 ± 4.14
29	thiophenyl	10.8 ± 1.46	15.0 ± 0.98	15.0 ± 2.13
30	pyridinyl	>100	64.8 ± 5.78	>100
31	furanyl	10.3 ± 1.26	2.1 ± 0.12	5.5 ± 0.57
32	benzofuranyl	5.3 ± 0.45	4.8 ± 0.84	4.3 ± 0.75
33	indolyl	>100	>100	>100
SH4-54		2.0 ± 0.24	5.6 ± 0.14	5.0 ± 0.15

[a] Data are calculated based on three independent experiments.

Further exploration the binding mode of compound **8** in a complex with the STAT3 SH2 domain suggested that the 2-phenylquinoline occupied both the Tyr705 and side pocket as we predicted (Fig. 2D). However, the C2-phenyl group of **8** just located on the threshold of the side pocket, not in the deep of the pocket mainly due to longer distance between C2-phenyl and C4-carbamoyl of quinoline than that between side pocket and Leu706 pocket. We surmised that shortening the distance between C2-phenyl and C4-carbamoyl may enhance the binding affinity with SH2 domain and translate to increased cell growth inhibitory activity. To test this hypothesis, compound **34** was designed and synthesized by replacing the 2-phenylquinoline with 2-phenylimidazo[1,2-*a*]pyridine, which is also defined as a privileged structure and represents one of the most important structural fragments for new drug discovery (Fig. 3) [41—45]. Unfortunately, compound **34** showed no inhibitory
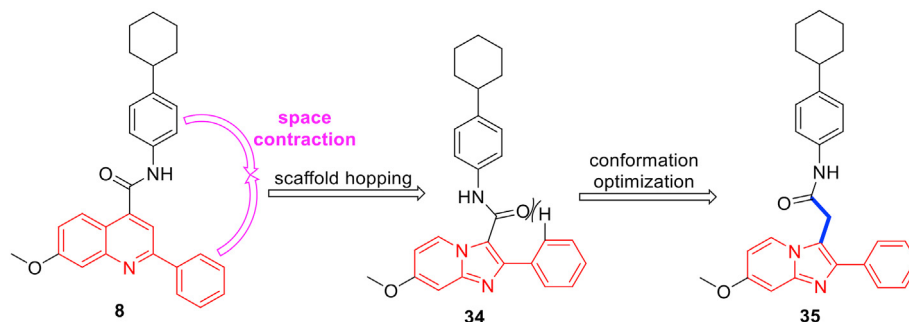
Fig. 3. Design of imidazo[1, 2-a]pyridine-based STAT3 inhibitor.

activity on cancer cell proliferation. We hypothesized that the abolished activity of compound **34** could be largely attributed to its torsion force derived from a repulsive interaction between the oxygen of C3- carbamoyl and the hydrogen at the C-2' position of C2-phenyl. To address this issue, compound **35** was prepared by adding a methylene linker between 3-carbamoyl and the imidazo [1,2-*a*]pyridine core structure with the aim of eliminating the torsion force of compound **34** (Fig. 3). To our delight, compound **35** recovered cancer cell growth inhibitory activity and exhibited comparable ability as compared to **8**. Next, a number of control compounds were designed and synthesized to test the essentiality of our new core structure. As showed in Table 3, both biphenyl derivative **36** and 4-(furan-2-yl)phenyl derivative **37** displayed similar tendency as in **24** and **31**. Furthermore, we replaced 4-cyclohexylphenyl of compound **35** with benzo[*b*]thiophene-1,1-dioxide, which is reported to be a pharmacophore model for the inhibition of STAT3 and predicted to bind to the SH2 domain [46—50]. Surprisingly, the desired compound **38** showed good inhibitory activity against the three test cancer cell lines with IC$_{50}$ values of 1.2 μM, 1.5 μM and 1.1 μM, respectively. In view of the

structural novelty and high potency, we selected compound **38** as our lead STAT3 inhibitor for further structural optimization.

First, we fixed the phenyl group at the C-2 position of imidazo [1,2-a]pyridine and then examined effect on the inhibitory potency with various substituents on the pyridine scaffold. As described in Table 4, removal of the C-7 methoxy in **38** afforded compound **39** exhibiting comparable antiproliferative activity with IC$_{50}$ values of around 1.0 μM. Replacement of C-7 methoxy with halogen atoms, such as chlorine (**40**) and bromine (**41**) was tolerated, especially for **41** displaying submicromolar inhibitory activity against the three cancer cell lines. The C-7 methyl derivative **42** also showed good activity. Moving the methoxy from C7 position to C8 (**43**) and C6 (**44**) position of imidazo[1,2-a]pyridine led to slightly decreased inhibitory activity as compared to **38**. Installation of the bromo group at the C-6 position of imidazo[1,2-a]pyridine afforded **45** displaying less potent anticancer activity against MDA-MB-231 and MGC-803 cells than **41**, but retaining potency against A549 cells. These results implied that the C-7 position of imidazo[1,2-a]pyridine may be a favorable spot for further optimization. Therefore, larger groups such as aryl or heteroaryl group were included in compounds **46**-**48**, and significant discrepancy in cell growth inhibitory activity was observed. For instance, C7-phenyl derivative **46** showed slightly weaker activity than **38**. In contrast, C7-*para*-methoxyphenyl derivative **47** recovered the potency against the three test cancer cell lines. Surprisingly, pyrazol derivative **48** also displayed good potency with submicromolar inhibitory activity against MGC-803 and A549 cells.

Afterwards, with imidazo[1,2-a]pyridine core structure substituted with C7 methoxy group, we explored the effect of various substitutions of the C2 phenyl ring in compound **38** on inhibitory activity. The para-substituted phenyl derivatives (**49**-**52**) were firstly explored. The fluoro derivative **49** exhibited good inhibitory activity against MGC-803 cells and A549 cells, but showed a decreased potency against MDA-MB-231 cells with an IC$_{50}$ value greater than 5 μM. However, compound **50** bearing a trifluoromethyl demonstrated significantly increased potency against the three tested cancer cells with IC$_{50}$ values of 0.7 μM, 0.4 μM and 0.4 μM, respectively, which is the most active compound in this study, probably due to the strong hydrophobic nature of the trifluoromethyl group. To test this hypothesis, we investigated the antiproliferative effects of low hydrophobic or high hydrophilic groups, such as nitro (**51**) and methylsulfonyl (**52**). Nitro derivative **51** demonstrated weaker inhibitory activity than **38**. The high hydrophilic methylsulfonyl substituted **53** showed significantly reduced anticancer activity against all tested cancer cells with IC$_{50}$ values greater than 5 μM. Next, replacement of C-2 phenyl with thiophenyl (**53**) and naphthalenyl (**54**) were also investigated, and it was revealed that both compounds showed good antiproliferation activity with IC$_{50}$ values of around 1.0 μM. In addition, compounds **55**-**57** were also designed with a core structure of C6-

Table 3
Antiproliferative activity of imidazo[1, 2-a]pyridine derivatives **34**-**38** against human cancer cell lines.[a]
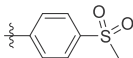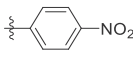

Compd	N	R	IC$_{50}$ (μM)		
			MDA-MB-231	MGC-803	A549
34	0		>100	>100	>100
35	1		5.4 ± 0.45	4.7 ± 0.32	5.6 ± 0.51
36	1		10.5 ± 1.21	3.5 ± 0.23	3.2 ± 0.24
37	1		10 ± 0.87	2.5 ± 0.35	6.6 ± 0.54
38	1		1.2 ± 0.29	1.0 ± 0.17	0.6 ± 0.14
SH4-54			2.0 ± 0.24	5.6 ± 0.14	5.0 ± 0.15

[a] Data are calculated based on three independent experiments.

Table 4
Antiproliferative activity of imidazo[1, 2-a]pyridine derivative **38-61** against human cancer cell lines.[a]
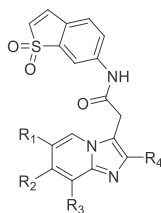
Compd	R$_1$	R$_2$	R$_3$	R$_4$	IC$_{50}$ (μM)		
					MDA-MB-231	MGC-803	A549
38	H	OMe	H		1.2 ± 0.29	1.0 ± 0.17	0.6 ± 0.14
39	H	H	H		1.2 ± 0.13	1.6 ± 0.06	1.1 ± 0.11
40	H	Cl	H		1.1 ± 0.08	1.3 ± 0.13	0.7 ± 0.05
41	H	Br	H		0.9 ± 0.12	0.9 ± 0.07	0.8 ± 0.06
42	H	Me	H		1.6 ± 0.12	1.0 ± 0.06	0.7 ± 0.07
43	H	H	OMe		2.2 ± 0.17	1.7 ± 0.22	1.0 ± 0.05
44	OMe	H	H		2.1 ± 0.13	1.7 ± 0.15	1.2 ± 0.08
45	Br	H	H		2.0 ± 0.42	1.5 ± 0.24	0.8 ± 0.06
46	H		H		2.4 ± 0.34	1.7 ± 0.26	1.1 ± 0.06
47	H		H		1.0 ± 0.04	0.5 ± 0.09	0.7 ± 0.11
48	H		H		1.4 ± 0.07	0.7 ± 0.07	0.8 ± 0.08
49	H	OMe	H		5.1 ± 0.56	0.9 ± 0.06	1.3 ± 0.16
50	H	OMe	H		0.7 ± 0.11	0.4 ± 0.12	0.4 ± 0.10
51	H	OMe	H		4.4 ± 0.32	2.6 ± 0.14	1.7 ± 0.11
52	H	OMe	H		5.8 ± 0.78	6.4 ± 0.34	5.8 ± 0.48
53	H	OMe	H		1.4 ± 0.04	1.3 ± 0.05	1.1 ± 0.06
54	H	OMe	H		1.4 ± 0.05	1.5 ± 0.24	1.0 ± 0.15
55	Me	H	H		2.1 ± 0.45	1.8 ± 0.22	0.9 ± 0.05
56	Me	H	H		2.0 ± 0.15	2.4 ± 0.15	2.5 ± 0.07
57	Me	H	H		2.0 ± 0.06	1.6 ± 0.08	1.2 ± 0.06
58	H	H	H		4.1 ± 0.25	2.7 ± 0.10	5.5 ± 0.23

Table 4 (*continued*)

Compd	R₁	R₂	R₃	R₄	IC₅₀ (μM)		
					MDA-MB-231	MGC-803	A549
59	H	H	H	⟨benzene–SO₂CH₃⟩	6.4 ± 0.32	6.9 ± 0.42	7.5 ± 1.12
60	H	H	H	⟨benzene–NO₂⟩	6.5 ± 0.83	5.2 ± 0.36	5.4 ± 0.87
61	H	H	H	H	20.2 ± 2.3	22.5 ± 1.21	23.4 ± 2.28

[a] Data are calculated based on three independent experiments.

methylated imidazo[1,2-a]pyridine, a privileged structure derived from the drug Zolpidem.[51] The three compounds demonstrated moderate to high cell growth inhibitory activity against the tested three cancer cell lines with IC₅₀ values ranging from 0.9 μM to 2.5 μM. Removing C6-methyl from compound **55** afforded compound **58**, resulting in less potent activity. Methylsulfonyl **59** and nitro **60** exhibited similar tendency as in compounds **52** and **51**. However, it should be noted that removal of C-2 phenyl group from imidazo[1,2-a]pyridine was not tolerated and led to dramatically decreased potency with IC₅₀ values greater than 20 μM for compound **61** as compared to compound **39**.

***In vitro* metabolic stability assessment**. Based on the antiproliferative activity mentioned above as well as the solubility observed in the preparation, compound **38**, **39** and **50** were selected out for *in vitro* metabolic stability study in human liver microsome (HLM). As shown in Table 5, compound **38** and **50** exhibited poor stability in HLM with the $T_{1/2}$ of 10.1 min and 4.4 min, respectively, while compound **39** offered an improved microsomal stability in HLM with the $T_{1/2}$ of 24.2 min. Taken together, compound **39** showed the best combination of microsomal stability and cell growth inhibitory potency, and was selected for further evaluation.

Compound 39 directly bound to STAT3 protein. To confirm a direct interaction between compound **39** and STAT3, a surface plasmon resonance (SPR) assay was performed, for which purified STAT3 was immobilized on CM5 sensor chips. As shown in Fig. 4, compound **39** exhibited high binding affinity with STAT3 with an equilibrium dissociation constant (K_D) value of 0.432 μM, indicating that compound **39** directly binds to the STAT3 protein and might therefore block its activation via inhibition of STAT3 phosphorylation at Tyr705.

Compound 39 selectively inhibited STAT3 Tyr705 phosphorylation. To evaluate the effect of compound **39** on inhibiting phosphorylation of STAT3, we performed western blotting assays to detect the protein levels of phosphorylated STAT3 (pSTAT3) and total STAT3 in triple negative breast cancer (TNBC) cell lines with constitutively activated STAT3, including MDA-MB-231, MDA-MB-468, HCC70 and MDA-MB231-4175. Western blotting assays showed that compound **39** inhibited STAT3 phosphorylation at Tyr705 in a dose-dependent manner in these four cell lines, but had no effect on the total STAT3 (Fig. 5A), indicating that the reduced pSTAT3 levels did not dependent on the total level of STAT3 protein. In addition, we also evaluated the ability of compound **39** to inhibit

STAT3 phosphorylation at Ser727, which also contributes to the transcriptional activity of STAT3. It was revealed that compound **39** slightly suppressed phosphorylation of Ser727 compared to Tyr705 in MDA-MB-231 and MDA-MB-231-4175 cells at 3 μM, and did not inhibit Ser727 phosphorylation in MDA-MB-468 and HCC cells at 3 μM. These results suggest that compound **39** mainly binds to STAT3 SH2 domain as we designed.

To address the selectivity of compound **39** among STAT isoforms, we further investigated the effects of compound **39** on phosphorylation of STAT1 and STAT5. As shown in Fig. 5B, compound **39** did not affect the total or phosphorylated levels of STAT1 and STAT5 in MDA-MB-231 and HCC cells even at the concentration of 3 μM, indicating that compound **39** selectively inhibits STAT3 over STAT1 and STAT5.

Compound 39 significantly inhibited STAT3 dimerization. Activated STAT3 proteins form a homodimer via reciprocal interaction between pY705 within one monomer and the SH2 domian of the other. To validate whether compound **39** disrupts STAT3 dimerization, HEK-293T cells were transfected with Flag-tagged STAT3 and HA-tagged STAT3 for co-localization and co-immunoprecipitation studies. HEK-293T cells that stably co-express HA-STAT3 and Flag-STAT3 were treated with compound **39** and DMSO as the solvent control. Then the cells were processed for immunofluorescence staining for Flag-STAT3 (red) and HA-STAT3 (green) and analyzed by confocal microscopy. As shown in Fig. 6A, the co-location (yellow) of HA-STAT3 and Flag-STAT3 was significantly reduced by compound **39** in a dose-dependent manner, suggesting that dimerization of HA-STAT3 and Flag-STAT3 was disrupted.

Next, we treated the HEK-293T cells with compound **39** for immunoprecipitation analysis and revealed that compound **39** dose-dependently inhibited dimerization of HA-STAT3 and Flag-STAT3 after IL-6 stimulation (Fig. 6B). These results further validate that compound **39** binds to the STAT3-SH2 domain and inhibits STAT3 dimerization in intact cells.
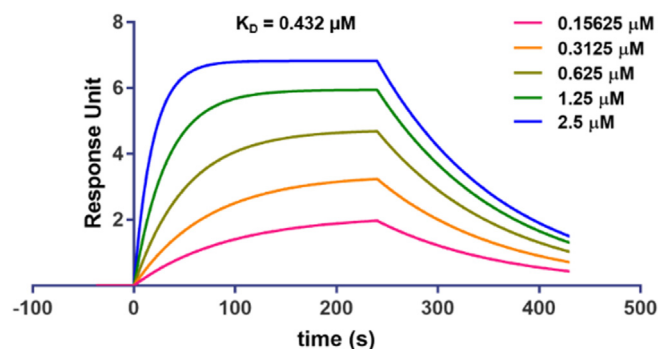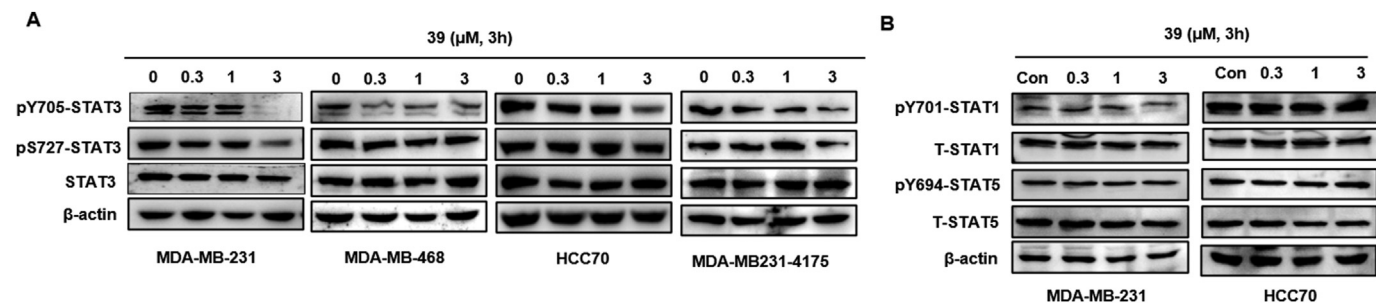
Table 5
In vitro metabolic stability in human liver microsomes.

	HLM	
Compd	clearance (mL/min/g)	$T_{1/2}$ (min)
38	208.4	10.1
39	87.0	24.2
50	478.0	4.4

Fig. 4. SPR analysis of compound **39** binding to STAT3 protein. Representative data from three independent experiments are shown.

Fig. 5. Effects of compound **39** on phosphorylation of STAT3 (A), STAT1 and STAT5 (B) analyzed by western blotting. Representative images from three independent experiments are shown.
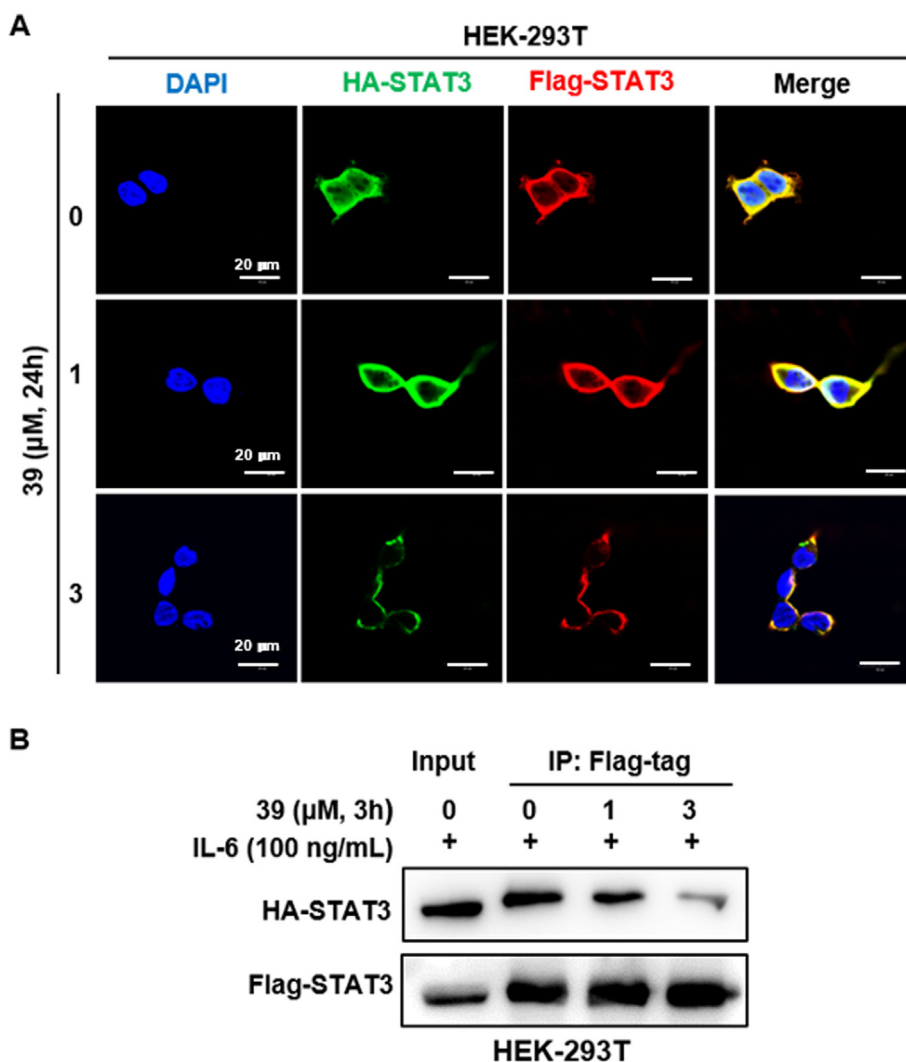

Fig. 6. Effects of compound **39** on STAT3 dimerization. (A) colocalization study of compound **39** in HEK-293T cells with HA-STAT3 (green) and FLAG-STAT3 (red). DAPI nuclear was stained in blue. (B) Coimmunoprecipitation assay of compound **39** in HEK-293T cells. Representative images from three independent experiments are shown.

Compound 39 inhibited nuclear translocation of pY705-STAT3. To demonstrate whether compound **39** would inhibit the nuclear translocation of pY705-STAT3, MDA-MB-231 breast cancer cells, which contain constitutively activated STAT3, were treated with either vehicle or compound **39** for 12 h and then were subjected to immunofluorescence staining by a specific p-STAT3 primary antibody and Alexa Fluor secondary antibody. It was revealed that pY705-STAT3 was localized predominantly in the nucleus in

the absence of compound **39** (Fig. 7). In contrast, compound **39** treatment inhibited the translocation of pY705-STAT3 to the nucleus in a dose-dependent manner.

Compound 39 inhibited STAT3 DNA-binding and STAT3-dependent transcriptional activation. After translocation from the cytoplasm to the nucleus, STAT3 dimers bind to STAT3-specific DNA-response elements and activate their transcriptional activity. Therefore, we next evaluated the effects of compound **39** on DNA-
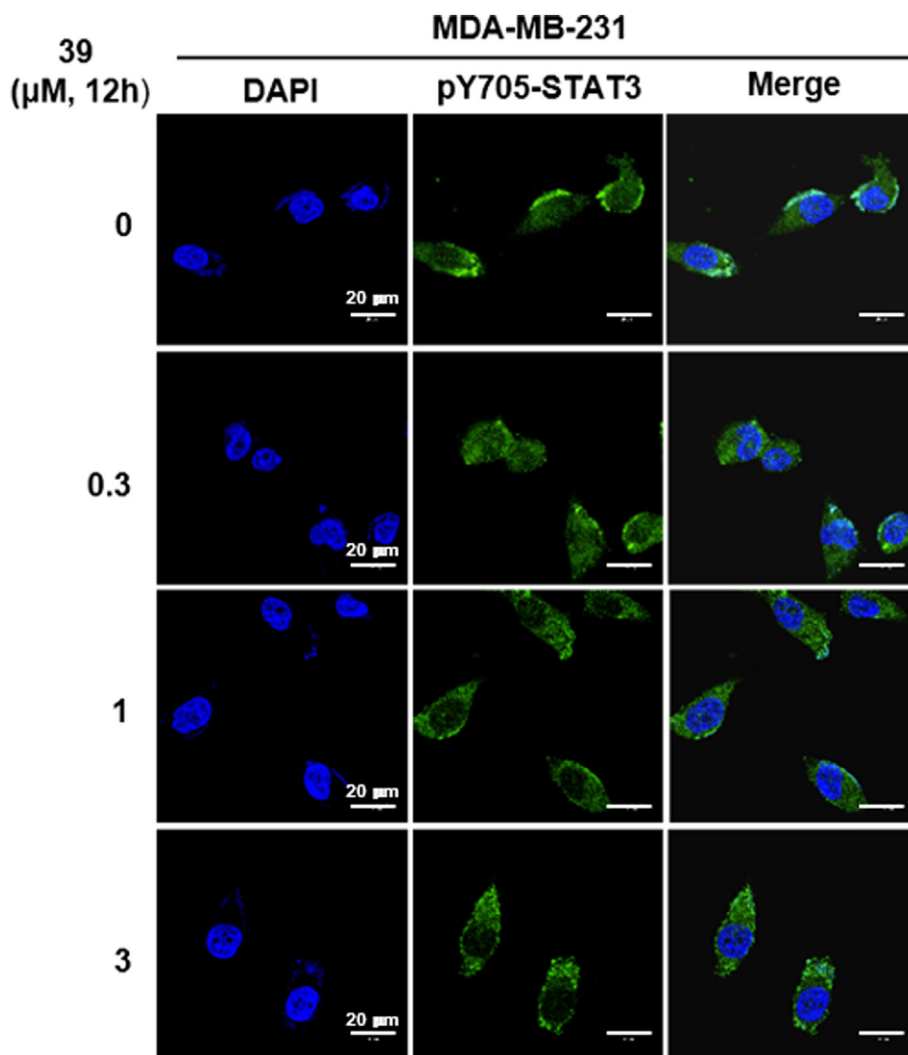
Fig. 7. Effects of compound **39** on nuclear translocation of phosphorylated STAT3 in MDA-MB-231 cell line. Representative images from three independent experiments are shown.
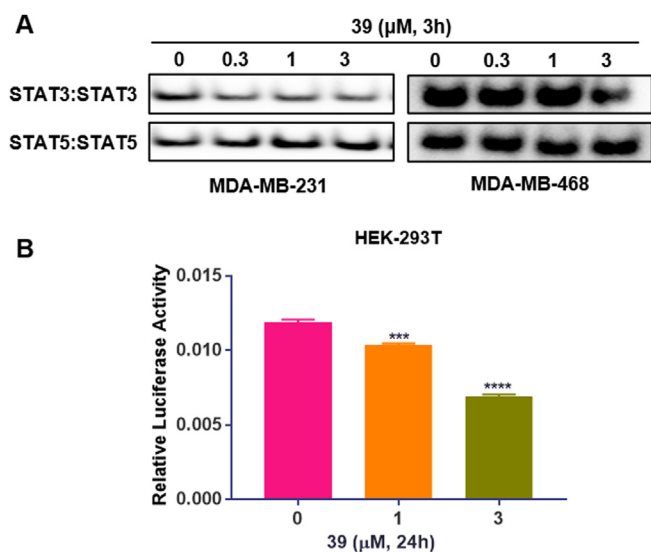
binding ability and transcriptional activation of STAT3. Electrophoretic mobility shift assay (EMSA) was first performed to assess whether compound **39** blocks STAT3 DNA-binding activity. As shown in Fig. 8A, compound **39** remarkably decreased the DNA-binding of STAT3 in MDA-MB-231 and MDA-MB-468 cells at the concentrations of 0.3 μM and 1 μM, respectively. However, the DNA-binding of STAT5 was not affected even at 3 μM. This suggests the preferential potential of compound **39** to inhibit DNA-binding ability of STAT3 over STAT5 in cancer cells.

We next investigated whether STAT3-dependent transcriptional activation was disrupted by compound **39** using a luciferase reporter assay. HEK-293T cells were transiently co-transfected with pGL3-STAT3 (a STAT3-responsive promoter-firefly luciferase reporter) and renilla reporter (as normalization control) to act as gene reporter model to examine the effect of compound **39** on STAT3-dependent transcriptional activation. Compared to the control group, the cells treated with 1 or 3 μM compound **39** for 24 h had lower luciferase activity (Fig. 8B), indicating that compound **39** inhibits STAT3-dependent transcriptional activity.

Compound 39 downregulated the expression of STAT3 target genes. In an effort to further provide evidence that compound **39** inhibits STAT3-dependent transcriptional activity, we evaluated the effect of compound **39** on regulating the expression of STAT3 target genes. TNBC cell lines, including MDA-MB-231, MDA-MB-468, HCC70 and MDA-MB-231-4175, were treated with compound **39** for 24 h, and then were processed for western blotting. Fig. 9 shows that compound **39** downregulated the expression of STAT3 target genes, including Bcl-xL, c-Myc and Mcl-1.

Compound 39 inhibited cancer cell proliferation and colony formation. To further evaluate the antiproliferative activities of compound **39** in cell models, its effects on TNBC cancer cell growth and colony survival were evaluated. MDA-MB-231-4175, MDA-MB-468 and HCC70 containing hyperactivated STAT3 were treated with various concentrations of compound **39** for 72 h, and subsequently examined by Cell Counting Kit-8. As shown in Fig. 10A, compound **39** concentration-dependently reduced the proliferation of MDA-MB-231-4175, HCC70, and MDA-MB-468 cells with the IC_{50} values of 2.5 μM, 1.1 μM and 2.5 μM, respectively. Interestingly, **39** showed much weaker growth inhibition in MCF-7 (breast cancer cells without persistent activated STAT3) and normal cells (H9C2: cardiomyocyte) with IC_{50} values of 7.22 μM and 6.79 μM, respectively, indicating its selectivity for STAT3 persistently activated cancer cell lines. Furthermore, compound **39** also significantly suppressed the colony formation of MDA-MB-231, MDA-MB-468, MDA-MB-231-4175 (Fig. 10B) and HCC70 (Figure S1) at as low as 0.3 μM concentration.

A

B

Fig. 8. Effects of compound **39** on STAT3 DNA-binding and STAT3-dependent transcriptional activation. (A) EMSA analysis of STAT3 or STAT5 DNA-binding activity in nuclear extracts prepared from MDA-MB-231 and MDA-MB-468 cells after treatment of compound **39**. (B) Luciferase reporter assay of compound **39** in HEK-293T cells. Representative images from three independent experiments are shown. (***) p < 0.001; (****) p < 0.0001.

To further demonstrate the specificity of compound **39** on STAT3 signaling pathway in MDA-MB-231 cells, endogenous STAT3 was knocked down using siRNA. As shown in Figure S2A, STAT3 was successfully knocked down by siSTAT3. Cell viability test (Figure S2B and Figure S2C) revealed that STAT3 siRNA treatment of MDA-MB-231 led to loss of sensitivity to inhibition of **39**, indicating that STAT3 is required for anticancer activity of compound **39**.
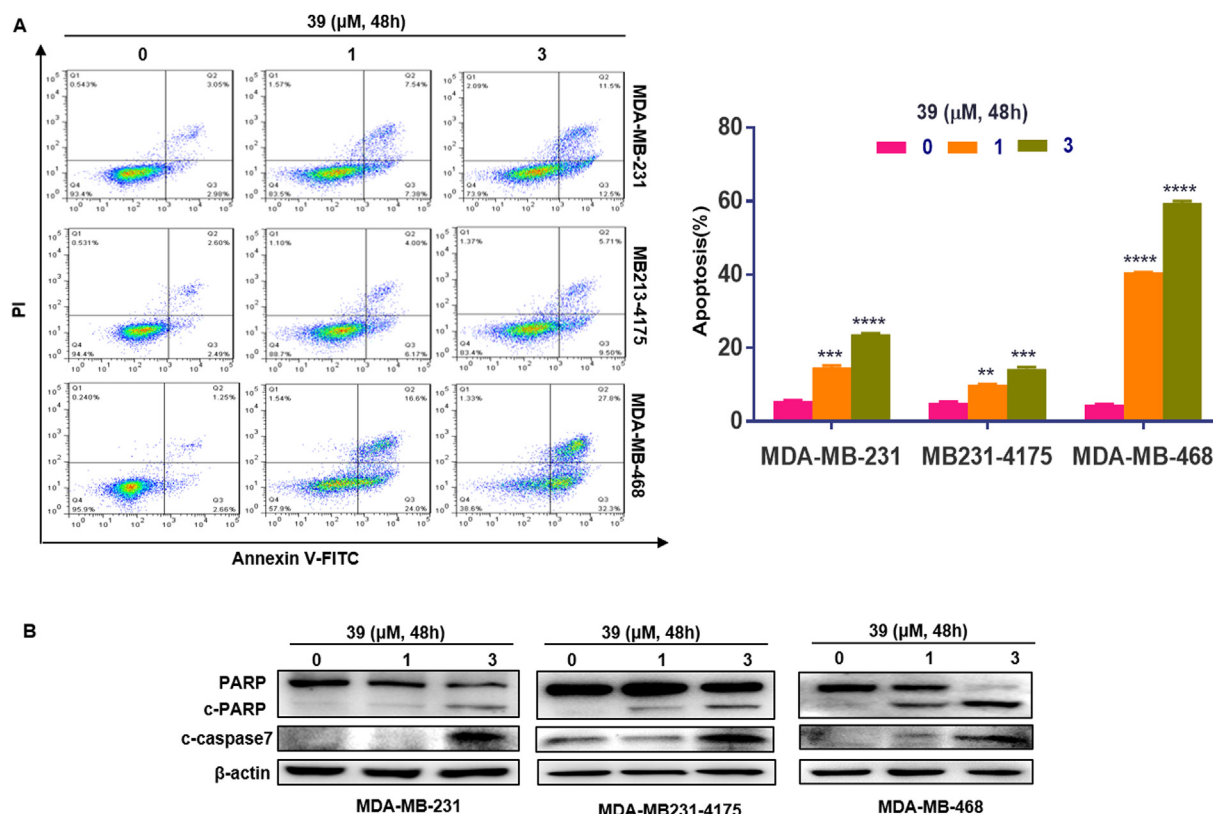
Compound 39 induced apoptosis in TNBC cancer cells. To assess whether the proliferative inhibition induced by compound **39** in cancer cells was attributed to apoptosis [51–55], TNBC cells were incubated with compound **39** at different concentrations for 48 h. Annexin V-FITC/propidium iodide (PI) staining was performed and the percentages of apoptotic cells were determined by flow cytometry. As shown in Fig. 11A, compound **39** induced apoptosis in MDA-MB-231, MDA-MB-231-4175 and MDA-MB-468 cells in a dose-dependent manner with the apoptotic percentages of 14.6%, 10.0% and 40.6% at 3 μM, respectively. To further elucidate the potential mechanisms of apoptosis induced by compound **39**, several proteins as markers of apoptosis were determined by western blotting. As shown in Fig. 11B, cleavage of PARP and caspase 7 was induced after treatment of compound **39** at 1 μM in MDA-MB-231-4175 and MDA-MB-468 cells and at 3 μM in MDA-MB-231 cells, suggesting that compound **39** induces the apoptosis in TNBC cells at least partially through increasing the expression of cleaved-PARP and cleaved-caspase7.
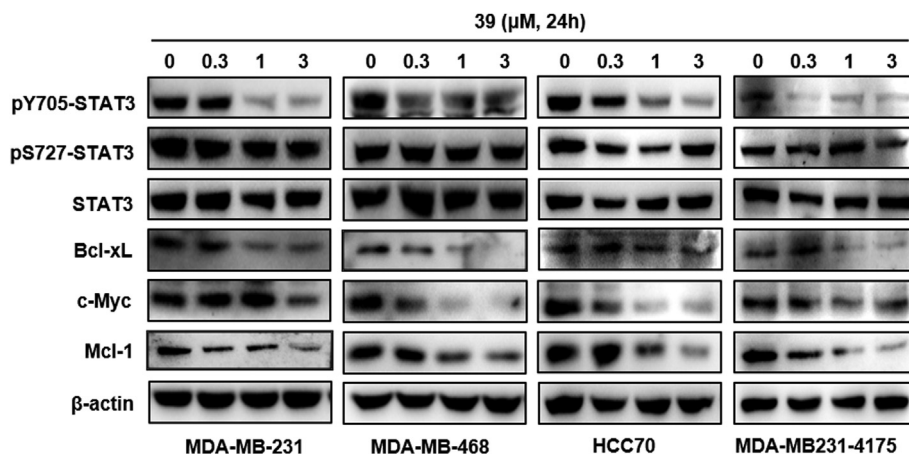
Fig. 9. Western blotting analysis was used to examine the phosphorylation of STAT3 and expression of STAT3-regulated genes in TNBC cells treated with different doses of compound **39** for 24 h. Representative data from three independent experiments are shown.
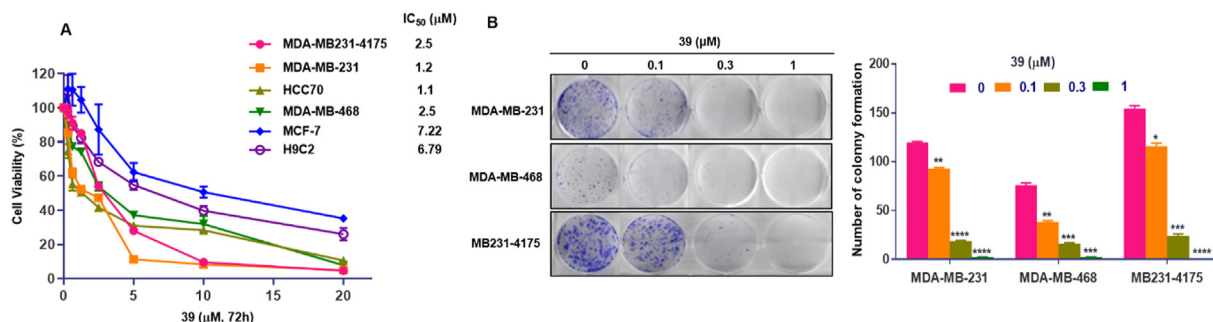
Fig. 10. Effects of compound **39** on proliferation and colony formation of TNBC cells. (A) Cell viability of cancer cell lines treated with compound **39** using the MTT assay. (B) Inhibitory effects of compound **39** on colony formation of TNBC cells. Representative data from three independent experiments are shown. (*) p < 0.05; (**) p < 0.01; (***) p < 0.001; (****) p < 0.0001.

Fig. 11. Effects of compound **39** on inducing apoptosis and cleavage of PARP and caspase 7 in breast cancer cells. (A) Apoptosis induced by compound **39** at different concentrations was examined by a annexin V-FITC/PI-staining based flow cytometry. (**) $p < 0.01$; (***) $p < 0.001$; (****) $p < 0.0001$. (B) Western blot analysis of the effect of compound **39** on cleaved- PARP and cleaved-caspase7. β-Action was used as the loading control. Representative data from three independent experiments are shown.

Compound 39 inhibited cancer cell migration and invasion. Constitutively activated STAT3 is also reported to be correlated with cancer cell migration and invasion, which contribute to cancer metastasis and lead to poor patient survival. Therefore, compound **39** was also investigated for its effects on cancer cell migration and invasion in wound healing and transwell assays. In the wound healing assay, MDA-MB-231, MDA-MB-468, MDA-MB-231-4175 and HCC70 cells were treated with compound **39** at the indicated concentrations for 12−96 h. As shown in Fig. 12A, the cells migrated to fill the scratched area in the absence of compound **39**, whereas compound **39** treatment prevented this migration dose-dependently. Next, the ability of compound **39** to inhibit invasion was evaluated in transwell assay. As shown in Fig. 12 B, compound **39** inhibited invasion in MDA-MB-231, MDA-MB-231-4175, HCC70 and MDA-MB-468 cells in a dose-dependent manner. Together, these results imply that compound **39** inhibits migration and invasion of cancer cells *in vitro*.

***In vivo* Pharmacokinetic Properties of compound 39**. As compound **39** exhibited high potency *in vitro*, the pharmacokinetic (PK) profiles were next evaluated in male SD rats after oral administration at 10 mg/kg (Table 6). Compound **39** exhibited a quick oral absorption ($T_{max} = 1.67$ h) with short half-life ($T_{1/2} = 1.67$ h). The maximum plasma concentration (C_{max}) was determined to be 23.8 ng/mL and small area under the curve (AUC) values were also observed.

Compound 39 exhibited antitumor activity *in vivo*. Upon the basis of the promising *in vitro* profile of the STAT3 inhibitor compound **39**, we then evaluated its anticancer efficacy *in vivo*. First, the *in vivo* antitumor effect of compound **39** was performed in the MDA-MB-231-4175 xenograft model in mice via intraperitoneal injection every day for 20 consecutive days. As shown in Fig. 13,

compound **39** inhibited tumor growth in a dose-dependent manner as measured by tumor volume (Fig. 13A) and weight (Fig. 13C), with tumor growth inhibition (TGI) of 20.1% at 5 mg/kg and 40.2% at 15 mg/kg. Meanwhile, compound **39** was found to be well tolerated and showed no apparent body weight loss during the treatment (Fig. 13B). Compound **39** was also evaluated for its effects on the tumor mitotic index (Ki67) and the STAT3 signaling in MDA-MB-231-4175 tumor tissues by immunohistochemistry analysis and western blotting. It was revealed that the expression of Ki67 was significantly reduced in compound **39**-treated groups compared to control group (Fig. 13D), suggesting that the number of the proliferating tumor cells was significantly decreased and tumor progression was slowed down in the mice after treatment of compound **39**. Afterwards, the expression of pY705-STAT3, STAT3, Bcl-xL and Mcl-1 in the tumor tissue was examined by western blotting. Compound **39** apparently reduced the level of pY705-STAT3 and subsequently downregulated the expression of STAT3 target genes Bcl-xL and Mcl-1 as shown in Fig. 13E. It is also noteworthy that no morphological change was observed in heart, liver, spleen, lung and kidney tissues for compound **39** treatment groups in HE staining (Fig. 13F). These results suggested that compound **39** inhibits the growth of MDA-MB-231-4175 xenograft tumor *in vivo* through inhibiting the STAT3 signaling pathway and shows no obvious toxicity.

Next, the antitumor efficacy of compound **39** was assessed in TNBC patient-derived xenograft (PDX) model in mice. The PDX model was performed in NOD/SCID mice and the mice were treated with compound **39** via intraperitoneal administration for 20 days with 5 mg/kg or 15 mg/kg per day. As shown in Fig. 14, compound **39** exhibited enhanced antitumor effects in the PDX model compared to that in the MDA-MB-231-4175 xenograft model
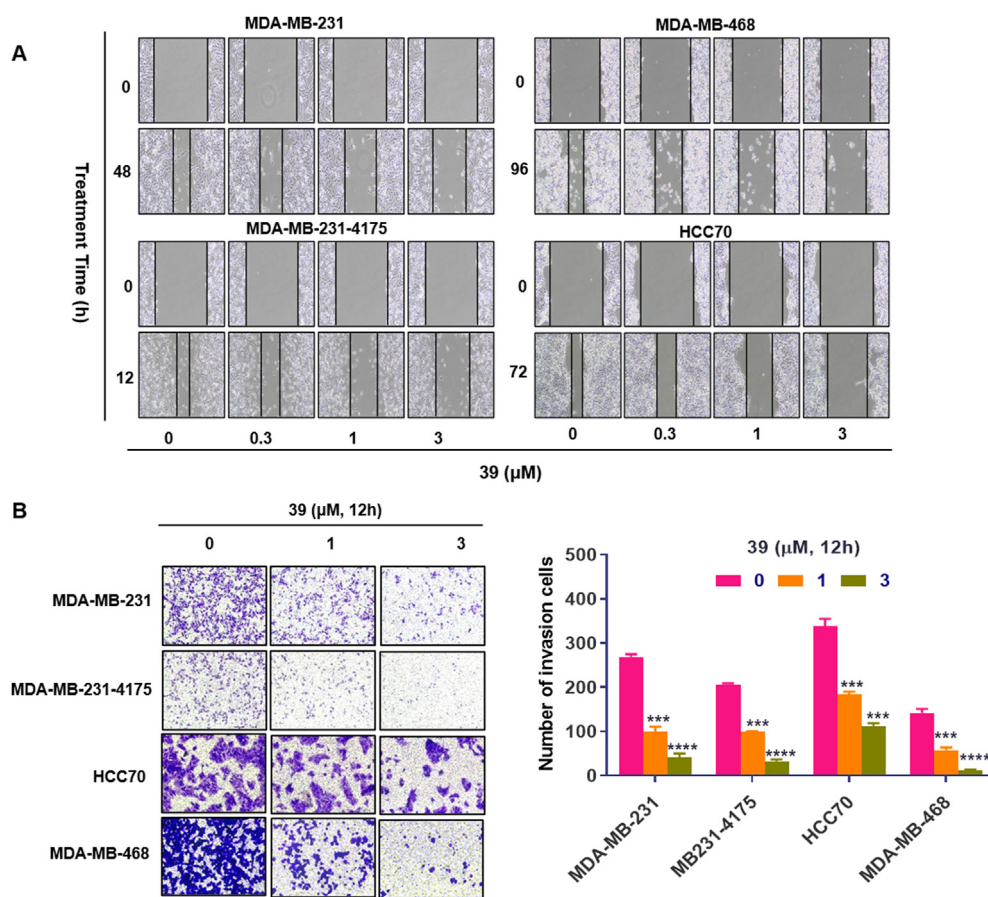
Fig. 12. Effects of compound **39** on cell migration and invasion. (A) Inhibition of cell migration by compound **39** in wound healing assay. (B) Inhibition of cell invasion by compound **39** in transwell assays. Representative images from three independent experiments are shown. (***) P < 0.001, (****) p < 0.0001.

Table 6
In vivo PK Parameters for compound 39.[a]

$T_{1/2}$ (h)	T_{max} (h)	C_{max} (ng/mL)	AUC_{0-last} (h*ng/mL)	AUC_{0-inf} (h*ng/mL)
1.46	1.67	23.8	54.6	56.1

[a] Values are the average of three runs. Vehicle: DMSO/0.5% HPMC (5/95, v/v/). $T_{1/2}$, half-life; T_{max}, time of maximum concentration; C_{max}, maximum concentration; AUC, area under the plasma concentration-time curve.

(Fig. 14A and C), with TGI of 32.7% at 5 mg/kg and 68.9% at 15 mg/kg. The expression of Ki67 in the tumor tissues was also decreased in the compound **39** treatment groups in immunohistochemistry assay (Fig. 14D), which is similar to that in MDA-MB-231-4175 xenograft mice model. The immunoblotting results showed that compound **39** reduced the level of pY705-STAT3 and STAT3 target genes including Bcl-xL and Mcl-1 (Fig. 14E), while HE staining analysis displayed that no morphological change was observed in heart, liver, spleen, lung and kidney tissues in compound **39** treatment groups (Fig. 14F). Moreover, no apparent body weight loss (Fig. 14B) or other obvious signs of toxicity, such as loss of appetite, decreased activity, or lethargy were observed during the studies. Taken together, compound **39** inhibited STAT3 signaling and tumor growth in animal studies with no obvious toxicity *in vivo*.

To compare the *in vivo* antitumor efficacy between compound **39** and the positive controls, **SH4-54** and **STX-119**, we further evaluated these three compounds in TNBC PDX model in mice for 20 days at 15 mg/kg per day via intraperitoneal administration. As

shown in Figure S3, compound **39** exhibited more potent *in vivo* efficacy than **STX-119** and **SH4-54** (Figure S3A, B, C) with TGI of 85.1%, 63.6% and 414.8%, respectively. No apparent body weight loss (Figure S3D) was observed during the studies. Moreover, Compound **39** also showed more potent activity in reduction of the level of pY705-STAT3 and subsequent downregulation of the expression of STAT3 target genes c-Myc and Bcl-xL as shown in Figure S3E.

2.1. Chemistry

As shown in Scheme 1, condensation of acids **62a-c** with 4-cyclohexylaniline **63a** or (4-cyclohexylphenyl)methanamine **63b** afforded amides **7-9** and **12-14**. Among them, hydroxyl **9** and **14** were alkylated with ethyl 2-bromoacetate to provide **10** and **15**, followed by hydrolysis under alkaline condition to give carboxylic acid **11** and **16**.

As illustrated in Scheme 2, acid **62b** was condensed with substituted amines **64a-q** to afford amides **17-27**. On the other hand, amide **17** underwent Suzuki−Miyaura coupling reaction with suitable arylboronic acids to give amides **28-33**.

As shown in Scheme 3, 2-aminepyridine **65** was condensed with ketone **66** to yield ester **67**, which was then hydrolyzed to acid **68**. Acid **68** was coupled with aniline **63a** to provide amide **34**.

Imidazo[1,2-a]pyridine **69** was alkylated with ethyl diazoacetate in the presence of a Rh(II) catalyst to give ester **70** as we reported previously [56], which was then subjected to hydrolysis and condensation with various amine to afford amides **35-38** (Scheme 4).
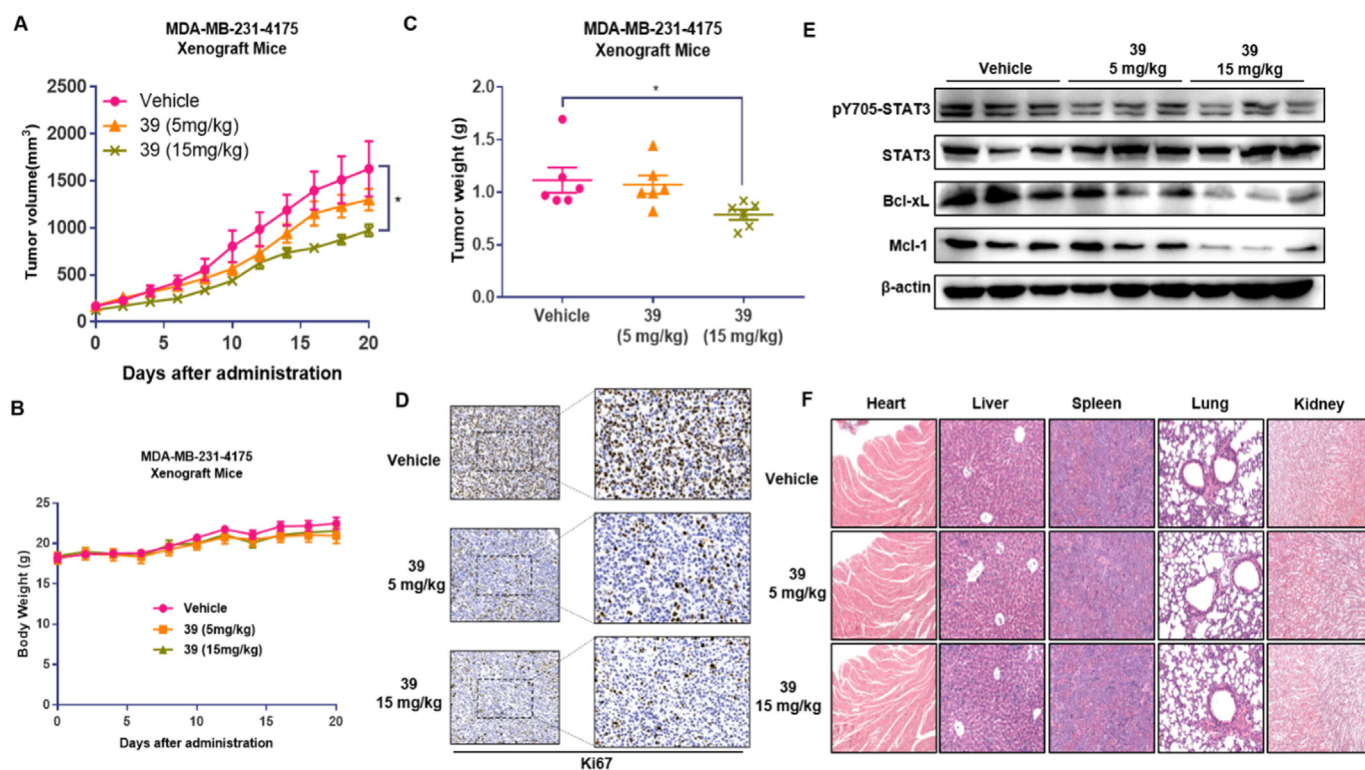
Fig. 13. Antitumor activity of compound **39** in MDA-MB–231-4175 xenograft model in mice. Tumor volume (A), body weight (B), and tumor weight (C) of the mice with the indicated treatment of compound **39**. (D) Tumor proliferation biomarker Ki67 detection of tumor tissues by immunohistochemistry after treatment with compound **39**. (E) pY705-STAT3, STAT3, Bcl-xL and Mcl-1 immunoblot in tumor tissue lysates. (F) Morphological images of heart, liver, spleen, lung and kidney tissues from treated mice. Values, mean $\pm$ SEM, n = 6. (*) P < 0.05.
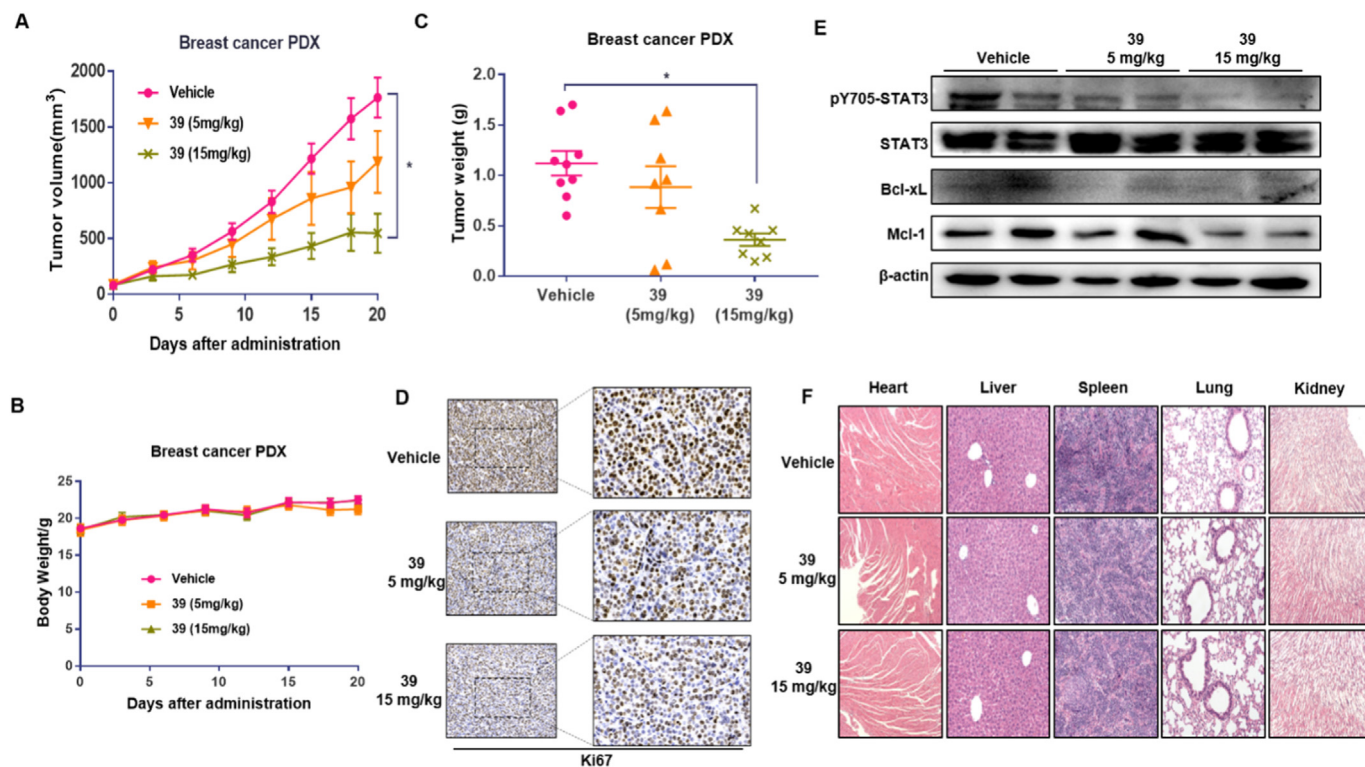

Fig. 14. Antitumor activity of compound **39** in breast cancer PDX model in mice. Tumor volume (A), body weight (B), and tumor weight (C) of the mice with the indicated treatment of compound **39**. (D) Tumor proliferation biomarker Ki67 detection of tumor tissues after treatment with compound **39**. (E) pY705-STAT3, STAT3, Bcl-xL and Mcl-1 immunoblot in tumor tissue lysates. (F) Morphological images of heart, liver, spleen, lung and kidney tissues from treated mice. Values, mean $\pm$ SEM, n = 6. (*) P < 0.05.
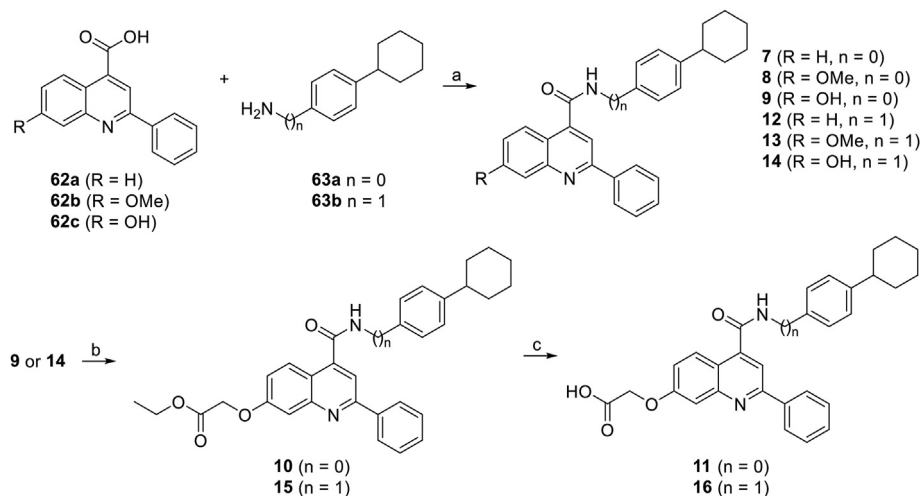
Scheme 1. Synthesis of compounds 7-16[a]. [a] Reagents and conditions: (a) HOAt, EDC, DIPEA, DMF, rt, 4 h, 80%; (b) ethyl 2-bromoacetate, Cs$_2$CO$_3$, DMF, rt, 6 h, 76%; (c) LiOH·H$_2$O, MeOH-H$_2$O (2:3), rt, 1 h, 88%.
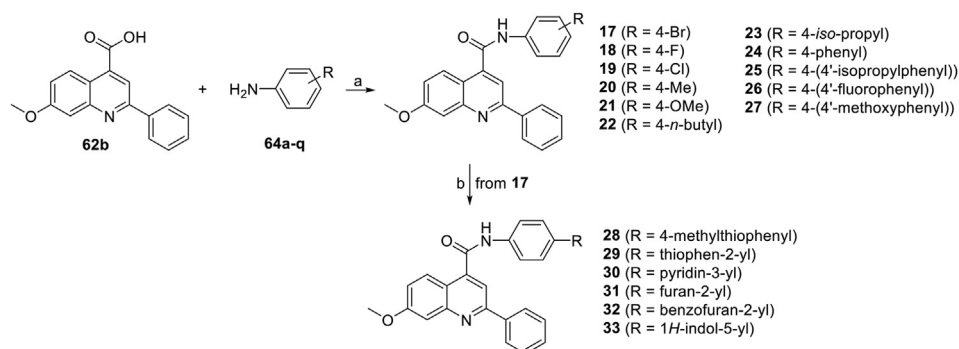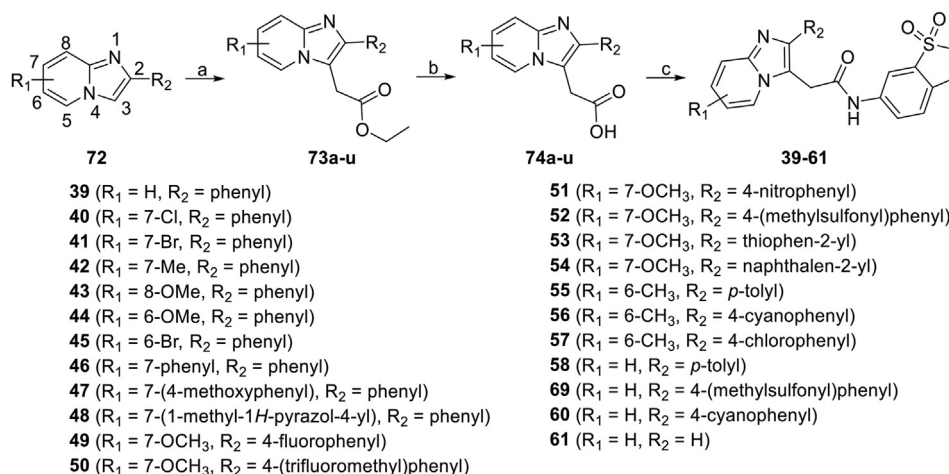

Scheme 2. Synthesis of compounds 17-33[a]. [a] Reagents and conditions: (a) HOAt, EDC, DIPEA, DMF, rt, 4 h, 60−80%; (b) suitable arylboronic acid, Pd(PPh$_3$)$_4$, K$_2$CO$_3$, 1,4-dioxane-H$_2$O (4:1), reflux, overnight, 75−79%.
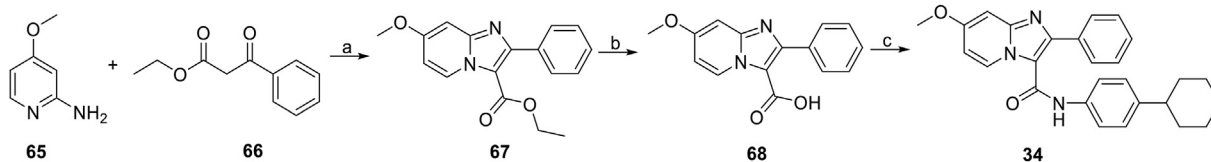
Scheme 3. Synthesis of compound 34[a]. [a] Reagents and conditions: (a) CBr$_4$, CH$_3$CN, 80 °C, 4 h, 85%; (b) LiOH·H$_2$O, MeOH-H$_2$O (2:3), rt, 1 h, 92%; (c) 63a, HATU, DIPEA, DMF, 0°C-rt, 5 h, 85%.
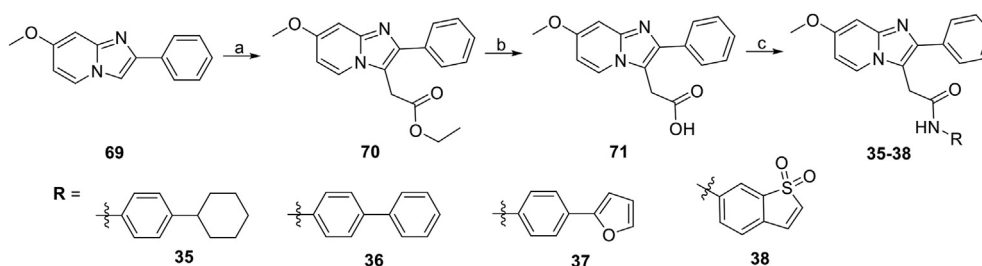
Scheme 4. Synthesis of compounds 35-38[a]. [a] Reagents and conditions: (a) ethyl diazoacetate, Rh$_2$(oct)$_4$, CHCl$_3$, rt, 4 h, 85%; (b) LiOH·H$_2$O, MeOH-H$_2$O (2:3), rt, 1 h, 80%; (c) HOAt, EDC, DIPEA, DMF, rt, 4 h, 65−75%.

39 (R₁ = H, R₂ = phenyl)
40 (R₁ = 7-Cl, R₂ = phenyl)
41 (R₁ = 7-Br, R₂ = phenyl)
42 (R₁ = 7-Me, R₂ = phenyl)
43 (R₁ = 8-OMe, R₂ = phenyl)
44 (R₁ = 6-OMe, R₂ = phenyl)
45 (R₁ = 6-Br, R₂ = phenyl)
46 (R₁ = 7-phenyl, R₂ = phenyl)
47 (R₁ = 7-(4-methoxyphenyl), R₂ = phenyl)
48 (R₁ = 7-(1-methyl-1*H*-pyrazol-4-yl), R₂ = phenyl)
49 (R₁ = 7-OCH₃, R₂ = 4-fluorophenyl)
50 (R₁ = 7-OCH₃, R₂ = 4-(trifluoromethyl)phenyl)

51 (R₁ = 7-OCH₃, R₂ = 4-nitrophenyl)
52 (R₁ = 7-OCH₃, R₂ = 4-(methylsulfonyl)phenyl)
53 (R₁ = 7-OCH₃, R₂ = thiophen-2-yl)
54 (R₁ = 7-OCH₃, R₂ = naphthalen-2-yl)
55 (R₁ = 6-CH₃, R₂ = *p*-tolyl)
56 (R₁ = 6-CH₃, R₂ = 4-cyanophenyl)
57 (R₁ = 6-CH₃, R₂ = 4-chlorophenyl)
58 (R₁ = H, R₂ = *p*-tolyl)
69 (R₁ = H, R₂ = 4-(methylsulfonyl)phenyl)
60 (R₁ = H, R₂ = 4-cyanophenyl)
61 (R₁ = H, R₂ = H)

Scheme 5. Synthesis of compounds 39-61[a]. [a] Reagents and conditions: (a) ethyl diazoacetate, Rh₂(oct)₄, CHCl₃, rt, 4 h, 70−95%; (b) LiOH·H₂O, MeOH-H₂O (2:3), rt, 1 h, 82−95%; (c) HOAt, EDC, DIPEA, DMF, rt, 4 h, 65−80%.

Recently, a novel synthetic route was developed to prepare esters **73a-u** [51] (Scheme 5), which were then subjected to hydrolysis and condensation with 6-aminobenzo[*b*]thiophene 1,1-dioxide to afford amides **39-61**.

3. Conclusions

In summary, we performed structure-based drug design approach to facilitate the discovery of novel STAT3 small-molecule inhibitors with desired druglike properties. Starting from the privileged structures in the previously reported STAT3 small-molecule inhibitors, a novel series of substituted 2-phenylquinolines were first designed and evaluated. Then, the core structure of 2-phenylquinoline was optimized to 2-arylimidazo[1,2-a]pyridine based on the molecular docking models. Further extensive optimization led to the identification of highly potent and selective STAT3 inhibitors, exemplified by compound **39** with the core structure of 2-phenylimidazo[1,2-*a*]pyridine. Compound **39** was able to selectively inhibit phosphorylation of STAT3, disrupt STAT3 dimerization, impair its nuclear translocation and DNA-binding ability, thereby downregulate transcriptional activity of STAT3, and ultimately suppress the growth, migration and invasion of human TNBC cells lines. Moreover, compound **39** demonstrated significant and dose-dependent tumor growth inhibition in both cell line-derived and patient derived xenograft tumor models in mice and was more potent than **SH4-54** and **STX-119**. Overall, these studies provide an example that highly potent and selective STAT3 small-molecule inhibitors with privileged structures can be successfully developed and compound **39** with favorable *in vitro* and *in vivo* pharmacological profiles deserves further investigation.

4. Experimental section

Chemical Reagents and General Method. All commercially available starting materials and solvents are reagent grade and used without further purification. Column chromatography was carried out on silica gel (200−300 mesh) manufactured by Qingdao Haiyang Chemical Group Co., Ltd. Analytical TLC was performed on silica gel plates and visualized under ultraviolet light (254 nm). ¹H and ¹³C NMR spectra were recorded on a Broker spectrometer with 400 or 500 MHz for proton (¹H NMR), and 101 MHz for carbon (¹³C NMR). Chemical shifts downfield from TMS were expressed in ppm, and the signals are described as br (broad singlet), d (doublet), dd

(doublet of doublet), m (multiple), q (quarter), s (singlet), and t (triplet). Coupling constants (*J* values) were given in Hz. HRMS (ESI) and LC-MS (ES) were recorded on SHIMADZU LCMS-IT-TOF mass spectrometer and Thermo TSQ QUANTUM LC-MS spectrometer, respectively. Purity of final compounds was confirmed by analytical HPLC analysis on an Agilent HPLC system. Conditions were as follows: XSelect HSS T3 reversed-phase column (150 mm × 4.60 mm, 5 μm); flow rate 1 mL/min; UV detection at 270 and 254 nM; gradient: from 70% methanol in 30% water to 95% methanol in 5% water (for compound **1**-**33**) and from 5% methanol in 95% water to 95% methanol in 5% water (for compound **34**-**61**). The purity of all final compounds for biological evaluation was greater than 95%.

N-(4-cyclohexylphenyl)-2-phenylquinoline-4-carboxamide (7). To a solution of 2-phenylquinoline-4-carboxylic acid **62a** (250 mg, 1 mmol) and 4-cyclohexylaniline **63a** (193 mg, 1.1 mmol) in anhydrous DMF (5 mL) were added HOAT (205 mg, 1.5 mmol), EDC (148 mg, 1.5 mmol) and DIPEA (194 mg, 1.5 mmol). The reaction mixture was stirred at room temperature for 4 h. Then, the mixture was poured into ice water and extracted with ethyl acetate (10 mL × 3). The combined organic layers were washed with brine and dried over anhydrous Na₂SO₄. After filtration, the solvent was removed under vacuum and the residue was purified by silica gel column chromatography (CHCl₃/MeOH = 20 : 1) to afford compound **7** (324 mg, 80%) as white solid, m.p. 233−235 °C. ¹H NMR (400 MHz, DMSO-*d₆*) δ 10.74 (s, 1H), 8.36 (d, *J* = 7.1 Hz, 2H), 8.31 (s, 1H), 8.18 (d, *J* = 8.5 Hz, 2H), 7.86 (t, *J* = 7.7 Hz, 1H), 7.73 (d, *J* = 8.5 Hz, 2H), 7.67 (t, *J* = 7.6 Hz, 1H), 7.63−7.52 (m, 3H), 7.26 (d, *J* = 8.5 Hz, 2H), 1.81 (d, *J* = 9.3 Hz, 4H), 1.72 (d, *J* = 12.4 Hz, 1H), 1.48−1.34 (m, 4H), 1.33−1.05 (m, 2H); ¹³C NMR (101 MHz, DMSO-*d₆*) δ 165.58, 156.32, 148.40, 144.05, 143.64, 138.63, 137.08, 130.80, 130.44, 130.10, 129.42, 127.85, 127.38, 125.58, 123.72, 120.56, 117.23, 43.77, 34.55, 26.84, 26.08; MS (EI) *m/z* 407.21 (M + H)⁺; HRMS (ESI) calcd for C₂₈H₂₆N₂O (M + H)⁺: 407.2118; found 407.2111. HPLC retention time 6.176 min, 100.00% pure.

Compounds **8-9** and **12**-**14** were prepared in a similar manner as described for compound **7**.

N-(4-cyclohexylphenyl)-7-methoxy-2-phenylquinoline-4-carboxamide (8). Yellow solid, 72% yield, m.p. 211−213 °C. ¹H NMR (400 MHz, DMSO-*d₆*) δ 10.70 (s, 1H), 8.34 (d, *J* = 7.1 Hz, 2H), 8.14 (s, 1H), 8.08 (d, *J* = 9.1 Hz, 1H), 7.72 (d, *J* = 8.0 Hz, 2H), 7.62−7.48 (m, 4H), 7.31 (d, *J* = 8.8 Hz, 1H), 7.24 (d, *J* = 8.0 Hz, 2H), 3.98 (s, 3H), 1.80 (d, *J* = 8.8 Hz, 4H), 1.71 (d, *J* = 12.5 Hz, 1H), 1.51−1.32 (m, 4H), 1.29−1.20 (m, 1H); ¹³C NMR (101 MHz, DMSO-*d₆*) δ 165.71, 161.13, 156.56, 150.41, 143.99, 143.37, 138.80, 137.12, 130.31, 129.36, 127.74,

127.35, 126.78, 120.56, 118.77, 115.01, 108.39, 56.08, 43.78, 34.55, 26.85, 26.09; MS (EI) m/z 437.22 (M + H)$^+$; HRMS (ESI) calcd for C$_{29}$H$_{28}$N$_2$O$_2$ (M + H)$^+$: 437.2224; found 437.2228. HPLC retention time 6.008 min, 97.58% pure.

N-(4-cyclohexylphenyl)-7-hydroxy-2-phenylquinoline-4-carboxamide (9). Yellow solid, 78% yield, m.p. 333−335 °C. ^{1}H NMR (400 MHz, DMSO-d_6) δ 10.31 (s, 1H), 9.45 (t, J = 5.8 Hz, 1H), 8.33 (d, J = 7.3 Hz, 2H), 8.10 (d, J = 9.1 Hz, 1H), 7.98 (s, 1H), 7.66 (dt, J = 13.7, 6.9 Hz, 3H), 7.35 (d, J = 2.2 Hz, 1H), 7.30 (d, J = 7.9 Hz, 2H), 7.21 (d, J = 7.9 Hz, 2H), 7.17 (d, J = 2.3 Hz, 1H), 2.40 (s, 1H), 1.80−1.74 (m, 4H), 1.58 (d, 1H), 1.40−1.32 (m, 4H), 1.30 (s, 1H); ^{13}C NMR (101 MHz, DMSO-d_6) δ 165.88, 159.53, 156.36, 150.44, 143.92, 143.40, 138.96, 137.15, 130.17, 129.30, 127.69, 127.33, 126.91, 120.51, 117.87, 114.17, 111.16, 43.77, 34.55, 26.84, 26.08; MS (EI) m/z 423.20 (M + H)$^+$; HRMS (ESI) calcd for C$_{28}$H$_{26}$N$_2$O$_2$ (M + H)$^+$: 423.2067; found 423.2066. HPLC retention time 4.213 min, 100.00% pure.

N-(4-cyclohexylbenzyl)-2-phenylquinoline-4-carboxamide (12). Yellow solid, 77% yield, m.p.162−164 °C. ^{1}H NMR (400 MHz, DMSO-d_6) δ 9.36 (s, 1H), 8.32 (d, J = 6.9 Hz, 2H), 8.24 (d, J = 8.1 Hz, 1H), 8.19 (s, 1H), 8.15 (d, J = 8.3 Hz, 1H), 7.83 (t, J = 7.1 Hz, 1H), 7.65 (t, J = 7.2 Hz, 1H), 7.61−7.52 (m, 3H), 7.35 (d, J = 7.2 Hz, 2H), 7.23 (d, J = 7.3 Hz, 2H), 4.59 (s, 2H), 1.78 (d, J = 9.4 Hz, 4H), 1.70 (d, J = 12.3 Hz, 1H), 1.38 (dd, J = 19.3, 10.5 Hz, 4H), 1.29−1.14 (m, 2H); ^{13}C NMR (101 MHz, DMSO-d_6) δ 167.10, 156.29, 148.46, 146.83, 143.27, 138.76, 136.81, 130.62, 130.34, 130.05, 129.37, 127.87, 127.61, 127.20, 125.82, 123.94, 117.23, 43.98, 43.02, 34.51, 26.84, 26.08; MS (EI) m/z 421.22 (M + H)$^+$; HRMS (ESI) calcd for C$_{29}$H$_{28}$N$_2$O (M + H)$^+$: 421.2274; found 421.2268. HPLC retention time 5.463 min, 100.00% pure.

N-(4-cyclohexylbenzyl)-7-methoxy-2-phenylquinoline-4-carboxamide (13). White solid, 80% yield, m.p. 173−175 °C. ^{1}H NMR (400 MHz, DMSO-d_6) δ 9.34 (t, J = 5.8 Hz, 1H), 8.30 (d, J = 7.1 Hz, 2H), 8.15 (d, J = 9.2 Hz, 1H), 8.02 (s, 1H), 7.56 (q, J = 14.5, 6.9 Hz, 3H), 7.52 (d, J = 2.3 Hz, 1H), 7.33 (d, J = 8.0 Hz, 2H), 7.29 (dd, J = 9.2, 2.6 Hz, 1H), 7.22 (d, J = 8.1 Hz, 2H), 4.55 (d, J = 5.8 Hz, 2H), 3.96 (s, 3H), 2.46 (s, 1H), 1.77 (d, J = 10.7 Hz, 4H), 1.69 (d, J = 12.4 Hz, 1H), 1.37 (dd, J = 18.5, 9.7 Hz, 4H), 1.26−1.23 (m, 1H); ^{13}C NMR (101 MHz, DMSO-d_6) δ 167.22, 161.03, 156.52, 150.45, 146.81, 142.95, 138.90, 136.85, 130.23, 129.32, 127.81, 127.10, 120.30, 118.97, 115.00, 108.31, 56.03, 43.98, 42.98, 34.51, 26.84, 26.08; MS (EI) m/z 451.23 (M + H)$^+$; HRMS (ESI) calcd for C$_{30}$H$_{30}$N$_2$O$_2$ (M + H)$^+$: 451.2380; found 451.2373. HPLC retention time 5.313 min, 100.00% pure.

N-(4-cyclohexylbenzyl)-7-hydroxy-2-phenylquinoline-4-carboxamide (14). Yellow solid, 84% yield, m.p. 158−160 °C. ^{1}H NMR (400 MHz, DMSO-d_6) δ 10.32 (s, 1H), 9.27 (t, J = 5.8 Hz, 1H), 8.25 (d, J = 7.3 Hz, 2H), 8.07 (d, J = 9.1 Hz, 1H), 7.91 (s, 1H), 7.54 (dt, J = 13.7, 6.9 Hz, 3H), 7.36 (d, J = 2.2 Hz, 1H), 7.32 (d, J = 7.9 Hz, 2H), 7.22 (d, J = 7.9 Hz, 2H), 7.19 (d, J = 2.3 Hz, 1H), 4.54 (d, J = 5.7 Hz, 2H), 2.46 (s, 1H), 1.81−1.74 (m, 4H), 1.68 (d, 1H), 1.42−1.33 (m, 4H), 1.23 (s, 1H); ^{13}C NMR (101 MHz, DMSO-d_6) δ 167.40, 159.42, 156.38, 150.49, 146.80, 142.99, 139.06, 136.88, 130.11, 129.29, 127.89, 127.67, 127.19, 120.23, 118.07, 114.21, 111.08, 43.97, 42.93, 34.51, 26.83, 26.07; MS (EI) m/z 437.22 (M + H)$^+$; HRMS (ESI) calcd for C$_{29}$H$_{28}$N$_2$O$_2$ (M + H)$^+$: 437.2224; found 437.2219. HPLC retention time 3.822 min, 97.91% pure.

N-(4-cyclohexylphenyl)-7-(2-ethoxy-2-oxoethoxy)-2-phenylquinoline-4-carboxamide (10). To a mixture of compound **9** (210 mg, 0.5 mmol) and Cs$_2$CO$_3$ (488 mg, 1.5 mmol) in anhydrous DMF was added ethyl bromoacetate (100 mg, 0.6 mmol) dropwise. The reaction mixture was stirred at room temperature for 4 h. Then, the mixture was poured into ice water and extracted with ethyl acetate (10 mL × 3). The combined organic layers were washed with brine and dried over anhydrous Na$_2$SO$_4$. After filtration, the solvent was removed under vacuum and the residue was purified by silica gel column chromatography (CHCl$_3$/MeOH = 20 : 1) to

afford compound **10** (193 mg, 76%) as yellow solid, m.p. 246−248 °C. ^{1}H NMR (400 MHz, DMSO-d_6) δ 10.71 (s, 1H), 8.33 (d, J = 7.1 Hz, 2H), 8.17 (s, 1H), 8.11 (d, J = 9.2 Hz, 1H), 7.72 (d, J = 8.4 Hz, 2H), 7.58 (dd, J = 13.9, 6.2 Hz, 3H), 7.50 (d, J = 2.6 Hz, 1H), 7.38 (dd, J = 9.2, 2.6 Hz, 1H), 7.25 (d, J = 8.5 Hz, 2H), 5.05 (s, 2H), 4.23 (q, J = 7.1 Hz, 2H), 1.81 (d, J = 9.2 Hz, 4H), 1.72 (d, J = 12.4 Hz, 1H), 1.40 (dd, J = 18.4, 9.9 Hz, 4H), 1.26−1.25 (m, 2H); ^{13}C NMR (101 MHz, DMSO-d_6) δ 168.93, 165.64, 159.35, 156.74, 150.08, 144.04, 143.37, 138.70, 137.08, 130.38, 129.38, 127.76, 127.36, 127.01, 120.58, 120.35, 119.10, 115.34, 109.50, 65.34, 61.30, 43.78, 34.55, 26.84, 26.08, 14.55; MS (EI) m/z 509.24 (M + H)$^+$; HRMS (ESI) calcd for C$_{32}$H$_{32}$N$_2$O$_4$ (M + H)$^+$: 509.2435; found 509.2439. HPLC retention time 5.227 min, 98.14% pure.

Ethyl 2-((4-((4-cyclohexylbenzyl)carbamoyl)-2-phenylquinolin-7-yl)oxy)acetate (15).

Compound **15** was synthesized according to the procedure for the preparation of compound **10**.

Starting from derivative **14**, compound **15** was obtained in in 72% yield, m.p. 164−166 °C. ^{1}H NMR (400 MHz, DMSO-d_6) δ 9.34 (t, J = 5.6 Hz, 1H), 8.28 (d, J = 7.3 Hz, 2H), 8.17 (d, J = 9.2 Hz, 1H), 8.04 (s, 1H), 7.59−7.52 (m, 3H), 7.46 (d, J = 2.1 Hz, 1H), 7.37 (d, J = 2.2 Hz, 1H), 7.33 (d, J = 8.0 Hz, 2H), 7.22 (d, J = 7.9 Hz, 2H), 5.03 (s, 2H), 4.55 (d, J = 5.6 Hz, 2H), 4.24−4.18 (m, 2H), 2.50 (s, 1H), 1.81−1.75 (m, 4H), 1.69 (d, J = 12.4 Hz, 1H), 1.43−1.28 (m, 5H), 1.23 (d, J = 7.0 Hz, 3H); ^{13}C NMR (101 MHz, DMSO-d_6) δ 168.93, 167.13, 159.25, 156.71, 150.13, 146.82, 142.95, 138.82, 136.83, 130.30, 129.34, 127.92, 127.21, 120.16, 119.30, 115.35, 109.44, 65.33, 61.28, 43.98, 42.99, 34.51, 26.84, 26.08, 14.55; MS (EI) m/z 523.25 (M + H)$^+$; HRMS (ESI) calcd for C$_{33}$H$_{34}$N$_2$O$_4$ (M + H)$^+$: 523.2591; found 523.2599. HPLC retention time 4.725 min, 99.66% pure.

N-(4-cyclohexylphenyl)-7-(carboxymethoxy)-2-phenylquinoline-4-carboxamide (11). To a solution of compound **10** (152 mg, 0.3 mmol) in MeOH (4 mL) was added the solution of LiOH.H$_2$O (38 mg, 0.9 mmol) in H$_2$O (6 mL). The reaction mixture was stirred at room temperature for 1 h. Then the mixture was concentrated in vacuum to 4 mL and was cooled to 0−4 °C. The resulting solution was acidified to pH = 2 with 4 N HCl and the precipitated solids were collected by filtration and dried to give compound **11** (127 mg, 88%) as yellow solid, m.p. 237−239 °C. ^{1}H NMR (500 MHz, DMSO-d_6) δ 10.73 (s, 1H), 8.34 (d, J = 7.4 Hz, 2H), 8.16 (s, 1H), 8.10 (d, J = 9.2 Hz, 1H), 7.73 (d, J = 8.4 Hz, 2H), 7.59−7.55 (m, 2H), 7.46 (d, J = 2.3 Hz, 1H), 7.36 (dd, J = 9.2, 2.4 Hz, 1H), 7.25 (d, J = 8.4 Hz, 2H), 4.92 (s, 2H), 2.47 (s, 1H), 1.83−1.78 (m, 4H), 1.71 (d, J = 12.6 Hz, 1H), 1.47−1.33 (m, 5H); ^{13}C NMR (101 MHz, DMSO-d_6) δ 170.38, 165.67, 159.59, 156.64, 150.12, 144.00, 143.36, 138.73, 137.11, 130.34, 129.36, 127.76, 127.35, 126.90, 120.57, 118.97, 115.19, 109.34, 65.41, 43.78, 34.55, 26.85, 26.09; MS (EI) m/z 481.24 (M + H)$^+$; HRMS (ESI) calcd for C$_{30}$H$_{28}$N$_2$O$_4$ (M + H)$^+$: 481.2122; found 481.2144. HPLC retention time 3.815 min, 100.00% pure.

2-((4-((4-cyclohexylbenzyl)carbamoyl)-2-phenylquinolin-7-yl)oxy)acetic acid (16).

Compound **16** was synthesized according to the procedure for the preparation of compound **11**. Compound **15** was used to afford compound **16** in 79% yield, m.p. 162−163 °C. ^{1}H NMR (500 MHz, DMSO-d_6) δ 9.35 (t, J = 5.0 Hz, 1H), 8.28 (d, J = 7.3 Hz, 2H), 8.10 (d, J = 9.1 Hz, 1H), 7.98 (s, 1H), 7.57−7.54 (m, 2H), 7.53−7.50 (m, 1H), 7.33 (d, J = 6.3 Hz, 4H), 7.28 (d, J = 9.1 Hz, 1H), 7.23 (d, J = 7.6 Hz, 2H), 4.57 (s, 2H), 4.55 (d, J = 5.3 Hz, 2H), 1.91 (s, 1H), 1.80−1.76 (m, 4H), 1.70 (d, J = 12.2 Hz, 1H), 1.42−1.36 (m, 4H), 1.24 (s, 1H); ^{13}C NMR (101 MHz, DMSO-d_6) δ 170.66, 167.28, 160.04, 156.45, 150.25, 146.80, 142.90, 138.87, 136.85, 130.20, 129.32, 127.89, 127.20, 126.80, 120.50, 118.88, 114.86, 109.18, 66.73, 43.97, 42.96, 34.51, 26.83, 26.07; MS (EI) m/z 495.22 (M + H)$^+$; HRMS (ESI) calcd for C$_{31}$H$_{30}$N$_2$O$_4$ (M + H)$^+$: 495.2278; found 495.2270. HPLC retention time 5.044 min, 98.49% pure.

Compounds **17-27** were synthesized according to the procedure for the preparation of compound **7**.

N-(4-bromophenyl)-7-methoxy-2-phenylquinoline-4-carboxamide (17). Yellow solid, 80% yield, m.p. 212−214 °C. ^{1}H NMR (400 MHz, DMSO-d_6) δ 10.96 (s, 1H), 8.36 (d, J = 7.2 Hz, 2H), 8.20 (s, 1H), 8.08 (d, J = 9.1 Hz, 1H), 7.82 (d, J = 8.3 Hz, 2H), 7.64−7.52 (m, 6H), 7.33 (d, J = 8.9 Hz, 1H), 3.99 (s, 3H); ^{13}C NMR (101 MHz, DMSO-d_6) δ 166.04, 161.16, 156.56, 150.41, 142.88, 138.73, 132.13, 130.35, 129.35, 127.77, 126.71, 122.44, 120.60, 118.63, 116.30, 115.18, 108.41, 56.09; MS (EI) m/z 433.05 (M + H)$^+$; HRMS (ESI) calcd for C$_{23}$H$_{17}$BrN$_2$O$_2$ (M + H)$^+$: 433.0546; found 433.0544. HPLC retention time 13.237 min, 100.00% pure.

N-(4-fluorophenyl)-7-methoxy-2-phenylquinoline-4-carboxamide (18). Yellow solid, 76% yield, m.p. 234−236 °C. ^{1}H NMR (400 MHz, DMSO-d_6) δ 11.05 (s, 1H), 8.37 (d, J = 7.2 Hz, 2H), 8.20 (s, 1H), 8.11 (d, J = 9.2 Hz, 1H), 7.90 (dd, J = 8.9, 5.1 Hz, 2H), 7.60−7.51 (m, 4H), 7.32 (dd, J = 9.2, 2.5 Hz, 1H), 7.25 (t, J = 8.8 Hz, 2H), 3.98 (s, 3H); ^{13}C NMR (126 MHz, DMSO-d_6) δ 165.84, 161.10, 158.96 (d, J = 240 Hz), 156.57, 150.41, 142.88, 138.81, 135.81, 130.30, 129.33, 127.81, 126.80, 122.38, 120.51, 118.74, 115.85 (d, J = 22.5 Hz), 115.33, 108.38, 56.08; MS (EI) m/z 373.13 (M + H)$^+$; HRMS (ESI) calcd for C$_{23}$H$_{17}$FN$_2$O$_2$ (M + H)$^+$: 373.1347; found 373.1351. HPLC retention time 10.037 min, 100.00% pure.

N-(4-chlorophenyl)-7-methoxy-2-phenylquinoline-4-carboxamide (19). Yellow solid, 76% yield, m.p. 210−212 °C. ^{1}H NMR (400 MHz, DMSO-d_6) δ 10.92 (s, 1H), 8.35 (d, J = 7.1 Hz, 2H), 8.20 (s, 1H), 8.08 (d, J = 9.2 Hz, 1H), 7.86 (d, J = 8.8 Hz, 2H), 7.63−7.52 (m, 4H), 7.48 (d, J = 8.8 Hz, 2H), 7.32 (dd, J = 9.2, 2.5 Hz, 1H), 3.98 (s, 3H); ^{13}C NMR (101 MHz, DMSO-d_6) δ 166.03, 161.17, 156.57, 150.43, 142.94, 138.74, 138.30, 130.34, 129.23, 128.24, 127.76, 126.71, 122.06, 120.61, 118.65, 115.13, 108.43, 56.08; MS (EI) m/z 389.10 (M + H)$^+$; HRMS (ESI) calcd for C$_{23}$H$_{17}$ClN$_2$O$_2$ (M + H)$^+$: 389.1051; found 389.1059. HPLC retention time 12.555 min, 100.00% pure.

7-Methoxy-2-phenyl-N-(p-tolyl)quinoline-4-carboxamide (20). Yellow solid, 68% yield, m.p. 209−211 °C. ^{1}H NMR (400 MHz, DMSO-d_6) δ 10.71 (s, 1H), 8.36 (d, J = 7.2 Hz, 2H), 8.16 (s, 1H), 8.09 (d, J = 9.2 Hz, 1H), 7.71 (d, J = 8.3 Hz, 2H), 7.61−7.53 (m, 4H), 7.32 (dd, J = 9.2, 2.5 Hz, 1H), 7.22 (d, J = 8.3 Hz, 2H), 3.99 (s, 3H), 2.32 (s, 3H); ^{13}C NMR (101 MHz, DMSO-d_6) δ 171.78, 165.72, 161.12, 156.57, 150.41, 143.33, 138.80, 136.85, 133.60, 130.31, 129.66, 129.35, 127.76, 126.79, 120.50, 118.77, 115.04, 108.38, 56.07, 21.03; MS (EI) m/z 369.15 (M + H)$^+$; HRMS (ESI) calcd for C$_{24}$H$_{20}$N$_2$O$_2$ (M + H)$^+$: 369.1598; found 369.1593. HPLC retention time 10.714 min, 100.00% pure.

7-Methoxy-N-(4-methoxyphenyl)-2-phenylquinoline-4-carboxamide (21). Yellow solid, 70% yield, m.p. 208−210 °C. ^{1}H NMR (400 MHz, DMSO-d_6) δ 10.68 (s, 1H), 8.36 (d, J = 6.8 Hz, 2H), 8.16 (s, 1H), 8.11 (d, J = 9.0 Hz, 1H), 7.75 (d, J = 8.1 Hz, 2H), 7.57 (d, J = 12.5 Hz, 4H), 7.32 (d, J = 8.8 Hz, 1H), 6.99 (d, J = 8.1 Hz, 2H), 3.99 (s, 3H), 3.78 (s, 3H); ^{13}C NMR (101 MHz, DMSO-d_6) δ 165.49, 161.11, 156.31, 150.43, 143.32, 138.84, 132.48, 130.28, 129.34, 127.77, 126.86, 122.10, 120.45, 118.83, 115.10, 114.39, 108.37, 56.06, 55.70; MS(EI) m/z 385.15(M + H)$^+$; HRMS (ESI) calcd for C$_{24}$H$_{20}$N$_2$O$_3$ (M + H)$^+$: 385.1547; found 385.1550. HPLC retention time 8.678 min, 100.00% pure.

N-(4-butylphenyl)-7-methoxy-2-phenylquinoline-4-carboxamide (22). Yellow solid, 74% yield, m.p. 244−246 °C. ^{1}H NMR (400 MHz, DMSO-d_6) δ 10.75 (s, 1H), 8.35 (d, J = 6.8 Hz, 2H), 8.16 (s, 1H), 8.09 (d, J = 9.1 Hz, 1H), 7.73 (d, J = 7.9 Hz, 2H), 7.57 (d, J = 12.7 Hz, 4H), 7.32 (d, J = 8.7 Hz, 1H), 7.22 (d, J = 7.7 Hz, 2H), 3.99 (s, 3H), 2.58 (t, J = 7.1 Hz, 2H), 1.61−1.52 (m, 2H), 1.38−1.29 (m, 2H), 0.92 (t, J = 7.0 Hz, 3H); ^{13}C NMR (101 MHz, DMSO-d_6) δ 165.73, 161.10, 156.57, 150.42, 143.23, 138.85, 138.58, 137.08, 130.27, 129.32, 128.97, 127.78, 126.82, 120.56, 118.81, 115.17, 108.39, 56.07, 34.79,

33.71, 22.15, 14.27. MS (EI) m/z 411.20(M + H)$^+$; HRMS (ESI) calcd for C$_{27}$H$_{26}$N$_2$O$_2$ (M + H)$^+$: 411.2067; found 411.2060. HPLC retention time 17.986min, 100.00% pure.

N-(4-isopropylphenyl)-7-methoxy-2-phenylquinoline-4-carboxamide (23). Yellow solid, 74% yield, m.p. 260−262 °C. ^{1}H NMR (400 MHz, DMSO-d_6) δ 10.72 (s, 1H), 8.34 (d, J = 7.1 Hz, 2H), 8.15 (s, 1H), 8.08 (d, J = 9.2 Hz, 1H), 7.73 (d, J = 8.4 Hz, 2H), 7.63−7.53 (m, 4H), 7.31 (dd, J = 9.2, 2.6 Hz, 1H), 7.27 (d, J = 8.4 Hz, 2H), 3.98 (s, 3H), 2.90 (dt, J = 13.9, 6.8 Hz, 1H), 1.22 (d, J = 6.9 Hz, 6H); ^{13}C NMR (101 MHz, DMSO-d_6) δ 165.73, 161.10, 150.41, 144.73, 143.24, 138.84, 137.14, 130.29, 129.33, 127.78, 126.95, 120.64, 120.47, 118.80, 115.15, 108.38, 56.07, 33.45, 24.45; MS (EI) m/z 397.19 (M + H)$^+$; HRMS (ESI) calcd for C$_{26}$H$_{24}$N$_2$O$_2$ (M + H)$^+$: 397.1911; found 397.1917. HPLC retention time 13.625 min, 100.00% pure.

N-([1,1′-biphenyl]-4-yl)-7-methoxy-2-phenylquinoline-4-carboxamide (24). Yellow solid, 62% yield, m.p. 213−214 °C. ^{1}H NMR (400 MHz, DMSO-d_6) δ 10.90 (s, 1H), 8.36 (d, 2H), 8.21 (s, 1H), 8.11 (d, J = 9.2 Hz, 1H), 7.94 (d, J = 8.6 Hz, 2H), 7.73 (dd, J = 14.8, 8.1 Hz, 4H), 7.62−7.54 (m, 4H), 7.48 (t, J = 7.7 Hz, 2H), 7.38−7.32 (m, 2H), 4.00 (s, 3H); ^{13}C NMR (101 MHz, DMSO-d_6) δ 165.97, 161.17, 156.59, 150.45, 143.21, 140.11, 138.79, 136.25, 130.34, 129.42, 127.77, 127.48, 126.83, 120.87, 120.59, 118.74, 115.10, 108.43, 56.08; MS (EI) m/z 431.17 (M + H)$^+$; HRMS (ESI) calcd for C$_{29}$H$_{22}$N$_2$O$_2$ (M + H)$^+$: 431.1754; found 431.1753. HPLC retention time 14.596 min, 100.00% pure.

N-(4′-isopropyl-[1,1′-biphenyl]-4-yl)-7-methoxy-2-phenylquinoline-4-carboxamide (25). White solid, 70% yield, m.p. 248−250 °C. ^{1}H NMR (500 MHz, DMSO-d_6) δ 10.89 (s, 1H), 8.37 (d, J = 7.2 Hz, 2H), 8.20 (s, 1H), 8.11 (d, J = 9.0 Hz, 1H), 7.91 (d, J = 7.8 Hz, 2H), 7.70 (d, J = 7.9 Hz, 2H), 7.63−7.52 (m, 6H), 7.33 (d, J = 7.7 Hz, 3H), 3.99 (s, 3H), 2.98−2.87 (m, 1H), 1.24 (d, J = 6.6 Hz, 6H); ^{13}C NMR (101 MHz, DMSO-d_6) δ 165.91, 161.16, 156.58, 150.43, 147.88, 143.23, 138.78, 138.55, 137.69, 136.28, 130.34, 129.37, 127.77, 127.34, 126.78, 120.84, 120.58, 118.74, 115.08, 108.42, 56.09, 33.57, 24.35; MS (EI) m/z 473.22 (M + H)$^+$; HRMS (ESI) calcd for C$_{32}$H$_{28}$N$_2$O$_2$ (M + H)$^+$: 473.2224; found 473.2224. HPLC retention time 15.478 min, 100.00% pure.

N-(4′-fluoro-[1,1′-biphenyl]-4-yl)-7-methoxy-2-phenylquinoline-4-carboxamide (26). White solid, 66% yield, m.p. 255−257 °C. ^{1}H NMR (500 MHz, DMSO-d_6) δ 10.91 (s, 1H), 8.37 (d, J = 7.4 Hz, 2H), 8.21 (s, 1H), 8.11 (d, J = 9.1 Hz, 1H), 7.93 (d, J = 8.2 Hz, 2H), 7.73 (t, J = 9.8 Hz, 4H), 7.61−7.52 (m, 4H), 7.31 (q, J = 20.1, 10.9 Hz, 3H), 3.99 (s, 3H). ^{13}C NMR (101 MHz, DMSO-d_6) δ 165.97, 163.17, 161.17, 156.58, 150.43, 143.19, 138.77, 136.61, 135.21, 130.35, 129.37, 128.80, 127.77, 127.44, 126.75, 120.86, 120.60, 118.72, 116.27, 116.10, 115.09, 108.42, 56.09; MS (EI) m/z 449.16 (M + H)$^+$; HRMS (ESI) calcd for C$_{29}$H$_{21}$FN$_2$O$_2$ (M + H)$^+$: 449.1660; found 449.1660. HPLC retention time 14.603 min, 100.00% pure.

7-Methoxy-N-(4′-methoxy-[1,1′-biphenyl]-4-yl)-2-phenylquinoline-4-carboxamide (27). Yellow solid, 72% yield, m.p. 252−254 °C. ^{1}H NMR (400 MHz, DMSO-d_6) δ 10.86 (s, 1H), 8.36 (d, J = 7.0 Hz, 2H), 8.20 (s, 1H), 8.10 (d, J = 9.2 Hz, 1H), 7.89 (d, J = 8.7 Hz, 2H), 7.66 (dd, J = 16.2, 8.7 Hz, 4H), 7.62−7.52 (m, 4H), 7.33 (dd, J = 9.2, 2.6 Hz, 1H), 7.09−6.99 (m, 2H), 3.99 (s, 3H), 3.80 (s, 3H); ^{13}C NMR (101 MHz, DMSO-d_6) δ 165.87, 161.16, 159.20, 156.58, 150.42, 143.25, 138.77, 138.15, 136.00, 132.51, 130.34, 129.37, 127.91, 126.83, 120.86, 120.58, 118.73, 115.07, 114.85, 108.41, 56.09, 55.66; MS (EI) m/z 461.18 (M + H)$^+$; HRMS (ESI) calcd for C$_{30}$H$_{24}$N$_2$O$_3$ (M + H)$^+$: 461.1860; found 461.1860. HPLC retention time 14.045 min, 98.26% pure.

Methoxy-N-(4′-(methylthio)-[1,1′-biphenyl]-4-yl)-2-phenylquinoline-4-carboxamide (28). To a mixture of compound **17** (215 mg, 0.5 mmol) and K$_2$CO$_3$ (207 mg, 1.5 mmol) in 1,4-dioxane (4 mL) and water (1 mL) was added 4-(methylthio)phenyl boronic acid (100 mg, 0.6 mmol). The mixture was degassed before addition

of tetrakis(triphenylphosphine)palladium (58 mg, 0.05 mmol) under nitrogen atmosphere. The mixture was heated under reflux overnight and concentrated under reduced pressure. The residue was purified by silica gel column chromatography (CHCl$_3$/ MeOH = 20 : 1) to afford compound **28** (179 mg, 75%) as white solid, m.p. 239−241 °C. ^{1}H NMR (400 MHz, DMSO-d_6) δ 10.89 (s, 1H), 8.39−8.35 (m, 2H), 8.21 (s, 1H), 8.11 (d, J = 9.2 Hz, 1H), 7.92 (d, J = 8.7 Hz, 2H), 7.73 (d, J = 8.7 Hz, 2H), 7.66 (d, J = 8.5 Hz, 2H), 7.61−7.53 (m, 4H), 7.38−7.32 (m, 3H), 3.99 (s, 3H), 2.52 (s, 3H); ^{13}C NMR (101 MHz, DMSO-d_6) δ 165.92, 161.16, 156.58, 150.42, 143.20, 138.73, 137.63, 136.60, 135.56, 135.12, 130.35, 129.37, 127.77, 127.01, 124.91, 121.04, 120.73, 118.72, 115.09, 108.42, 56.09, 15.22; MS (EI) m/z 477.16 (M + H)$^+$; HRMS (ESI) calcd for C$_{30}$H$_{24}$N$_2$O$_2$S (M + H)$^+$: 477.1631; found 477.1631. HPLC retention time 14.747 min, 100.00% pure.

Compounds **29-33** were synthesized according to the procedure for the preparation of compound **28**.

7-Methoxy-2-phenyl-N-(4-(thiophen-2-yl)phenyl)quinoline-4-carboxamide (29). White solid, 63% yield, m.p. 272−274 °C. ^{1}H NMR (400 MHz, DMSO-d_6) δ 10.86 (s, 1H), 8.36 (d, J = 7.0 Hz, 2H), 8.21 (s, 1H), 8.10 (d, J = 9.2 Hz, 1H), 7.93−7.84 (m, 3H), 7.78 (d, J = 8.7 Hz, 2H), 7.65 (dd, J = 5.0, 2.9 Hz, 1H), 7.62−7.51 (m, 5H), 7.33 (dd, J = 9.2, 2.6 Hz, 1H), 3.99 (s, 3H); ^{13}C NMR (101 MHz, DMSO-d_6) δ 165.87, 161.15, 156.57, 150.42, 143.19, 141.51, 138.77, 138.37, 131.49, 130.34, 129.37, 127.77, 127.54, 126.91, 126.53, 120.76, 120.58, 118.72, 115.09, 108.41, 56.09; MS (EI) m/z 437.12 (M + H)$^+$; HRMS (ESI) calcd for C$_{27}$H$_{20}$N$_2$O$_2$S (M + H)$^+$: 437.1318; found 437.1320. HPLC retention time 13.290 min, 100.00% pure.

7-Methoxy-2-phenyl-N-(4-(pyridin-3-yl)phenyl)quinoline-4-carboxamide (30). White solid, 69% yield, m.p. 118−120 °C. ^{1}H NMR (400 MHz, DMSO-d_6) δ 10.96 (s, 1H), 8.95 (d, J = 1.9 Hz, 1H), 8.57 (dd, J = 4.7, 1.5 Hz, 1H), 8.37 (d, J = 7.0 Hz, 2H), 8.22 (s, 1H), 8.15−8.07 (m, 2H), 7.97 (d, J = 8.7 Hz, 2H), 7.82 (d, J = 8.7 Hz, 2H), 7.64−7.54 (m, 4H), 7.50 (dd, J = 7.9, 4.8 Hz, 1H), 7.34 (dd, J = 9.2, 2.6 Hz, 1H), 3.99 (s, 3H); ^{13}C NMR (101 MHz, DMSO-d_6) δ 166.05, 161.18, 156.59, 150.43, 148.69, 147.87, 143.13, 139.45, 138.76, 135.50, 134.17, 133.05, 130.36, 129.37, 127.74, 126.74, 124.35, 120.97, 120.62, 118.69, 115.10, 108.43, 56.10; MS (EI) m/z 432.17 (M + H)$^+$; HRMS (ESI) calcd for C$_{28}$H$_{21}$N$_3$O$_2$ (M + H)$^+$: 432.1707; found 432.1709. HPLC retention time 9,878 min, 100.00% pure.

N-(4-(furan-2-yl)phenyl)-7-methoxy-2-phenylquinoline-4-carboxamide (31). White solid, 61% yield, m.p. 264−266 °C. ^{1}H NMR (400 MHz, DMSO-d_6) δ 10.91 (s, 1H), 8.37 (d, J = 7.0 Hz, 2H), 8.22 (s, 1H), 8.12 (d, J = 9.2 Hz, 1H), 7.91 (d, J = 8.8 Hz, 2H), 7.76 (d, J = 8.6 Hz, 3H), 7.61−7.51 (m, 4H), 7.34 (dd, J = 9.2, 2.6 Hz, 1H), 6.92 (d, J = 3.0 Hz, 1H), 6.61 (dd, J = 3.3, 1.8 Hz, 1H), 3.99 (s, 3H); ^{13}C NMR (101 MHz, DMSO-d_6) δ 166.34, 161.58, 156.99, 153.82, 150.85, 143.49, 139.18, 130.76, 129.78, 128.19, 127.18, 124.88, 121.15, 119.13, 115.54, 112.99, 108.83, 106.08, 56.50; MS (EI) m/z 421.15 (M + H)$^+$; HRMS (ESI) calcd for C$_{27}$H$_{20}$N$_2$O$_3$ (M + H)$^+$: 421.1547; found 421.1544. HPLC retention time 12.966 min, 100.00% pure.

N-(4-(benzofuran-2-yl)phenyl)-7-methoxy-2-phenylquinoline-4-carboxamide (32). Yellow solid, 77% yield, m.p. 247−249 °C. ^{1}H NMR (400 MHz, DMSO-d_6) δ 11.00 (s, 1H), 8.37 (d, J = 7.0 Hz, 2H), 8.23 (s, 1H), 8.11 (d, J = 9.2 Hz, 1H), 7.98 (s, 4H), 7.68−7.62 (m, 2H), 7.61−7.52 (m, 4H), 7.40 (d, J = 0.6 Hz, 1H), 7.36−7.25 (m, 3H), 3.99 (s, 3H); ^{13}C NMR (101 MHz, DMSO-d_6) δ 166.06, 161.18, 156.58, 155.59, 154.62, 150.43, 143.02, 139.89, 138.74, 130.36, 129.37, 127.77, 126.74, 125.84, 124.89, 123.73, 121.50, 120.73, 118.67, 115.15, 111.51, 108.43, 101.76, 56.10; MS (EI) m/z 471.17 (M + H)$^+$; HRMS (ESI) calcd for C$_{31}$H$_{22}$N$_2$O$_3$ (M + H)$^+$: 471.1703; found 471.1701. HPLC retention time 17.385 min, 100.00% pure.

N-(4-(1H-indol-6-yl)phenyl)-7-methoxy-2-phenylquinoline-4-carboxamide (33). Yellow solid, 79% yield, m.p. 228−230 °C. ^{1}H

NMR (400 MHz, DMSO-d_6) δ 11.15 (s, 1H), 10.85 (s, 1H), 8.38 (dd, J = 8.3, 1.3 Hz, 2H), 8.22 (s, 1H), 8.14 (d, J = 9.2 Hz, 1H), 7.92 (d, J = 8.7 Hz, 2H), 7.88−7.85 (m, 1H), 7.73 (d, J = 8.7 Hz, 2H), 7.62−7.52 (m, 4H), 7.50 (d, J = 8.4 Hz, 1H), 7.44 (dd, J = 8.5, 1.7 Hz, 1H), 7.39 (t, 1H), 7.35 (dd, J = 9.2, 2.6 Hz, 1H), 6.52−6.47 (m, 1H), 4.00 (s, 3H); ^{13}C NMR (101 MHz, DMSO-d_6) δ 165.83, 161.16, 156.59, 150.44, 143.33, 138.80, 138.17, 137.70, 135.86, 131.34, 130.34, 129.37, 128.75, 127.78, 127.32, 126.81, 126.54, 120.88, 120.64, 118.78, 118.28, 115.08, 112.27, 108.42, 101.98, 56.09; MS (EI) m/z 470.18 (M + H)$^+$; HRMS (ESI) calcd for C$_{31}$H$_{23}$N$_3$O$_2$ (M + H)$^+$: 470.1863; found 470.1857. HPLC retention time 11.307 min, 98.85% pure.

Compound **34** was synthesized according to the procedure for the preparation of compound **7**.

N-(4-cyclohexylphenyl)-7-methoxy-2-phenylimidazo[1,2-a] pyridine-3-carboxamide (34). White solid, 82% yield, m.p. 237−240 °C. ^{1}H NMR (500 MHz, CDCl$_3$) δ 9.42 (d, J = 7.6 Hz, 1H), 7.74 (d, J = 6.9 Hz, 2H), 7.54 (d, J = 6.3 Hz, 3H), 7.48 (s, 1H), 7.16 (d, J = 7.9 Hz, 2H), 7.10 (d, J = 7.8 Hz, 2H), 6.96 (s, 1H), 6.69 (d, J = 7.6 Hz, 1H), 3.90 (s, 3H), 2.44 (s, 1H), 1.82 (d, J = 7.4 Hz, 4H), 1.73 (d, J = 12.5 Hz, 1H), 1.36 (t, J = 9.6 Hz, 4H), 1.26 (s, 1H); ^{13}C NMR (101 MHz, CDCl$_3$) δ 159.85, 158.89, 148.82, 148.59, 144.12, 135.38, 134.03, 129.88, 129.64, 129.16, 129.03, 127.27, 119.58, 113.99, 108.25, 94.93, 55.64, 44.00, 34.49, 26.87, 26.13; MS (EI) m/z 426.21 (M + H)$^+$; HRMS (ESI) calcd for C$_{27}$H$_{27}$N$_3$O$_2$ (M + H)$^+$: 426.2176; found 426.2181. HPLC retention time 12.815min, 100.00% pure.

Ethyl 2-(7-methoxy-2-phenylimidazo[1,2-a]pyridin-3-yl)acetate (71). A dried flask was charged with 7-methoxy-2-phenylimidazo[1,2-a]pyridine (450 mg, 2 mmol), Ph$_2$(oct)$_4$ (78 mg, 0.1 mmol), and CHCl$_3$ (4 mL). Diazoester (342 mg, 3 mmol) was added into the mixture dropwise under a nitrogen atmosphere. The reaction mixture was stirred at room temperature for 4 h and then concentrated in vacuum. The crud product was purified by chromatography (EtOAc: Hexane = 1 : 2) to yield compound 71 (435 mg, 70%) as white solid. ^{1}H NMR (400 MHz, CDCl$_3$) δ 7.99−7.94 (m, 1H), 7.81 (d, J = 7.2 Hz, 2H), 7.46 (dd, J = 10.3, 4.9 Hz, 2H), 7.37 (d, J = 7.2 Hz, 1H), 6.97 (d, J = 1.7 Hz, 1H), 6.58 (dd, J = 7.4, 2.4 Hz, 1H), 4.21 (dd, J = 7.1, 3.2 Hz, 2H), 3.98 (s, 2H), 3.86 (s, 3H), 1.27 (s, 3H); MS (EI) m/z 310.13 (M + H)$^+$.

Compound **72** was synthesized according to the procedure for the preparation of compound **11**.

2-(7-methoxy-2-phenylimidazo[1,2-a]pyridin-3-yl)acetic acid (72). White solid, 75% yield. ^{1}H NMR (500 MHz, CD$_3$OD) δ 8.64 (s, 1H), 7.69 (s, 2H), 7.64−7.56 (m, 3H), 7.33 (s, 1H), 7.19 (s, 1H), 4.19 (s, 2H), 4.08 (s, 3H); MS (EI) m/z 282.10 (M + H)$^+$.

Compounds **35-38** were synthesized according to the procedure for the preparation of compound **7**.

N-(4-cyclohexylphenyl)-2-(7-methoxy-2-phenylimidazo[1,2-a]pyridin-3-yl)acetamide (35). White solid, 72% yield, m.p. 207−209 °C. ^{1}H NMR (400 MHz, DMSO-d_6) δ 10.35 (s, 1H), 8.29 (d, J = 7.1 Hz, 1H), 7.80 (d, J = 7.1 Hz, 2H), 7.57−7.44 (m, 4H), 7.35 (t, J = 6.4 Hz, 1H), 7.16 (d, J = 7.6 Hz, 2H), 7.00 (s, 1H), 6.72−6.64 (m, 1H), 4.21 (s, 2H), 3.86 (s, 3H), 2.47−2.39 (m, 1H), 1.81−1.72 (m, 4H), 1.71−1.66 (m, 1H), 1.40−1.31 (m, 4H), 1.26−1.22 (m, 1H); ^{13}C NMR (101 MHz, DMSO-d_6) δ 167.71, 157.80, 145.77, 143.28, 142.53, 137.26, 135.16, 128.97, 128.10, 127.70, 127.29, 126.13, 119.85, 114.59, 106.86, 94.74, 56.06, 43.68, 34.53, 31.99, 26.83, 26.07; MS (EI) m/z 440.22 (M + H)$^+$; HRMS (ESI) calcd for C$_{28}$H$_{29}$N$_3$O$_2$ (M + H)$^+$: 440.2333; found 440.2336. HPLC retention time 19.171 min, 100.00% pure.

([1,1′-biphenyl]-4-yl)-2-(7-methoxy-2-phenylimidazo[1,2-a] pyridin-3-yl)acetamide (36). White solid, 76% yield, m.p. 217−218 °C. ^{1}H NMR (500 MHz, DMSO-d_6) δ 10.46 (s, 1H), 8.24 (d, J = 7.5 Hz, 1H), 7.71 (d, J = 7.6 Hz, 2H), 7.66 (d, J = 8.1 Hz, 2H), 7.58 (d, J = 8.0 Hz, 4H), 7.39 (dt, J = 14.9, 7.4 Hz, 4H), 7.28 (dt, J = 11.8, 6.7 Hz, 2H), 6.93 (s, 1H), 6.62 (d, J = 7.4 Hz, 1H), 4.18 (s, 2H), 3.79 (s, 3H); ^{13}C NMR (101 MHz, DMSO-d_6) δ 168.04, 157.76, 145.84, 142.67, 140.12,

138.95, 135.59, 135.24, 129.38, 129.01, 128.07, 127.79, 127.57, 126.73, 126.16, 120.11, 114.43, 106.84, 94.80, 56.08, 32.10; MS (EI) m/z 434.18 (M + H)$^+$; HRMS (ESI) calcd for C$_{28}$H$_{23}$N$_3$O$_2$ (M + H)$^+$: 434.1865; found 434.1863. HPLC retention time 13.844 min, 100.00% pure.

N-(4-(furan-2-yl)phenyl)-2-(7-methoxy-2-phenylimidazo[1,2-a]pyridin-3-yl)acetamide(37). White solid, 74% yield, m.p. 212−214 °C. ^{1}H NMR (400 MHz, DMSO-d_6) δ 11.00 (s, 1H), 8.34 (d, J = 7.0 Hz, 1H), 7.77 (d, J = 6.8 Hz, 2H), 7.70 (d, J = 7.6 Hz, 2H), 7.63 (s, 1H), 7.58 (d, J = 7.5 Hz, 2H), 7.39 (t, J = 6.5 Hz, 2H), 7.28 (t, J = 6.9 Hz, 1H), 6.92 (s, 1H), 6.77 (s, 1H), 6.59 (d, J = 7.1 Hz, 1H), 6.49 (s, 1H), 4.24 (s, 2H), 3.79 (s, 3H); ^{13}C NMR (101 MHz, DMSO-d_6) δ 168.11, 157.72, 153.48, 145.77, 142.88, 142.67, 138.99, 135.23, 128.97, 128.08, 127.66, 126.26, 126.05, 124.38, 119.97, 114.54, 112.48, 106.80, 105.30, 94.78, 56.07, 32.04; MS (EI) m/z 424.16 (M + H)$^+$; HRMS (ESI) calcd for C$_{26}$H$_{21}$N$_3$O$_3$ (M + H)$^+$: 424.1656; found 424.1653. HPLC retention time 10.207 min, 100.00% pure.

N-(1,1-dioxidobenzo[b]thiophen-6-yl)-2-(7-methoxy-2-phenylimidazo[1,2-a]pyridin-3-yl) acetamide (38). White solid, 73% yield, m.p. 167−168 °C. ^{1}H NMR (500 MHz, DMSO-d_6) δ 10.93 (s, 1H), 8.31 (d, J = 7.4 Hz, 1H), 8.15 (s, 1H), 7.81−7.74 (m, 3H), 7.58 (dd, J = 16.8, 7.5 Hz, 2H), 7.48 (t, J = 7.4 Hz, 2H), 7.36 (t, J = 7.2 Hz, 1H), 7.29 (d, J = 6.8 Hz, 1H), 7.01 (s, 1H), 6.69 (d, J = 7.0 Hz, 1H), 4.29 (s, 2H), 3.38 (s, 3H); ^{13}C NMR (101 MHz, DMSO-d_6) δ 168.80, 157.83, 145.90, 142.80, 141.87, 137.69, 135.11, 133.29, 130.54, 129.06, 128.08, 127.77, 127.08, 126.23, 126.06, 123.79, 113.89, 111.94, 106.91, 94.77, 56.08, 32.23; MS (EI) m/z 446.11 (M + H)$^+$; HRMS (ESI) calcd for C$_{24}$H$_{19}$N$_3$O$_4$S (M + H)$^+$: 446.1169; found 446.1162. HPLC retention time 15.632 min, 100.00% pure.

Compounds **74a-u** were synthesized according to the procedure for the preparation of compound **11**.

2-(2-phenylimidazo[1,2-a]pyridin-3-yl)acetic acid (74a). White solid, 85% yield. ^{1}H NMR (400.

MHz, CD$_3$OD) δ 8.86 (d, J = 6.9 Hz, 1H), 8.11−8.06 (m, 1H), 8.02 (d, J = 8.9 Hz, 1H), 7.78−7.73 (m, 2H), 7.69−7.59 (m, 4H), 4.30 (s, 2H); MS (EI) m/z 252.15 (M + H)$^+$.

2-(7-chloro-2-phenylimidazo[1,2-a]pyridin-3-yl)acetic acid (74b). White solid, 82% yield. ^{1}H NMR (400 MHz, CD$_3$OD) δ 8.82 (d, J = 7.2 Hz, 1H), 8.04 (s, 1H), 7.72 (d, J = 6.0 Hz, 2H), 7.62 (dd, J = 19.0, 6.4 Hz, 4H), 4.24 (s, 2H); MS (EI) m/z 286.05 (M + H)$^+$.

2-(7-bromo-2-phenylimidazo[1,2-a]pyridin-3-yl)acetic acid (74c). White solid, 88% yield. ^{1}H NMR (500 MHz, CD$_3$OD) δ 8.78 (d, J = 6.9 Hz, 1H), 8.26 (s, 1H), 7.75 (d, J = 7.0 Hz, 3H), 7.67 (d, J = 6.6 Hz, 3H), 4.27 (s, 2H); MS (EI) m/z 330.00 (M + H)$^+$.

2-(7-methyl-2-phenylimidazo[1,2-a]pyridin-3-yl)acetic acid (74d). White solid, 81% yield. ^{1}H NMR (500 MHz, CD$_3$OD) δ 8.69 (d, J = 6.9 Hz, 1H), 7.75 (s, 1H), 7.73−7.68 (m, 2H), 7.64 (d, J = 7.0 Hz, 2H), 7.44 (d, J = 6.8 Hz, 1H), 4.29 (s, 2H), 2.65 (s, 3H); MS (EI) m/z 266.11 (M + H)$^+$.

2-(8-methoxy-2-phenylimidazo[1,2-a]pyridin-3-yl)acetic acid (74e). White solid, 84% yield. ^{1}H NMR (400 MHz, CD$_3$OD) δ 8.37 (s, 1H), 7.70 (d, J = 3.4 Hz, 2H), 7.63 (d, J = 3.7 Hz, 3H), 7.49 (s, 2H), 4.20 (d, J = 4.5 Hz, 5H); MS (EI) m/z 282.11 (M + H)$^+$.

2-(6-methoxy-2-phenylimidazo[1,2-a]pyridin-3-yl)acetic acid (74f). White solid, 79% yield. ^{1}H NMR (500 MHz, CDCl$_3$) δ 8.09 (s, 1H), 7.70 (d, J = 5.9 Hz, 3H), 7.50 (dd, J = 18.8, 6.7 Hz, 4H), 4.06 (s, 2H), 3.92 (s, 3H); MS (EI) m/z 282.12 (M + H)$^+$.

2-(6-bromo-2-phenylimidazo[1,2-a]pyridin-3-yl)acetic acid (74g). White solid, 81% yield. ^{1}H NMR (500 MHz, CDCl$_3$) δ 9.08 (s, 1H), 7.95 (dd, J = 48.2, 41.2 Hz, 3H), 7.61 (d, J = 43.9 Hz, 4H), 4.18 (d, J = 16.4 Hz, 2H); MS (EI) m/z 330.00 (M + H)$^+$.

2-(2,7-diphenylimidazo[1,2-a]pyridin-3-yl)acetic acid (74h). White solid, 85% yield. ^{1}H NMR (400 MHz, CD$_3$OD) δ 8.85 (s, 1H), 8.15 (s, 1H), 7.91 (s, 3H), 7.77 (s, 2H), 7.66 (d, J = 6.8 Hz, 3H), 7.58 (dd, J = 11.7, 6.6 Hz, 3H), 4.29 (s, 2H); MS (EI) m/z 328.12 (M + H)$^+$.

2-(7-(4-methoxyphenyl)-2-phenylimidazo[1,2-a]pyridin-3-

yl)acetic acid (74i). White solid, 86% yield. ^{1}H NMR (400 MHz, CD$_3$OD) δ 8.82 (s, 1H), 8.09 (s, 1H), 7.91 (d, J = 8.2 Hz, 4H), 7.77 (d, J = 6.4 Hz, 2H), 7.70−7.66 (m, 2H), 7.15 (d, J = 8.2 Hz, 2H), 4.29 (s, 2H), 3.90 (s, 3H); MS (EI) m/z 358.13 (M + H)$^+$.

2-(7-(1-methyl-1H-pyrazol-4-yl)-2-phenylimidazo[1,2-a]pyridin-3-yl)acetic acid (74j). White solid, 81% yield. ^{1}H NMR (400 MHz, CD$_3$OD) δ 8.75 (s, 1H), 8.44 (s, 1H), 8.18 (s, 1H), 8.04 (s, 1H), 7.82 (s, 1H), 7.73 (d, J = 6.3 Hz, 2H), 7.66 (d, J = 6.0 Hz, 3H), 4.31 (s, 2H), 4.01 (s, 3H); MS (EI) m/z 332.13 (M + H)$^+$.

2-(2-(4-fluorophenyl)-7-methoxyimidazo[1,2-a]pyridin-3-yl)acetic acid (74k). White solid, 83% yield. ^{1}H NMR (500 MHz, CD$_3$OD) δ 8.63 (d, J = 7.5 Hz, 1H), 7.74 (dd, J = 8.3, 5.2 Hz, 2H), 7.38 (t, J = 8.5 Hz, 2H), 7.30 (s, 1H), 7.20 (d, J = 7.3 Hz, 1H), 4.23 (s, 2H), 4.09 (s, 3H); MS (EI) m/z.300.09 (M + H)$^+$.

2-(7-methoxy-2-(4-(trifluoromethyl)phenyl)imidazo[1,2-a]pyridin-3-yl)acetic acid (74l). White solid, 78% yield. ^{1}H NMR (400 MHz, CD$_3$OD) δ 8.67 (s, 1H), 7.95 (s, 4H), 7.36 (s, 1H), 7.23 (s, 1H), 4.26 (s, 2H), 4.11 (s, 3H); MS (EI) m/z 350.09 (M + H)$^+$.

2-(7-methoxy-2-(4-nitrophenyl)imidazo[1,2-a]pyridin-3-yl)acetic acid (74m). White solid, 82% yield. ^{1}H NMR (500 MHz, CD$_3$OD) δ 8.66 (d, J = 6.3 Hz, 1H), 8.47 (d, J = 6.7 Hz, 2H), 7.99 (d, J = 6.5 Hz, 2H), 7.34 (s, 1H), 7.22 (d, J = 5.5 Hz, 1H), 4.26 (s, 2H), 4.10 (s, 3H); MS (EI) m/z 269.08 (M + H)$^+$.

2-(7-methoxy-2-(4-(methylsulfonyl)phenyl)imidazo[1,2-a]pyridin-3-yl)acetic acid (74n). White solid, 86% yield. ^{1}H NMR (500 MHz, CDCl$_3$) δ 8.11 (d, J = 7.5 Hz, 1H), 7.90 (q, J = 8.5 Hz, 4H), 6.80 (d, J = 2.3 Hz, 1H), 6.63 (dd, J = 7.5, 2.4 Hz, 1H), 3.84−3.76 (m, 5H), 3.02 (s, 3H); MS (EI) m/z 360.08 (M + H)$^+$.

2-(7-methoxy-2-(thiophen-2-yl)imidazo[1,2-a]pyridin-3-yl)acetic acid (74o). White solid, 82% yield. ^{1}H NMR (400 MHz, CD$_3$OD) δ 8.64 (s, 1H), 7.79 (s, 1H), 7.65 (s, 1H), 7.31 (s, 2H), 7.18 (s, 1H), 4.33 (s, 2H), 4.09 (s, 3H); MS (EI) m/z 288.06 (M + H)$^+$.

2-(7-methoxy-2-(naphthalen-2-yl)imidazo[1,2-a]pyridin-3-yl)acetic acid (74p). White solid, 71% yield. ^{1}H NMR (400 MHz, MeOD) δ 8.41 (s, 1H), 7.69 (m, 7H), 7.53 (s, 3H), 4.24 (d, J = 4.5 Hz, 5H); MS (EI) m/z 333.11 (M + H)$^+$.

2-(2-(4-cyanophenyl)-6-methylimidazo[1,2-a]pyridin-3-yl)acetic acid (74q). White solid, 86% yield. ^{1}H NMR (500 MHz, CD$_3$OD) δ 8.68 (s, 1H), 8.05−7.89 (m, 6H), 4.30 (s, 2H), 2.55 (s, 3H); MS (EI) m/z 291.10 (M + H)$^+$.

2-(2-(4-chlorophenyl)-6-methylimidazo[1,2-a]pyridin-3-yl)acetic acid (74r). White solid, 81% yield. ^{1}H NMR (400 MHz, CD$_3$OD) δ 8.65 (s, 1H), 7.92 (s, 2H), 7.71 (s, 2H), 7.66 (s, 2H), 4.28 (d, J = 16.9 Hz, 5H); MS (EI) m/z 300.07 (M + H)$^+$.

2-(2-(p-tolyl)imidazo[1,2-a]pyridin-3-yl)acetic acid (74s). White solid, 89% yield. ^{1}H NMR (500 MHz, CD$_3$OD) δ 8.83 (s, 1H), 8.02 (d, J = 16.8 Hz, 2H), 7.60 (d, J = 16.6 Hz, 3H), 7.45 (d, J = 6.7 Hz, 2H), 4.27 (s, 2H), 2.45 (s, 3H); MS (EI) m/z 266.11 (M + H)$^+$.

2-(2-(4-(methylsulfonyl)phenyl)imidazo[1,2-a]pyridin-3-yl)acetic acid (74t). White solid, 80% yield. ^{1}H NMR (400 MHz, MeOD) δ 8.65 (s, 1H), 7.97 (m, 4H), 7.26 (d, J = 34.0 Hz, 2H), 4.15 (d, J = 48.7 Hz, 5H); MS (EI) m/z 331.06 (M + H)$^+$.

2-(2-(4-cyanophenyl)imidazo[1,2-a]pyridin-3-yl)acetic acid (74u). White solid, 85% yield. ^{1}H NMR (400 MHz, MeOD) δ 8.87 (d, J = 6.0 Hz, 1H), 8.08 (m, 2H), 7.98 (s, 4H), 7.63 (s, 1H), 4.34 (s, 2H); MS (EI) m/z 278.08 (M + H)$^+$.

Compounds **39-61** were synthesized according to the procedure for the preparation of compound **7**.

N-(1,1-dioxidobenzo[b]thiophen-6-yl)-2-(7-methoxy-2-phenylimidazo[1,2-a]pyridin-3-yl) acetamide (39). White solid, 78% yield, m.p. 201−203 °C. ^{1}H NMR (400 MHz, DMSO-d_6) δ 10.99 (s, 1H), 8.46 (d, J = 6.7 Hz, 1H), 8.17 (s, 1H), 7.82−7.77 (m, 3H), 7.65 (d, J = 9.0 Hz, 1H), 7.59 (dd, J = 11.5, 7.6 Hz, 2H), 7.50 (t, J = 7.4 Hz, 2H), 7.40 (t, J = 7.2 Hz, 1H), 7.34−7.28 (m, 2H), 6.98 (t, J = 6.7 Hz, 1H), 4.36 (s, 2H); ^{13}C NMR (101 MHz, DMSO-d_6) δ 168.60, 144.52, 143.51,

141.86, 137.71, 134.86, 133.29, 130.56, 129.12, 128.38, 128.06, 127.08, 126.11, 125.53, 125.12, 123.83, 117.10, 115.19, 112.49, 111.99, 32.31; MS (EI) m/z 416.10 (M + H)$^+$; HRMS (ESI) calcd for $C_{24}H_{19}N_3O_4S$ (M + H)$^+$: 416.1063; found: 416.060. HPLC retention time 12.255 min, 96.70% pure.

2-(7-chloro-2-phenylimidazo[1,2-a]pyridin-3-yl)-N-(1,1-dioxidobenzo[b]thiophen-6-yl) acetamide (40). White solid, 76% yield, m.p. 230−232 °C. ^{1}H NMR (500 MHz, DMSO-d_6) δ 10.93 (s, 1H), 8.52 (d, J = 7.4 Hz, 1H), 8.12 (s, 1H), 7.81 (d, J = 2.0 Hz, 1H), 7.77−7.73 (m, 3H), 7.58 (dd, J = 16.4, 7.6 Hz, 2H), 7.50 (t, J = 7.7 Hz, 2H), 7.40 (t, J = 7.3 Hz, 1H), 7.29 (d, J = 6.9 Hz, 1H), 7.06 (dd, J = 7.3, 2.1 Hz, 1H), 4.35 (s, 2H); ^{13}C NMR (101 MHz, DMSO-d_6) δ 168.37, 144.23, 141.79, 137.68, 134.41, 133.29, 130.57, 130.26, 129.20, 128.33, 127.09, 126.79, 126.12, 123.83, 115.85, 113.48, 111.97, 32.21; MS (EI) m/z 450.06 (M + H)$^+$; HRMS (ESI) calcd for $C_{23}H_{16}ClN_3O_3S$ (M + H)$^+$: 450.0674; found: 450.0676. HPLC retention time 11.189 min, 97.88% pure.

(7-bromo-2-phenylimidazo[1,2-a]pyridin-3-yl)-N-(1,1-dioxidobenzo[b]thiophen-6-yl) acetamide (41). White solid, 71% yield, m.p. 247−249 °C. ^{1}H NMR (500 MHz, DMSO-d_6) δ 10.93 (s, 1H), 8.45 (d, J = 7.3 Hz, 1H), 8.12 (s, 1H), 7.96 (s, 1H), 7.75 (d, J = 7.2 Hz, 3H), 7.58 (dd, J = 16.7, 7.5 Hz, 2H), 7.50 (t, J = 7.6 Hz, 2H), 7.40 (t, J = 7.2 Hz, 1H), 7.29 (d, J = 6.9 Hz, 1H), 7.15 (d, J = 7.3 Hz, 1H), 4.34 (s, 2H); ^{13}C NMR (101 MHz, DMSO-d_6) δ 168.36, 144.63, 144.11, 141.85, 137.68, 134.40, 133.29, 130.55, 129.19, 128.36, 127.07, 126.72, 126.09, 123.83, 118.99, 118.09, 115.77, 111.98, 32.22; MS (EI) m/z 494.01 (M + H)$^+$; HRMS (ESI) calcd for $C_{23}H_{16}BrN_3O_3S$ (M + H)$^+$: 494.0168; found: 494.0161. HPLC retention time 11.676 min, 96.27% pure.

N-(1,1-dioxidobenzo[b]thiophen-6-yl)-2-(7-methyl-2-phenylimidazo[1,2-a]pyridin-3-yl) acetamide (42). White solid, 76% yield, m.p. 202−204 °C. ^{1}H NMR (500 MHz, DMSO-d_6) δ 10.95 (s, 1H), 8.29 (d, J = 6.8 Hz, 1H), 8.14 (s, 1H), 7.78 (t, J = 7.2 Hz, 3H), 7.61−7.56 (m, 2H), 7.49 (t, J = 7.6 Hz, 2H), 7.39 (t, J = 7.3 Hz, 1H), 7.29 (d, J = 6.9 Hz, 1H), 7.13 (d, J = 6.6 Hz, 1H), 6.89 (t, J = 6.8 Hz, 1H), 4.31 (s, 2H), 2.56 (s, 3H); ^{13}C NMR (101 MHz, DMSO-d_6) δ 168.63, 144.86, 142.95, 141.85, 137.69, 134.96, 133.29, 130.55, 129.07, 128.43, 127.98, 127.09, 126.56, 126.08, 123.81, 123.26, 115.55, 112.51, 111.93, 32.42, 17.06; MS (EI) m/z 430.12 (M + H)$^+$; HRMS (ESI) calcd for $C_{24}H_{19}N_3O_3S$ (M + H)$^+$: 430.1220; found: 430.1220. HPLC retention time 12.859 min, 100.00% pure.

N-(1,1-dioxidobenzo[b]thiophen-6-yl)-2-(8-methoxy-2-phenylimidazo[1,2-a]pyridin-3-yl) acetamide (43). White solid, 78% yield, m.p. 219−221 °C. ^{1}H NMR (500 MHz, DMSO-d_6) δ 11.07 (s, 1H), 8.16 (s, 1H), 8.06 (d, J = 6.5 Hz, 1H), 7.79 (d, J = 6.2 Hz, 3H), 7.66−7.56 (m, 2H), 7.49 (t, J = 7.2 Hz, 2H), 7.37 (t, J = 6.9 Hz, 1H), 7.29 (d, J = 6.7 Hz, 1H), 6.88 (t, J = 6.9 Hz, 1H), 6.73 (d, J = 7.3 Hz, 1H), 4.33 (s, 2H), 3.98 (s, 3H); ^{13}C NMR (101 MHz, DMSO-d_6) δ 168.57, 148.81, 142.48, 141.87, 138.84, 137.67, 134.82, 133.30, 130.54, 129.07, 128.28, 127.96, 127.07, 126.07, 123.80, 118.11, 116.08, 112.55, 111.92, 102.02, 56.23, 32.50; MS (EI) m/z 446.11 (M + H)$^+$; HRMS (ESI) calcd for $C_{24}H_{19}N_3O_4S$ (M + H)$^+$: 446.1169; found: 446.1166. HPLC retention time 14.234 min, 98.64% pure.

N-(1,1-dioxidobenzo[b]thiophen-6-yl)-2-(6-methoxy-2-phenylimidazo[1,2-a]pyridin-3-yl) acetamide (44). White solid, 71% yield, m.p. 233−234 °C. ^{1}H NMR (500 MHz, DMSO-d_6) δ 11.34 (s, 1H), 8.17 (d, J = 27.5 Hz, 2H), 7.81 (dd, J = 21.5, 8.0 Hz, 3H), 7.61−7.55 (m, 3H), 7.48 (t, J = 7.5 Hz, 2H), 7.36 (t, J = 7.0 Hz, 1H), 7.28 (d, J = 6.8 Hz, 1H), 7.12 (d, J = 9.7 Hz, 1H), 4.39 (s, 2H), 3.84 (s, 3H); ^{13}C NMR (101 MHz, DMSO-d_6) δ 168.70, 149.09, 141.97, 141.42, 137.67, 134.82, 133.31, 130.51, 129.08, 128.13, 127.91, 127.08, 126.04, 123.77, 119.99, 117.34, 116.47, 111.89, 107.59, 57.07, 32.40; MS (EI) m/z 446.11 (M + H)$^+$; HRMS (ESI) calcd for $C_{24}H_{19}N_3O_4S$ (M + H)$^+$: 446.1169; found: 446.1164. HPLC retention time 14.748 min, 98.68% pure.

2-(6-bromo-2-phenylimidazo[1,2-a]pyridin-3-yl)-N-(1,1-

dioxidobenzo[b]thiophen-6-yl) acetamide (45). White solid, 72% yield, m.p. 223−225 °C. ^{1}H NMR (400 MHz, DMSO-d_6) δ 10.95 (s, 1H), 8.86 (s, 1H), 8.13 (s, 1H), 7.79−7.73 (m, 3H), 7.64−7.56 (m, 3H), 7.50 (t, J = 7.6 Hz, 2H), 7.45−7.37 (m, 2H), 7.29 (d, J = 6.9 Hz, 1H), 4.37 (s, 2H); ^{13}C NMR (101 MHz, DMSO-d_6) δ 168.46, 144.10, 143.03, 141.85, 137.70, 134.39, 133.29, 130.56, 129.21, 128.30, 128.02, 127.11, 126.08, 125.81, 123.79, 118.19, 116.13, 111.91, 106.47, 32.23; MS (EI) m/z 494.01 (M + H)$^+$; HRMS (ESI) calcd for $C_{23}H_{16}BrN_3O_3S$ (M + H)$^+$: 494.0168; found: 446.0168. HPLC retention time 13.345 min, 100.00% pure.

N-(1,1-dioxidobenzo[b]thiophen-6-yl)-2-(2,7-diphenylimidazo[1,2-a]pyridin-3-yl)acetamide (46). White solid, 71% yield, m.p. 146−148 °C. ^{1}H NMR (500 MHz, DMSO-d_6) δ 11.11 (s, 1H), 8.55 (d, J = 7.2 Hz, 1H), 8.30 (d, J = 4.6 Hz, 1H), 8.16 (s, 1H), 7.96 (s, 1H), 7.87−7.81 (m, 3H), 7.59 (q, J = 6.7 Hz, 2H), 7.52 (q, J = 8.0 Hz, 2H), 7.41−7.38 (m, 2H), 7.29 (d, J = 6.8 Hz, 1H), 7.18 (d, J = 8.2 Hz, 1H), 6.88 (d, 1H), 6.69 (d, J = 8.2 Hz, 1H), 6.10 (s, 1H), 4.40 (s, 2H); ^{13}C NMR (101 MHz, DMSO-d_6) δ 168.60, 144.97, 144.26, 141.86, 138.38, 137.71, 136.63, 134.84, 133.29, 130.57, 129.58, 129.16, 128.70, 128.32, 127.05, 126.11, 125.70, 123.83, 115.17, 113.34, 111.85, 32.35; MS (EI) m/z 492.13 (M + H)$^+$; HRMS (ESI) calcd for $C_{29}H_{21}N_3O_3S$ (M + H)$^+$: 492.1376; found: 492.1378. HPLC retention time 15.083 min, 98.37% pure.

N-(1,1-dioxidobenzo[b]thiophen-6-yl)-2-(7-(4-methoxyphenyl)-2-phenylimidazo[1,2-a]   pyridin-3-yl)acet-amide (47). White solid, 78% yield, m.p. 136−138 °C. ^{1}H NMR (400 MHz, DMSO-d_6) δ 10.98 (s, 1H), 8.49 (d, J = 7.2 Hz, 1H), 8.15 (s, 1H), 7.88 (d, J = 1.0 Hz, 1H), 7.83 (s, 1H), 7.82−7.75 (m, 4H), 7.63−7.56 (m, 2H), 7.50 (t, J = 7.6 Hz, 2H), 7.39 (t, J = 7.4 Hz, 1H), 7.34 (dd, J = 7.3, 1.8 Hz, 1H), 7.29 (d, J = 6.9 Hz, 1H), 7.08 (d, J = 8.8 Hz, 2H), 4.37 (s, 2H), 3.83 (s, 3H); ^{13}C NMR (101 MHz, DMSO-d_6) δ 168.64, 159.98, 145.11, 144.00, 141.86, 137.70, 136.40, 134.88, 133.30, 130.61, 129.14, 128.27, 128.06, 127.10, 126.09, 125.56, 123.81, 115.00, 112.19, 111.94, 111.56, 55.74, 32.33; MS (EI) m/z 522.14 (M + H)$^+$; HRMS (ESI) calcd for $C_{30}H_{23}N_3O_4S$ (M + H)$^+$: 522.1482; found: 522.1483. HPLC retention time 13.398 min, 99.57% pure.

N-(1,1-dioxidobenzo[b]thiophen-6-yl)-2-(7-(1-methyl-1H-pyrazol-4-yl)-2-phenylimidazo [1,2-a]pyridin-3-yl)acetamide (48). White solid, 79% yield, m.p. 135−136 °C. ^{1}H NMR (400 MHz, DMSO-d_6) δ 10.94 (s, 1H), 8.44 (d, J = 7.1 Hz, 1H), 8.34 (s, 1H), 8.14 (s, 1H), 8.07 (s, 1H), 7.83−7.76 (m, 4H), 7.59 (dd, J = 11.2, 7.6 Hz, 2H), 7.50 (t, J = 7.6 Hz, 2H), 7.39 (d, J = 7.3 Hz, 1H), 7.30−7.22 (m, 2H), 4.34 (s, 2H), 3.90 (s, 3H). MS(EI) m/z 496.14 (M + H)$^+$; ^{13}C NMR (101 MHz, DMSO-d_6) δ 168.66, 145.08, 143.52, 141.85, 137.70, 137.07, 134.84, 133.29, 130.56, 129.85, 129.12, 128.23, 128.02, 127.09, 126.09, 125.64, 123.82, 120.76, 114.94, 111.97, 111.19, 110.23, 32.29, 19.03; MS (EI) m/z 496.14 (M + H)$^+$; HRMS (ESI) calcd for $C_{27}H_{21}N_5O_3S$ (M + H)$^+$: 496.1438; found: 496.1436. HPLC retention time 10.522 min, 97.28% pure.

N-   (1,1-dioxidobenzo[b]thiophen-6-yl)-2-(2-(4-fluorophenyl)-7-methoxyimidazo[1,2-a]   Pyridin-3-yl)acet-amide (49). White solid, 73% yield, m.p. 207−209 °C. ^{1}H NMR (500 MHz, DMSO-d_6) δ 10.95 (s, 1H), 8.31 (d, J = 7.5 Hz, 1H), 8.14 (s, 1H), 7.78 (t, J = 6.6 Hz, 2H), 7.58 (dd, J = 17.1, 7.6 Hz, 2H), 7.30 (dd, J = 15.2, 7.7 Hz, 3H), 7.00 (d, J = 2.0 Hz, 1H), 6.69 (dd, J = 7.5, 2.3 Hz, 1H), 5.76 (s, 1H), 4.26 (s, 2H), 3.86 (s, 3H); ^{13}C NMR (126 MHz, DMSO-d_6) δ 168.74, 162.07 (d, J = 244.4 Hz), 157.88, 145.89, 141.84, 137.68, 133.29, 131.63, 130.55, 129.97, 127.06, 126.08, 123.82, 116.03, 115.86, 113.76, 111.97, 106.98, 94.77, 56.09, 32.16; MS (EI) m/z 464.10 (M + H)$^+$; HRMS (ESI) calcd for $C_{24}H_{18}FN_3O_4S$ (M + H)$^+$: 464.1075; found: 464.1074. HPLC retention time 16.149 min, 100.00% pure.

N-(1,1-dioxidobenzo[b]thiophen-6-yl)-2-(7-methoxy-2-(4-(trifluoromethyl)phenyl)imidazo [1,2-a]pyridin-3-yl)acetamide (50). White solid, 77% yield, m.p. 213−216 °C. ^{1}H NMR (500 MHz, DMSO-d_6) δ 10.93 (s, 1H), 8.34 (d, J = 7.5 Hz, 1H), 8.14 (s, 1H), 7.98 (d,

$J = 8.1$ Hz, 2H), 7.84 (d, $J = 8.2$ Hz, 2H), 7.76 (s, 1H), 7.58 (dd, $J = 16.3$, 7.5 Hz, 2H), 7.29 (d, $J = 6.9$ Hz, 1H), 7.04 (d, $J = 2.0$ Hz, 1H), 6.72 (d, $J = 7.4$ Hz, 1H), 4.32 (s, 2H), 3.87 (s, 3H); ^{13}C NMR (101 MHz, DMSO-d_6) δ 168.52, 158.13, 146.17, 141.79, 141.26, 139.17, 137.68, 133.28, 130.58, 128.54, 127.81, 127.06, 126.35, 126.03, 123.88, 115.21, 112.03, 107.42, 94.84, 56.16, 32.18; MS (EI) m/z 514.10 (M + H)$^+$; HRMS (ESI) calcd for C$_{25}$H$_{18}$F$_3$N$_3$O$_4$S (M + H)$^+$: 514.1043; found: 514.1042. HPLC retention time 14.887 min, 97.07% pure.

N-(1,1-dioxidobenzo[b]thiophen-6-yl)-2-(7-methoxy-2-(4-nitrophenyl)imidazo[1,2-a] pyridin-3-yl)acetamide (51). White solid, 80% yield, m.p. 245−247 °C. For compound 52:^{1}H NMR (400 MHz, DMSO-d_6) δ 11.01 (s, 1H), 8.35 (dd, $J = 14.0$, 8.3 Hz, 3H), 8.14 (s, 1H), 8.07 (d, $J = 8.9$ Hz, 2H), 7.79 (dd, $J = 8.2$, 1.9 Hz, 1H), 7.58 (dd, $J = 11.3$, 7.6 Hz, 2H), 7.28 (d, $J = 6.9$ Hz, 1H), 7.04 (d, $J = 2.4$ Hz, 1H), 6.74 (dd, $J = 7.5$, 2.5 Hz, 1H), 4.37 (s, 2H), 3.88 (s, 3H); ^{13}C NMR (101 MHz, DMSO-d_6) δ 168.36, 158.31, 146.64, 146.35, 141.82, 140.52, 137.64, 133.29, 130.56, 128.66, 127.03, 126.40, 126.13, 124.37, 123.91, 116.31, 112.06, 107.72, 94.82, 56.18, 32.22; MS (EI) m/z 491.10 (M + H)$^+$; HRMS (ESI) calcd for C$_{24}$H$_{18}$N$_4$O$_6$S (M + H)$^+$: 491.1020; found: 491.1017. HPLC retention time 13.263 min, 97.66% pure.

N-(1,1-dioxidobenzo[b]thiophen-6-yl)-2-(7-methoxy-2-(4-(methylsulfonyl)phenyl)imidazo [1,2-a]pyridin-3-yl)acetamide (52). White solid, 69% yield, m.p. 153−155 °C. ^{1}H NMR (500 MHz, DMSO-d_6) δ 11.00 (s, 1H), 8.36 (d, $J = 7.6$ Hz, 1H), 8.14 (s, 1H), 8.09−7.97 (m, 4H), 7.81−7.76 (m, 1H), 7.58 (dd, $J = 14.8$, 7.5 Hz, 2H), 7.29 (d, $J = 6.7$ Hz, 1H), 7.04 (d, $J = 2.3$ Hz, 1H), 6.73 (dd, $J = 7.5$, 1.3 Hz, 1H), 4.34 (s, 2H), 3.87 (s, 3H), 3.25 (s, 3H); ^{13}C NMR (101 MHz, DMSO-d_6) δ 168.44, 158.18, 146.24, 141.77, 141.03, 140.09, 139.62, 137.67, 133.25, 130.57, 128.50, 127.80, 127.03, 126.33, 126.14, 123.91, 115.60, 112.07, 107.50, 94.85, 56.16, 44.07, 32.21; MS (EI) m/z 524.09 (M + H)$^+$; HRMS (ESI) calcd for C$_{25}$H$_{21}$N$_3$O$_6$S$_2$ (M + H)$^+$: 524.0945; found: 524.0951. HPLC retention time 10.781 min, 100.00% pure.

N-(1,1-dioxidobenzo[b]thiophen-6-yl)-2-(7-methoxy-2-(thiophen-2-yl)imidazo[1,2-a] pyridin-3-yl)acetamide (53). White solid, 80% yield, m.p. 146−148 °C. ^{1}H NMR (400 MHz, DMSO-d_6) δ 10.95 (s, 1H), 8.33 (d, $J = 7.4$ Hz, 1H), 8.11 (s, 1H), 7.78 (d, $J = 8.1$ Hz, 1H), 7.56 (dd, $J = 14.2$, 4.7 Hz, 3H), 7.40 (s, 1H), 7.27 (d, $J = 5.9$ Hz, 1H), 7.15 (s, 1H), 6.99 (s, 1H), 6.67 (d, $J = 7.4$ Hz, 1H), 4.36 (s, 2H), 3.86 (s, 3H); ^{13}C NMR (101 MHz, DMSO-d_6) δ 168.46, 158.03, 145.89, 141.84, 138.48, 137.69, 137.48, 133.28, 130.54, 128.44, 127.09, 126.14, 124.01, 123.74, 113.12, 111.86, 106.97, 94.56, 56.11, 31.99; MS (EI) m/z 452.07 (M + H)$^+$; HRMS (ESI) calcd for C$_{22}$H$_{17}$N$_3$O$_4$S$_2$ (M + H)$^+$: 452.0733; found: 452.0742. HPLC retention time 12.357 min, 98.68% pure.

N-(1,1-dioxidobenzo[b]thiophen-6-yl)-2-(7-methoxy-2-(naphthalen-2-yl)imidazo[1,2-a] pyridin-3-yl)acetamide (54). White solid, 78% yield, m.p. 136−138 °C. ^{1}H NMR (500 MHz, DMSO-d_6) δ 11.01 (s, 1H), 8.36 (d, $J = 7.5$ Hz, 1H), 8.24 (s, 1H), 8.17 (s, 1H), 8.01 (d, $J = 8.6$ Hz, 1H), 7.99−7.91 (m, 3H), 7.81 (dd, $J = 8.2$, 1.7 Hz, 1H), 7.59 (dd, $J = 12.6$, 7.6 Hz, 2H), 7.56−7.50 (m, 2H), 7.29 (d, $J = 6.9$ Hz, 1H), 7.04 (d, $J = 2.4$ Hz, 1H), 6.71 (dd, $J = 7.5$, 2.4 Hz, 1H), 4.41 (d, $J = 25.1$ Hz, 2H), 3.88 (s, 3H); ^{13}C NMR (101 MHz, DMSO-d_6) δ 168.89, 157.91, 146.05, 142.62, 141.90, 137.71, 133.30, 132.66, 130.56, 128.61, 128.04, 127.11, 126.82, 126.52, 126.28, 126.11, 123.84, 114.43, 111.97, 106.99, 94.78, 56.11, 32.36; MS (EI) m/z 496.13 (M + H)$^+$; HRMS (ESI) calcd for C$_{28}$H$_{21}$N$_3$O$_4$S (M + H)$^+$: 496.1326; found: 496.1324. HPLC retention time 12.366 min, 96.04% pure.

N-(1,1-dioxidobenzo[b]thiophen-6-yl)-2-(6-methyl-2-(p-tolyl)imidazo[1,2-a]pyridin-3-yl) acetamide (55). White solid, 75% yield, m.p. 252−254 °C. ^{1}H NMR (400 MHz, DMSO-d_6) δ 10.92 (s, 1H), 8.26 (s, 1H), 8.14 (s, 1H), 7.78 (dd, $J = 8.2$, 1.9 Hz, 1H), 7.63 (d, $J = 8.1$ Hz, 2H), 7.61−7.56 (m, 2H), 7.52 (d, $J = 9.1$ Hz, 1H), 7.28 (d, $J = 7.0$ Hz, 3H), 7.16 (dd, $J = 9.2$, 1.5 Hz, 1H), 4.28 (s, 2H), 2.34 (d, $J = 8.6$ Hz, 6H); ^{13}C NMR (101 MHz, DMSO-d_6) δ 168.70, 143.52,

141.90, 137.69, 137.17, 133.31, 132.22, 130.53, 129.67, 128.12, 127.83, 127.10, 126.04, 123.77, 122.81, 121.49, 116.46, 114.47, 111.89, 32.32, 21.28, 18.28; MS (EI) m/z 444.13 (M + H)$^+$; HRMS (ESI) calcd for C$_{25}$H$_{21}$N$_3$O$_3$S (M + H)$^+$: 444.1376; found: 444.1376. HPLC retention time 8.613 min, 100.00% pure.

2-(2-(4-cyanophenyl)-6-methylimidazo[1,2-a]pyridin-3-yl)-N-(1,1-dioxidobenzo[b]thiophen-6-yl)acetamide (56). White solid, 71% yield, m.p. 229−231 °C. ^{1}H NMR (400 MHz, DMSO-d_6) δ 11.01 (s, 1H), 8.32 (s, 1H), 8.15 (s, 1H), 8.00−7.92 (m, 4H), 7.79 (d, $J = 8.2$ Hz, 1H), 7.59 (dd, $J = 11.7$, 7.8 Hz, 3H), 7.29 (d, $J = 6.9$ Hz, 1H), 7.22 (d, $J = 9.1$ Hz, 1H), 4.35 (s, 2H), 2.33 (s, 3H); ^{13}C NMR (101 MHz, DMSO-d_6) δ 168.29, 143.84, 141.81, 141.34, 139.65, 137.66, 133.30, 133.07, 130.56, 128.67, 127.07, 126.13, 123.87, 122.94, 122.27, 119.45, 116.79, 116.45, 112.01, 110.17, 32.28, 18.27; MS (EI) m/z 455.11 (M + H)$^+$; HRMS (ESI) calcd for C$_{25}$H$_{18}$N$_4$O$_3$S (M + H)$^+$: 455.1172; found: 455.1177. HPLC retention time 8.357 min, 98.80% pure.

2-(2-(4-chlorophenyl)-6-methylimidazo[1,2-a]pyridin-3-yl)-N-(1,1-dioxidobenzo [b]thiophen -6-yl)acetamide (57). White solid, 73% yield, m.p. 217−219 °C. ^{1}H NMR (500 MHz, DMSO-d_6) δ 10.94 (s, 1H), 8.29 (s, 1H), 8.15 (s, 1H), 7.79−7.75 (m, 3H), 7.61−7.53 (m, 5H), 7.29 (d, $J = 6.9$ Hz, 1H), 7.20 (d, $J = 9.2$ Hz, 1H), 4.29 (s, 2H), 2.33 (s, 3H); ^{13}C NMR (101 MHz, DMSO-d_6) δ 168.44, 143.49, 141.82, 137.69, 133.67, 133.28, 132.73, 130.56, 129.87, 129.15, 128.53, 127.07, 126.12, 123.87, 122.92, 122.05, 116.44, 115.21, 112.01, 32.22, 18.26; MS (EI) m/z 464.08 (M + H)$^+$; HRMS (ESI) calcd for C$_{24}$H$_{18}$ClN$_3$O$_3$S (M + H)$^+$: 464.0830; found: 464.0837. HPLC retention time 11.831 min, 100.00% pure.

N-(1,1-dioxidobenzo[b]thiophen-6-yl)-2-(2-(p-tolyl)imidazo[1,2-a]pyridin-3-yl)acetamide (58). White solid, 71% yield, m.p. 225−227 °C. ^{1}H NMR (400 MHz, DMSO-d_6) δ 10.92 (s, 1H), 8.46 (d, $J = 6.9$ Hz, 1H), 8.13 (s, 1H), 7.77 (dd, $J = 8.2$, 1.8 Hz, 1H), 7.61 (m, 5H), 7.31 (m, 4H), 7.00 (t, $J = 6.5$ Hz, 1H), 4.33 (s, 2H), 2.36 (s, 3H); ^{13}C NMR (101 MHz, DMSO-d_6) δ 168.52, 141.80, 137.54, 133.25, 130.56, 129.73, 128.29, 127.06, 126.10, 125.58, 123.81, 116.72, 114.98, 112.66, 111.95, 32.24, 21.29; MS (EI) m/z 430.12 (M + H)$^+$; HRMS (ESI) calcd for C$_{24}$H$_{19}$N$_3$O$_3$S (M + H)$^+$: 430.1220; found: 430.1219. HPLC retention time 10.558 min, 100.00% pure.

N-(1,1-dioxidobenzo[b]thiophen-6-yl)-2-(2-(4-(methylsulfonyl)phenyl)imidazo[1,2-a] pyridine-3-yl)acetamide(59). White solid, 62% yield, m.p. 156−159 °C. ^{1}H NMR (500 MHz, DMSO-d_6) δ 11.34 (s, 1H), 8.55 (s, 1H), 8.07 (d, $J = 31.7$ Hz, 5H), 7.84 (s, 1H), 7.63 (d, $J = 34.5$ Hz, 3H), 7.32 (d, $J = 38.3$ Hz, 2H), 7.01 (s, 1H), 4.45 (s, 2H), 3.26 (s, 3H); ^{13}C NMR (101 MHz, DMSO-d_6) δ 168.38, 144.76, 141.89, 141.61, 139.92, 137.67, 133.30, 130.57, 128.87, 127.86, 127.04, 126.12, 125.76, 123.88, 117.38, 116.82, 112.96, 112.04, 44.08, 32.20; MS (EI) m/z 494.08 (M + H)$^+$; HRMS (ESI) calcd for C$_{24}$H$_{19}$N$_3$O$_5$S$_2$ (M + H)$^+$: 494.0839; found: 494.0835. HPLC retention time 9.322 min, 100.00% pure.

2-(2-(4-cyanophenyl)imidazo[1,2-a]pyridin-3-yl)-N-(1,1-dioxidobenzo[b]thiophen-6-yl) acetamide (60). White solid, 66% yield, m.p. 243−244 °C. ^{1}H NMR (500 MHz, DMSO-d_6) δ 10.99 (s, 1H), 8.48 (d, $J = 6.9$ Hz, 1H), 8.13 (s, 1H), 8.01 (d, $J = 8.2$ Hz, 2H), 7.95 (d, $J = 8.2$ Hz, 2H), 7.78 (d, $J = 8.1$ Hz, 1H), 7.67 (d, $J = 9.1$ Hz, 1H), 7.59 (dd, $J = 15.4$, 7.5 Hz, 2H), 7.36 (m, 1H), 7.29 (d, $J = 6.8$ Hz, 1H), 7.02 (t, $J = 6.7$ Hz, 1H), 4.39 (s, 2H); ^{13}C NMR (101 MHz, DMSO-d_6) δ 168.23, 144.75, 141.74, 141.56, 139.50, 137.68, 133.27, 133.11, 130.61, 128.86, 127.08, 126.18, 125.84, 125.67, 123.90, 119.42, 117.39, 116.79, 113.01, 112.04, 110.37, 32.27; MS (EI) m/z 441.10 (M + H)$^+$; HRMS (ESI) calcd for C$_{24}$H$_{18}$ClN$_3$O$_3$S (M + H)$^+$: 441.1016; found:441.1017. HPLC retention time 9.322 min, 98.00% pure.

N-(1,1-dioxidobenzo[b]thiophen-6-yl)-2-(imidazo[1,2-a]pyridin-3-yl)acetamide (61). White solid, 82% yield, m.p. 222−224 °C. ^{1}H NMR (500 MHz, DMSO-d_6) δ 10.87 (s, 1H), 8.41 (d, $J = 6.8$ Hz, 1H), 8.12 (s, 1H), 7.74 (d, $J = 8.2$ Hz, 1H), 7.55 (m, 4H), 7.25 (dd, $J = 13.3$, 7.3 Hz, 2H), 6.93 (t, $J = 6.7$ Hz, 1H), 4.19 (s, 2H); ^{13}C NMR (101 Hz,

DMSO-d_6) δ 168.46, 145.36, 141.92, 137.70, 133.27, 133.22, 130.51, 127.03, 125.99, 125.50, 124.30, 123.69, 118.96, 117.41, 112.20, 111.81, 32.23; MS (EI) m/z 340.07 (M + H)$^+$; HRMS (ESI) calcd for $C_{17}H_{13}N_3O_3S$ (M + H)$^+$: 340.0750; found: 340.0743. HPLC retention time 6.732 min, 100.00% pure.

Cell lines and cell culture. HEK-293T cells, triple-negative breast cancer MDA-MB-231 and MDA-MB231-4175 cell lines were obtained from American Type Culture Collection and cultured in Dulbecco Modified Eagle Medium (DMEM, Gibco, USA) plus 10% (v/v) fetal bovine serum (FBS, Gibco, USA), 50 μg/mL penicillin and 50 μg/mL streptomycin (Gibco). A549, MGC-803, HCC70 and MDA-MB-468 cell lines were obtained from American Type Culture Collection and cultured in RPMI 1640 medium (Gibco, USA) with 10% (v/v) FBS, 50 μg/mL penicillin and 50 μg/mL streptomycin (Gibco, USA). All cells were incubated at 37 °C in an incubator containing 5% CO_2.

Reagents and antibodies. The compound **39** was dissolved in sterile dimethyl sulfoxide (DMSO; MP, 196055) and stored at −20 °C. For animal studies, **39** was dissolved in PBS (0.01 M; 8.1 mM $Na_2HPO_4 \cdot 12H_2O$, 1.9 mM $NaH_2PO_4 \cdot 2H_2O$ and 145 mM NaCl, pH 7.2−7.4; cat# G0002, Servicebio, China) containing 15% Cremophor EL (Millipore, 238470-1SET). The primary antibodies for phosphorylated (p-)STAT3 (Y705, #9145; S727, #9134), phosphorylated (p-)STAT1 (Y701, #9167), phosphorylated (p-)STAT5 (Y694, #9351), STAT5 (#25656), β-actin (#3700), c-myc (#5605), Mcl-1 (#4572), HA-tag (#3742), PARP (#9542), cleaved-caspase7 (#9491), second-fluorescence antibodies Alexa Fluor® 488 Conjuate2 (#4412) and Alexa Fluor® 555 Conjuate2 (#4409) were purchased from Cell Signaling Technology, Inc. The antibodies against STAT3 (10253-2-AP) and STAT1 (10144-2-AP) were purchased from ProteinTech Group, Inc. Bcl-xL antibody (sc-8392) was from Santa Cruz Biotechnology. Monoclonal ANTI-FLAG® M2 antibody was from Sigma-Aldrich. The second antibodies Goat Anti-Rabbit IgG H&L (HRP) (ab6721) and Goat Anti-Mouse IgG H&L (HRP) (ab6789) antibodies were purchased from Abcam.

Plasmids. pGL3-STAT3 is a STAT3-dependent luciferase reporter with seven copies of the Stat3-specific binding sequence (AATCC-CAGAA) in the C-reactive protein gene promoter. This new construct was verified by sequencing. STAT3C (or CSTAT3) is a an engineered constitutively dimerizeable STAT3, through substituting cysteine residues for specific amino acids within the C-terminal loop in the SH2 domain. Flag-STAT3 was purchased from FulenGen (#EX-Z2385-M35, Guangzhou, China) and STAT3 sequence was confirmed by sequence. HA-STAT3 in pCDNA3.1 backbone was purchased from PPL (#BC00627, Nanjing, China). STAT3 protein expression plasmid was constructed by inserting full length STAT3 into plasmid pET28a. The insert was confirmed by DNA sequencing.

Molecular docking. In this study, the STAT3 crystal structure (PDB ID: 1BG1) was obtained from the PDB database, and the Maestro 11.1 (Schrodinger, Inc.) was used for molecular docking. Firstly, the "Protein Preparation Wizard" module in Schrodinger software is used to optimize the structure of STAT3 protein, including removing water molecules, hydrogenation, energy minimization and treatment of metal ions and disulfide bonds. The small molecule was imported into the software and then optimized by the "Lig Prep" module, including the formation of 3D structure and low energy conformation. Next, the SH2 domain of the protein was extracted as the active pocket center, and the "Receptor Grid Generation" module in the software was applied to generate the pocket Grid points. Finally, we dock STAT3 protein and small molecule by using the "Ligand Docking" module in Schrodinger software. During docking, the STAT3 protein is considered rigid, while the small molecule is considered flexible. The Glide Score scoring function was applied to calculate the interaction and binding capacity of small molecule and STAT3 protein. As the main docking parameter, XP precision can calculate the binding free energy of ligand and receptor. The greater the negative absolute value is, the greater the affinity between ligand and receptor is. In addition, we also used the "Protein Surface Analyzer" module to analyze the STAT3 protein structure based on electronegativity and marked with different colors.

***In vitro* Metabolic Stability Study**. Microsomes in 0.1 M TRIS buffer pH 7.4 (final concentration 0.33 mg/mL), co-factor $MgCl_2$ (final concentration 5 mM) and tested compound (final concentration 0.1 μM, co-solvent (0.01% DMSO) and 0.005% Bovin serum albumin (BSA)) were incubated at 37 °C for 10 min. The reaction was started by the addition of NADPH (final concentration 1 mM). Aliquots were sampled at 0, 7, 17, 30 and 60 min respectively and methanol (cold in 4 °C) was added to terminate the reaction. After centrifugation (4000 rpm,5 min), samples were then analyzed by LC-MS/MS.

Surface Plasmon Resonance (SPR) analysis. SPR assay was performed using Biacore 8K (GE Healthcare, USA). Purified STAT3 protein (0.1 mg/mL) was dissolved in PBS and immobilized onto the CM5 chip (GE Healthcare, USA). Different concentrations of **39** were dissolved in PBS (0.1% DMSO) and passed over the chip to produce diverse response signals. The binding affinity (K_D) was evaluated using the Biacore Insight Evaluation Software.

Cell viability assay. Cell viability assay was performed using Cell Counting Kit-8 (Bimake, B34302) to measure anti-proliferative activity of designed compounds. The cells were seeded in 96-well plates with 1000−8000 cells per well and allowed to grow overnight. Subsequently, cells were treated with vehicle (0.1% DMSO, as the solvent control) or different concentrations of compounds for 72 h. Before testing, the cells were added to 1/10 volume of CCK-8 each well and incubated for 0.5−4 h at 37 °C until the OD values of vehicle are about 0.8−1.5. Then, the absorbance (also called optical density, OD) of each hole at 480 nm was determined by microplate reader (FLUOstar Omega ACU, Germany). Cell viability (%) = ($OD_{compounds}$-OD_{blank})/($OD_{vehicle}$-OD_{blank}) X 100%. "Blank" represents medium only. Finally, the IC_{50} values were evaluated by GraphPad Prism 7. The concentration range used for this assay was from 0.1 μM to 100 μM.

Colony formation assay. Colony formation assay was performed to examine the effect of **39** on cell colony survival. MDA-MB-231, MDA-MB-468, MDA-MB231-4175 and HCC70 cells were seeded in 6-well plates with 0.5×10^3−1×10^3 cells per well. The second day, various concentrations of **39** were added into the cells. After that, the cell culture medium was changed and the corresponding concentration of **39** was added every 2−3 days until the colonies visible. About 10−15 days later, the cells were fixed using 4% paraformaldehyde fix solution (Beyotime, China) and stained with crystal violet (Beyotime, China). The results of colonies were scanned by printer, processed with image J and analyzed with GraphPad Prism 7. All experiments were set in triplicate.

Wounding healing assay. Wounding healing assay was performed to measure whether **39** inhibit TNBC cells migration. MDA-MB-231, MDA-MB-468, MDA-MB231-4175 and HCC70 cells were seeded in 6-well plates with 0.8×10^6−1.2×10^6 cells per well. When the cell fusion degree reaches 100%, the cells were scratched with pipette tips. Then, the cells were treated with 0−3 μM **39** until the vehicle cells migrate into the scratched area. About 12−96 h later, pictures of the cells were taken with microscope. All experiments were set in triplicate.

Transwell assay for cell invasion. Invasion assay was performed in 24-well Transwell® plates with 8.0 μm pore polycarbonate filters (Corning, USA). MDA-MB-231, MDA-MB-468, MDA-MB231-4175 and HCC70 cells were seeded in the top chamber of insert at 1.5×10^4−3×10^4 cells/well. Then, the cells were treated with different concentrations of **39**. After the treatment

with **39** for 12 h, the cells in the top chamber were carefully removed by cotton and then washed with PBS twice, and the invaded cells in the bottom chamber were fixed with 4% para-formaldehyde and stained with crystal violet. Finally, the invaded cells were photographed and calculated. All experiments were set in triplicate.

Apoptosis assay. Annexin V-fluorescein isothiocyanate (FITC)/propidium iodide (PI) Cell Death Detection Kit (BestBio, China) was applied in cell apoptosis assay. The MDA-MB-231, MDA-MB-468 and MDA-MB231-4175 cells were seeded in 6-well plates and treated with vehicle (0.1% DMSO, as the solvent control) or **39** for 48 h. Then, the cells were digested with trypsin without EDTA, then, washed with cold PBS twice and resuspended in 400 μL 1X binding buffer solution. Subsequently, the cells were incubated with Annexin V-FITC (5 μl) for 5 min and PI (10 μl) for 15 min at 4 °C in the dark. Finally, the samples were detected within 1 h by flow cytometry (Millipore, USA) and processed by FlowJo 7.6 software. All experiments were set in triplicate.

RNA interference. MDA-MB-231 cells were seeded into 6-well or 96-well plates. After incubating for 18−24 h, cells grew to 60−70%. According to the manufacturer's protocol of DharmaFECT (T-2001-03, Dharmacon, USA), cells were transfected with negative control or siRNA targeting STAT3. For STAT3 interference, the sequence of siRNA targeting STAT3:

STAT3-F: 5′-UCCAGUUUCUUAAUUUGUUGACGGGUC-3′;
STAT3-R: 5′-GACCCGUCAACAAAUUAAGAAACUGGA-3′;

A nonspecific oligonucleotide without complementary to any human gene was used as negative control. All above siRNAs were synthesized by Sangon Biotech (Guangdong, China).

Western blotting analysis. The human breast cancer cells were treated with vehicle (0.1% DMSO, as the solvent control) and various concentrations of **39** for 3, 24 or 48 h. Subsequently, the cells were lysed with RIPA buffer(50 mM Tris (pH 7.4), 150 mM NaCl, 1% Triton X-100, 1% sodium deoxycholate, 0.1% SDS sodium orthovanadate, sodium fluoride, EDTA, leupeptin containing 1 mM PMSF (Beyotime, China) and 1% phosphatase inhibitor cocktail (Bimake, China) and the specimen were quantified with Pierce™ BCA Protein Assay Kit (Thermo, 23225). The cell lysates containing 20−50 μg of proteins were denatured by boiling and then analyzed by electrophoresis on 8 or 12% SDS-PAGE gels and transferred onto polyvinylidene difluoride membranes (Millipore, USA). The membranes were blocked with 5% Bovine Serum Albumin (Beyotime, China) for 1 h at room temperature, and then, incubated with primary antibodies (pY705-STAT3, pS727-STAT3, STAT3, Mcl-1, Bcl-xL, c-Myc, β-actin, PARP and cleaved-caspase7) overnight at 4 °C. After washed three times with TBST (TBS with 0.1% Tween-20) buffer, the membranes were incubated with corresponding anti-rabbit (Abcam, ab6721) or anti-mouse (Abcam, ab6789) HRP-conjugated secondary antibodies for 1 h at room temperature. Finally, the membranes were washed with TBST buffer three times for 10 min each time and then developed with ECL kit (Tanon, China) following the manufacturer's protocol.

Immunofluorescence for colocalization. HEK-293T cells were seeded in confocal dishes and incubated overnight. Then, the cells were transfected with HA-STAT3 and Flag-STAT3. 24 h later, HEK-293T cells were treated with vehicle (0.1% DMSO) and **39** for 24 h. The cells were added to 100 ng/mL IL-6 (PeproTech, China) for 30 min before imaged. Subsequently, HEK-293T cells were fixed with 4% paraformaldehyde for 15 min and permeabilized with 0.3% Triton X-100 for 10 min. The samples were blocked with goat serum (Boster, China) for 1 h at room temperature, and then, incubated with HA-tag and Flag-tag antibody at 1: 500 dilution (in goat serum) at 4 °C overnight. After washed three times with PBS, the cells were incubated with two Alexa Fluor secondary antibodies, Alexa Fluor 555 Conjugate and Alexa Fluor 488 Conjugate for Flag-

STAT3 and HA-STAT3 detection, respectively, for 1 h at room temperature in the dark. Then, the cells were rinsed with DAPI (Yeasen, China) for 10 min in the dark followed by washed three times with PBS. Finally, the specimens were examined by Laser Scanning Confocal Microscope FV3000 (Olympus, Japan) and imaged using Olympus software.

Co-immunoprecipitation. HEK-293T cells were seeded into 6-well plates with the concentration of 5×10^5 cells per well and allowed to grow overnight. Then, the cells were transiently transfected with 2500 ng HA-STAT3 and 2500 ng Flag-STAT3. After 24 h, HEK-293T cells, which stably express HA- and Flag-tagged STAT3, were treated with vehicle (0.1% DMSO, as the solvent control) and **39** for 3 h. Then, the cells were added to 100 ng/mL IL-6 to stimulate the interaction between HA-STAT3 and Flag-STAT3 proteins. Subsequently, the cell lysates were extracted for IP by cell lysis buffer (Beyotime, China) containing 1 mM PMSF and 1% phosphatase inhibitor cocktail. Anti-Flag Affinity Gel (Bimake, B23101) was washed three times with PBST (PBS with 0.2% Tween) and incubated with 600−800 μg lysates at 4 °C overnight. Then, the mixtures were washed three times with PBST to remove unbound proteins and boiled in 50 μL 1 × SDS-PAGE loading buffer for 5 min. Finally, the samples were run on SDS-PAGE gel, transferred to polyvinylidene difluoride membranes and then blotted for HA-tag and Flag-tag antibodies.

Reporter gene assay for STAT3 transcriptional activity. HEK-293T cells were plated into 96-well plates with 2.5×10^4 cells per well and incubated overnight. Subsequently, the cells were transiently transfected with 50 ng pGL3-STAT3 (a STAT3-dependent luciferase reporter, containing seven copies of the Stat3-specific binding sequence (AATCCCAGAA), 50 ng STAT3C and 40 ng TK-Renilla as control. After 24 h, HEK-293T cells were treated with vehicle and **39** for 24 h. Samples were processed with Dual Luciferase Reporter Gene Assay Kit (Beyotime, China) following the manufacturer's protocol. The luciferase activity was measured in the luminometer (Promega, GloMax® Navigator, USA).

Electrophoretic Mobility Shift Assay. MDA-MB-231 and MDA-MB-468 cells were treated with vehicle and **39** for 3 h. Then, nuclear extract preparations of the cells were collected with Nuclear and Cytoplasmic Protein Extraction Kit (Beyotime, China) following the manufacturer's protocol and quantified with Pierce™ BCA Protein Assay Kit (Thermo, USA). 8−10 μg nuclear proteins were incubated with biotin-STAT3 (Beyotime, China) or biotin-STAT5 probe (Beyotime, China) prior to EMSA. The STAT3 or STAT5 DNA-protein complexes were separated in 6% native polyacrylamide gels and transferred to a positively charged nylon membrane. The membrane was detected by EMSA/gel-shift Kit (Beyotime, China) following the manufacturer's instructions.

Pharmacokinetic study. Compound **39** was dissolved in DMSO/0.5% HPMC = (5/95, v/v) and was given to SD rats by oral administration. Animal procedures were performed according to institutional ethical guidelines of animal care. The blood samples were collected at 0.25, 0.5, 1, 2, 4, 8, 24h after administration, and then plasma samples were harvested. 20 μL plasma samples were precipitated by 200 μL acetonitrile/methanol (1/1, v/v), and the supernatant was mixed with equal volume of water before analysis. The analysis was performed on a LC-MS/MS system consisted of triple quadrupole mass spectrometer (TQ-S; Waters; America) and liquid chromatography (ACQUITY I-Class; Waters; USA). The chromatographic separation was performed on an ACQUITY UPLCr BEH Phenyl 1.7 μm column (50 mm × 2.1 mm I.D., 1.7 μm) (Waters; USA). The mobile phase consisted of 0.1% formic acid in water and 0.1% formic in acetonitrile.

Animal studies. In human breast carcinoma cells xenograft tumor model, $2 \times 10^6 − 3 \times 10^6$ MDA-MB231-4175 cells were subcutaneously injected into the flank of 4-5-week-old NOD-SCID

female mice (SCXK 2018-0008). In human triple-negative breast cancer patient-derived tumor xenograft (TNBC PDX) model, we used the tumor tissues from the TNBC patient (No. J00099327, Jackson Lab, USA) in serum-free DMEM, which was then cut into pieces. Approximately 2 mm^3 patient tumor tissue fragments were subcutaneously implanted into the flank of female NOD-SCID mice (SCXK 2018-0008) using a trocar. For these two models, when tumor volume reached about 100 mm^3, the mice were randomly divided into three groups (n = 6/group) including vehicle (treated with PBS containing 15% Cremophor EL), 5 mg/kg and 15 mg/kg **39** (diluted in PBS containing 15% Cremophor EL). Mice were administered with different doses of **39** by intraperitoneal injection every day. The volume (V) of the tumor was measured every 2–3 days and calculated using the formula, $V = \pi/6 \times S^2 \times L$, where S is the minor axis and L is the major axis. At day 20, the mice were sacrificed and their tumor tissues were harvested and weighed. The tumor tissues were detected by immunohistochemistry assay using Ki67 antibody. The hearts, livers, spleen, lungs, kidneys of the mice were also collected for hematological analysis to study the toxicology of **39**. For immunoblot assay, we gained the protein samples of tumor lysed with RIPA buffer (Beyotime, China) subjecting to western blot analysis as described above. All animal procedures were approved by Animal Care and Use Committee of Sun Yat-Sen Univeristy, Guangzhou, China.

Declaration of competing interest

The authors declare that they have no known competing financial interests or personal relationships that could have appeared to influence the work reported in this paper.

Acknowledgments

Appendix A. Supplementary data

Supplementary data to this article can be found online at https://doi.org/10.1016/j.ejmech.2021.113525.

References

[1] B. Debnath, S. Xu, N. Neamati, Small molecule inhibitors of signal transducer and activator of transcription 3 (Stat3) protein, J. Med. Chem. 55 (2012) 6645–6668.

[2] Q. Huang, Y. Zhong, H. Dong, Q. Zheng, S. Shi, K. Zhu, X. Qu, W. Hu, X. Zhang, Y. Wang, Revisiting signal transducer and activator of transcription 3 (STAT3) as an anticancer target and its inhibitor discovery: where are we and where should we go? Eur. J. Med. Chem. 187 (2020) 111922.

[3] K. Al Zaid Siddiquee, J. Turkson, STAT3 as a target for inducing apoptosis in solid and hematological tumors, Cell Res. 18 (2008) 254–267.

[4] P. Sansone, J. Bromberg, Targeting the interleukin-6/Jak/stat pathway in human malignancies, J. Clin. Oncol. 30 (2012) 1005–1014.

[5] G. Miklossy, T.S. Hilliard, J. Turkson, Therapeutic modulators of STAT signalling for human diseases, Nat. Rev. Drug Discov. 12 (2013) 611–629.

[6] D.E. Johnson, R.A. O'Keefe, J.R. Grandis, Targeting the IL-6/JAK/STAT3 signalling axis in cancer, Nat. Rev. Clin. Oncol. 15 (2018) 234–248.

[7] J.D. Beebe, J.Y. Liu, J.T. Zhang, Two decades of research in discovery of anticancer drugs targeting STAT3, how close are we? Pharmacol. Ther. 191 (2018) 74–91.

[8] H. Yu, H. Lee, A. Herrmann, R. Buettner, R. Jove, Revisiting STAT3 signalling in cancer: new and unexpected biological functions, Nat. Rev. Canc. 14 (2014) 736–746.

[9] D.L. Ma, L.J. Liu, K.H. Leung, Y.T. Chen, H.J. Zhong, D.S. Chan, H.M. Wang, C.H. Leung, Antagonizing STAT3 dimerization with a rhodium(III) complex, Angew Chem. Int. Ed. Engl. 53 (2014) 9178–9182.

[10] G. La Sala, C. Michiels, T. Kukenshoner, T. Brandstoetter, B. Maurer, A. Koide, K. Lau, F. Pojer, S. Koide, V. Sexl, L. Dumoutier, O. Hantschel, Selective inhibition of STAT3 signaling using monobodies targeting the coiled-coil and N-terminal domains, Nat. Commun. 11 (2020) 4115.

[11] C. Zhao, H. Li, H.J. Lin, S. Yang, J. Lin, G. Liang, Feedback activation of STAT3 as a cancer drug-resistance mechanism, Trends Pharmacol. Sci. 37 (2016) 47–61.

[12] H.J. Lee, G. Zhuang, Y. Cao, P. Du, H.J. Kim, J. Settleman, Drug resistance via feedback activation of Stat3 in oncogene-addicted cancer cells, Canc. Cell 26 (2014) 207–221.

[13] M. Spitzner, R. Ebner, H.A. Wolff, B.M. Ghadimi, J. Wienands, M. Grade, STAT3: a novel molecular mediator of resistance to chemoradiotherapy, Cancers (Basel) 6 (2014) 1986–2011.

[14] I. Pavlinov, M. Salkovski, L.N. Aldrich, Beclin 1-ATG14L protein-protein interaction inhibitor selectively inhibits autophagy through disruption of VPS34 complex I, J. Am. Chem. Soc. 142 (2020) 8174–8182.

[15] K. McAulay, E.A. Hoyt, M. Thomas, M. Schimpl, M.S. Bodnarchuk, H.J. Lewis, D. Barratt, D. Bhavsar, D.M. Robinson, M.J. Deery, D.J. Ogg, G.J.L. Bernardes, R.A. Ward, M.J. Waring, J.G. Kettle, Alkynyl benzoxazines and dihydroquinazolines as cysteine targeting covalent warheads and their application in identification of selective irreversible kinase inhibitors, J. Am. Chem. Soc. 142 (2020) 10358–10372.

[16] T. Wang, G. Niu, M. Kortylewski, L. Burdelya, K. Shain, S. Zhang, R. Bhattacharya, D. Gabrilovich, R. Heller, D. Coppola, W. Dalton, R. Jove, D. Pardoll, H. Yu, Regulation of the innate and adaptive immune responses by Stat-3 signaling in tumor cells, Nat. Med. 10 (2004) 48–54.

[17] Y. Wang, Y. Shen, S. Wang, Q. Shen, X. Zhou, The role of STAT3 in leading the crosstalk between human cancers and the immune system, Canc. Lett. 415 (2018) 117–128.

[18] T.A. Karakasheva, E.W. Lin, Q. Tang, E. Qiao, T.J. Waldron, M. Soni, A.J. Klein-Szanto, V. Sahu, D. Basu, S. Ohashi, K. Baba, Z.T. Giaccone, S.R. Walker, D.A. Frank, E.P. Wileyto, Q. Long, M.C. Dunagin, A. Raj, J.A. Diehl, K.K. Wong, A.J. Bass, A.K. Rustgi, IL-6 mediates cross-talk between tumor cells and activated fibroblasts in the tumor microenvironment, Canc. Res. 78 (2018) 4957–4970.

[19] H. Kitamura, Y. Ohno, Y. Toyoshima, J. Ohtake, S. Homma, H. Kawamura, N. Takahashi, A. Taketomi, Interleukin-6/STAT3 signaling as a promising target to improve the efficacy of cancer immunotherapy, Canc. Sci. 108 (2017) 1947–1952.

[20] N.M. Song Tl, Y. Laurensia, J. Lim, J. Tan, Z. Li, W. Pang, A. Kizhakeyil, G. Wijaya, D. Huang, S. Nagarajan, B.K. Chia, D. Cheah, Y. Liu, F. Zhang, H. Rao, T. Tang, E.K. Wong, J. Bei, J. Iqbal, N. Grigoropoulos, S. Ng, W. Chng, B. Teh, S. Tan, N.K. Verma, H. Fan, S. Lim, C. Ong, Oncogenic activation of the STAT3 pathway drives PD-L1 expression in natural killer-T-cell lymphoma, Blood 132 (2018) 1146–1158.

[21] V. Atsaves, N. Tsesmetzis, D. Chioureas, L. Kis, V. Leventaki, E. Drakos, T. Panaretakis, D. Grander, L.J. Medeiros, K.H. Young, G.Z. Rassidakis, PD-L1 is commonly expressed and transcriptionally regulated by STAT3 and MYC in ALK-negative anaplastic large-cell lymphoma, Leukemia 31 (2017) 1633–1637.

[22] R. Huang, X. Jing, X. Huang, Y. Pan, Y. Fang, G. Liang, Z. Liao, H. Wang, Z. Chen, Y. Zhang, Bifunctional naphthoquinone aromatic amide-oxime derivatives exert combined immunotherapeutic and antitumor effects through simultaneous targeting of indoleamine-2,3-dioxygenase and signal transducer and activator of transcription 3, J. Med. Chem. 63 (2020) 1544–1563.

[23] K. Matsuno, Y. Masuda, Y. Uehara, H. Sato, A. Muroya, O. Takahashi, T. Yokotagawa, T. Furuya, T. Okawara, M. Otsuka, N. Ogo, T. Ashizawa, C. Oshita, S. Tai, H. Ishii, Y. Akiyama, A. Asai, Identification of a new series of STAT3 inhibitors by virtual screening, ACS Med. Chem. Lett. 1 (2010) 371–375.

[24] B.D. Page, S. Fletcher, P. Yue, Z. Li, X. Zhang, S. Sharmeen, A. Datti, J.L. Wrana, S. Trudel, A.D. Schimmer, J. Turkson, P.T. Gunning, Identification of a non-phosphorylated, cell permeable, small molecule ligand for the Stat3 SH2 domain, Bioorg. Med. Chem. Lett 21 (2011) 5605–5609.

[25] S. Haftchenary, H.A. Luchman, A.O. Jouk, A.J. Veloso, B.D. Page, X.R. Cheng, S.S. Dawson, N. Grinshtein, V.M. Shahani, K. Kerman, D.R. Kaplan, C. Griffin, A.M. Aman, R. Al-Awar, S. Weiss, P.T. Gunning, Potent targeting of the STAT3 protein in brain cancer stem cells: a promising route for treating glioblastoma, ACS Med. Chem. Lett. 4 (2013) 1102–1107.

[26] R.W. Hui Song, Shaomeng Wang, Jiayuh Lin, A low-molecular weight compound discovered through virtual database screening inhibits Stat 3 function in breast cancer cells, Proc. Natl. Acad. Sci. U.S.A. 102 (2005), 4700-1705.

[27] T.A. Karakasheva, E.W. Lin, Q. Tang, E. Qiao, T.J. Waldron, M. Soni, A.J. Klein-Szanto, V. Sahu, D. Basu, S. Ohashi, K. Baba, Z.T. Giaccone, S.R. Walker, D.A. Frank, E.P. Wileyto, Q. Long, M.C. Dunagin, A. Raj, J.A. Diehl, K.K. Wong, A.J. Bass, A.K. Rustgi, IL-6 mediates cross-talk between tumor cells and activated fibroblasts in the tumor microenvironment, Canc. Res. 78 (2018) 4957–4970.

[28] L. Bai, H. Zhou, R. Xu, Y. Zhao, K. Chinnaswamy, D. McEachern, J. Chen, C.Y. Yang, Z. Liu, M. Wang, L. Liu, H. Jiang, B. Wen, P. Kumar, J.L. Meagher, D. Sun, J.A. Stuckey, S. Wang, A potent and selective small-molecule degrader of STAT3 achieves complete tumor regression in vivo, Canc. Cell 36 (2019) 498–511 e417.

[29] H. Zhou, L. Bai, R. Xu, Y. Zhao, J. Chen, D. McEachern, K. Chinnaswamy, B. Wen,

L. Dai, P. Kumar, C.Y. Yang, Z. Liu, M. Wang, L. Liu, J.L. Meagher, H. Yi, D. Sun, J.A. Stuckey, S. Wang, Structure-based discovery of SD-36 as a potent, selective, and efficacious PROTAC degrader of STAT3 protein, J. Med. Chem. 62 (2019) 11280−11300.

[30] G.B. Becker S, C.W. Müller, Three-dimensional structure of the Stat3beta homodimer bound to DNA, Nature 394 (1998) 145−151.

[31] R. Musharrafieh, J. Zhang, P. Tuohy, N. Kitamura, S.S. Bellampalli, Y. Hu, R. Khanna, J. Wang, Discovery of quinoline analogues as potent antivirals against enterovirus D68 (EV-D68), J. Med. Chem. 62 (2019) 4074−4090.

[32] T. Felicetti, R. Cannalire, D. Pietrella, G. Latacz, A. Lubelska, G. Manfroni, M.L. Barreca, S. Massari, O. Tabarrini, K. Kiec-Kononowicz, B.D. Schindler, G.W. Kaatz, V. Cecchetti, S. Sabatini, 2-Phenylquinoline S. aureus NorA efflux pump inhibitors: evaluation of the importance of methoxy group introduction, J. Med. Chem. 61 (2018) 7827−7848.

[33] M.K. Krapf, M. Wiese, Synthesis and biological evaluation of 4-Anilino-quinazolines and -quinolines as inhibitors of breast cancer resistance protein (ABCG2), J. Med. Chem. 59 (2016) 5449−5461.

[34] T.D. Cushing, X. Hao, Y. Shin, K. Andrews, M. Brown, M. Cardozo, Y. Chen, J. Duquette, B. Fisher, F. Gonzalez-Lopez de Turiso, X. He, K.R. Henne, Y.L. Hu, R. Hungate, M.G. Johnson, R.C. Kelly, B. Lucas, J.D. McCarter, L.R. McGee, J.C. Medina, T. San Miguel, D. Mohn, V. Pattaropong, L.H. Pettus, A. Reichelt, R.M. Rzasa, J. Seganish, A.S. Tasker, R.C. Wahl, S. Wannberg, D.A. Whittington, J. Whoriskey, G. Yu, L. Zalameda, D. Zhang, D.P. Metz, Discovery and in vivo evaluation of (S)-N-(1-(7-fluoro-2-(pyridin-2-yl)quinolin-3-yl)ethyl)-9H-purin-6-amine (AMG319) and related PI3Kdelta inhibitors for inflammation and autoimmune disease, J. Med. Chem. 58 (2015) 480−511.

[35] S. Sabatini, F. Gosetto, N. Iraci, M.L. Barreca, S. Massari, L. Sancineto, G. Manfroni, O. Tabarrini, M. Dimovska, G.W. Kaatz, V. Cecchetti, Re-evolution of the 2-phenylquinolines: ligand-based design, synthesis, and biological evaluation of a potent new class of Staphylococcus aureus NorA efflux pump inhibitors to combat antimicrobial resistance, J. Med. Chem. 56 (2013) 4975−4989.

[36] J.T. Madak, C.R. Cuthbertson, Y. Miyata, S. Tamura, E.M. Petrunak, J.A. Stuckey, Y. Han, M. He, D. Sun, H.D. Showalter, N. Neamati, Design, synthesis, and biological evaluation of 4-quinoline carboxylic acids as inhibitors of dihydroorotate dehydrogenase, J. Med. Chem. 61 (2018) 5162−5186.

[37] B.M. Fox, K. Sugimoto, K. Iio, A. Yoshida, J.K. Zhang, K. Li, X. Hao, M. Labelle, M.L. Smith, S.M. Rubenstein, G. Ye, D. McMinn, S. Jackson, R. Choi, B. Shan, J. Ma, S. Miao, T. Matsui, N. Ogawa, M. Suzuki, A. Kobayashi, H. Ozeki, C. Okuma, Y. Ishii, D. Tomimoto, N. Furakawa, M. Tanaka, M. Matsushita, M. Takahashi, T. Inaba, S. Sagawa, F. Kayser, Discovery of 6-phenylpyrimido[4,5-b][1,4]oxazines as potent and selective acyl CoA:diacylglycerol acyltransferase 1 (DGAT1) inhibitors with in vivo efficacy in rodents, J. Med. Chem. 57 (2014) 3464−3483.

[38] H. Mohammad, A.S. Mayhoub, A. Ghafoor, M. Soofi, R.A. Alajlouni, M. Cushman, M.N. Seleem, Discovery and characterization of potent thiazoles versus methicillin- and vancomycin-resistant Staphylococcus aureus, J. Med. Chem. 57 (2014) 1609−1615.

[39] J.A. Kodra Jt, B. Andersen, C. Behrens, C.L. Brand, I.T. Christensen, M. Guldbrandt, C.B. Jeppesen, L.B. Knudsen, P. Madsen, E. Nishimura, C. Sams, U.G. Sidelmann, R.A. Pedersen, F.C. Lynn, J. Lau, Novel glucagon receptor antagonists with improved selectivity over the glucose-dependent insulinotropic polypeptide receptor, J. Med. Chem. 51 (2008) 5387−5396.

[40] B.C. Lau J, U.G. Sidelmann, L.B. Knudsen, B. Lundt, C. Sams, L. Ynddal, C.L. Brand, L. Pridal, A. Ling, D. Kiel, M. Plewe, S. Shi, P. Madsen, New beta-alanine derivatives are orally available glucagon receptor antagonists, J. Med. Chem. 50 (2007) 113−128.

[41] K. Yakoub, S. Jung, C. Sattler, H. Damerow, J. Weber, A. Kretzschmann, A.S. Cankaya, M. Piel, F. Rosch, A.S. Haugaard, B. Frolund, T. Schirmeister, H. Luddens, Structure-function evaluation of imidazopyridine derivatives selective for delta-subunit-containing gamma-aminobutyric acid type A (GABAA) receptors, J. Med. Chem. 61 (2018) 1951−1968.

[42] Y. Ma, G. Sun, D. Chen, X. Peng, Y.L. Chen, Y. Su, Y. Ji, J. Liang, X. Wang, L. Chen, J. Ding, B. Xiong, J. Ai, M. Geng, J. Shen, Design and optimization of a series of 1-sulfonylpyrazolo[4,3-b]pyridines as selective c-Met inhibitors, J. Med. Chem. 58 (2015) 2513−2529.

[43] L.V. Denora N, M.G. Pisu, R. Dore, L. Murru, A. Latrofa, G. Trapani, E. Sanna, 2-Phenyl-imidazo[1,2-a]pyridine compounds containing hydrophilic groups as potent and selective ligands for peripheral benzodiazepine receptors: synthesis, binding affinity and electrophysiological studies, J. Med. Chem. 51 (2008) 6876−6888.

[44] L.J. Cai L, S.S. Zoghbi, J. Cuevas, C. Baetas, J. Hong, H.U. Shetty, N.M. Seneca, A.K. Brown, R. Gladding, S.S. Temme, M.M. Herman, R.B. Innis, V.W. Pike, Synthesis and evaluation of N-methyl and S-methyl 11C-labeled 6-methylthio-2-(4'-N,N-dimethylamino)phenylimidazo[1,2-a]pyridines as radioligands for imaging beta-amyloid plaques in Alzheimer's disease, J. Med. Chem. 51 (2008) 148−158.

[45] L.V. Trapani G, N. Denora, A. Trapani, A. Lopedota, A. Latrofa, M. Franco, M. Serra, M.G. Pisu, I. Floris, E. Sanna, G. Biggio, G. Liso, Structure-activity relationships and effects on neuroactive steroid synthesis in a series of 2-phenylimidazo[1,2-a]pyridineacetamide peripheral benzodiazepine receptors ligands, J. Med. Chem. 48 (2005) 292−305.

[46] J. Schust, B. Sperl, A. Hollis, T.U. Mayer, T. Berg, Stattic: a small-molecule inhibitor of STAT3 activation and dimerization, Chem. Biol. 13 (2006) 1235−1242.

[47] H. Chen, Z. Yang, C. Ding, L. Chu, Y. Zhang, K. Terry, H. Liu, Q. Shen, J. Zhou, Fragment-based drug design and identification of HJC0123, a novel orally bioavailable STAT3 inhibitor for cancer therapy, Eur. J. Med. Chem. 62 (2013) 498−507.

[48] H. Chen, Z. Yang, C. Ding, A. Xiong, C. Wild, L. Wang, N. Ye, G. Cai, R.M. Flores, Y. Ding, Q. Shen, J. Zhou, Discovery of potent anticancer agent HJC0416, an orally bioavailable small molecule inhibitor of signal transducer and activator of transcription 3 (STAT3), Eur. J. Med. Chem. 82 (2014) 195−203.

[49] W. Zhang, T. Ma, S. Li, Y. Yang, J. Guo, W. Yu, L. Kong, Antagonizing STAT3 activation with benzo[b]thiophene 1, 1-dioxide based small molecules, Eur. J. Med. Chem. 125 (2017) 538−550.

[50] P. Ji, X. Xu, S. Ma, J. Fan, Q. Zhou, X. Mao, C. Qiao, Novel 2-Carbonylbenzo[b]thiophene 1,1-dioxide derivatives as potent inhibitors of STAT3 signaling pathway, ACS Med. Chem. Lett. 6 (2015) 1010−1014.

[51] K.J. Wu, H.J. Zhong, G. Yang, C. Wu, J.M. Huang, G. Li, D.L. Ma, C.H. Leung, Small molecule Pin1 inhibitor blocking NF-kappaB signaling in prostate cancer cells, Chem. Asian J. 13 (2018) 275−279.

[52] C.C. Hsu, J.C. Lien, C.W. Chang, C.H. Chang, S.C. Kuo, T.F. Huang, Yuwen02f1 suppresses LPS-induced endotoxemia and adjuvant-induced arthritis primarily through blockade of ROS formation, NFkB and MAPK activation, Biochem. Pharmacol. 85 (2013) 385−395.

[53] K.J. Wu, H.J. Zhong, G. Li, C. Liu, H.D. Wang, D.L. Ma, C.H. Leung, Structure-based identification of a NEDD8-activating enzyme inhibitor via drug repurposing, Eur. J. Med. Chem. 143 (2018) 1021−1027.

[54] Q. Huang, L. Zhan, H. Cao, J. Li, Y. Lyu, X. Guo, J. Zhang, L. Ji, T. Ren, J. An, B. Liu, Y. Nie, J. Xing, Increased mitochondrial fission promotes autophagy and hepatocellular carcinoma cell survival through the ROS-modulated coordinated regulation of the NFKB and TP53 pathways, Autophagy 12 (2016) 999−1014.

[55] R.P. Nishanth, R.G. Jyotsna, J.J. Schlager, S.M. Hussain, P. Reddanna, Inflammatory responses of RAW 264.7 macrophages upon exposure to nanoparticles: role of ROS-NFkappaB signaling pathway, Nanotoxicology 5 (2011) 502−516.

[56] Q. Huang, H. Dong, B. Li, W. Hu, Y. Wang, Rhodium catalyzed direct C3-ethoxycarbonylmethylation of imidazo[1,2-a]pyridines with ethyl diazoacetate, Tetrahedron (2020) 76.